INFORMATION TO USERS

This manuscript has been reproduced from the microfilm master. UMI films the text directly from the original or copy submitted. Thus, some thesis and dissertation copies are in typewriter face, while others may be from any type of computer printer.

The quality of this reproduction is dependent upon the quality of the copy submitted. Broken or indistinct print, colored or poor quality illustrations and photographs, print bleedthrough, substandard margins, and improper alignment can adversely affect reproduction.

In the unlikely event that the author did not send UMI a complete manuscript and there are missing pages, these will be noted. Also, if unauthorized copyright material had to be removed, a note will indicate the deletion.

Oversize materials (e.g., maps, drawings, charts) are reproduced by sectioning the original, beginning at the upper left-hand corner and continuing from left to right in equal sections with small overlaps.

University Of Alberta

Numerical Solution of the Forward Problem in Electroencephalography

by

Vladislav E. Agapov

©

Thesis submitted to the Faculty of Graduate Studies and Research in partial fulfillment

of the requirements for the degree of

Doctor of Philosophy in Applied Mathematics.

Department of Mathematical Sciences.

Edmonton, Alberta

Spring 2002.

The author has granted a non-exclusive licence allowing the National Library of Canada to reproduce, loan, distribute or sell copies of this thesis in microform, paper or electronic formats.

The author retains ownership of the copyright in this thesis. Neither the thesis nor substantial extracts from it may be printed or otherwise reproduced without the author's permission.

L'auteur a accordé une licence non exclusive permettant à la Bibliothèque nationale du Canada de reproduire, prêter, distribuer ou vendre des copies de cette thèse sous la forme de microfiche/film, de reproduction sur papier ou sur format électronique.

L'auteur conserve la propriété du droit d'auteur qui protège cette thèse. Ni la thèse ni des extraits substantiels de celle-ci ne doivent être imprimés ou autrement reproduits sans son autorisation.

0-612-69325-4

Canada

University of Alberta

Library Release Form

Name of Author: Vladislav E. Agapov

Title: Numerical Solution of the Forward Problem in Electroencephalography.

Degree: Doctor of Philosophy

Granted: 2001

Permission is hereby granted to the University of Alberta Library to reproduce single copies of this thesis and to lend or sell copies for private, academic, or scientific research purposes only.

The author reserves all other publications and all other rights with respect to the copyright of this thesis, and except as previously stated, neither this thesis nor any substantial portion thereof may be printed or otherwise reproduced in any material form without the author's prior written permission.

Vladislav Agapov

6595 Cote Saint Luc Road, Apt. 703

Montreal, Quebec

Canada, H4V 1G7

Nov. 1/01
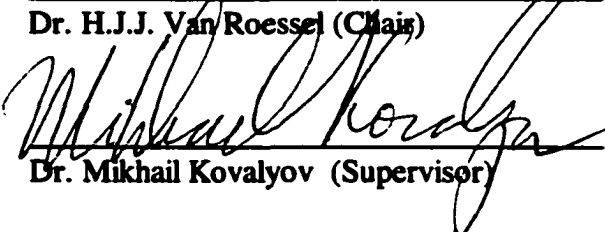
UNIVERSITY OF ALBERTA

Faculty of Graduate Studies and Research

The undersigned certify that they have read, and recommend to the Faculty of Graduate Studies and Research for acceptance, a thesis entitled **Numerical Solution of the Forward Problem in Encephalography** submitted by **Vladislav E. Agapov** in partial fulfillment of the requirements for the degree of **Doctor of Philosophy** in **Applied Mathematics**.

Dr. H.J.J. Van Roessel (Chair)

Dr. Mikhail Kovalyov (Supervisor)

Dr. Zoltan J. Koles (Co-supervisor)
(Biomedical Engineering)

Dr. John C. Lind (Alberta Hospital)

Dr. Walter Allegretto

Dr. Martin Legaré

Dr. Vladimir L. Makarov (Inst. of Math of NAS of Ukraine)

Date: Oct 23/2001

Abstract.

The localization of areas of excessive electrical activity in the human brain system by multi-channel electroencephalography (EEG) recordings is one of the most important problems in Clinical Neurophysiology. This activity can be approximated by equivalent dipole [15], which generates the potential distribution all over the brain system. 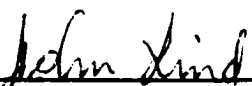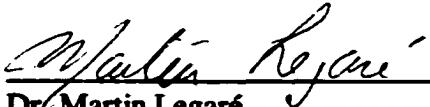The essential part of the source localization procedure is the forward problem solution, i.e. computation of the potential on the surface of the head given the location and orientation of the dipole. In this work, the forward problem is solved with the use of the Finite Volume Method (FVM). The implementation of the FVM is done in such a way that the same algorithm can be applied for the realistic head model made by using Magnetic Resonance Imaging (MRI) scans of the head of the real patient. The main objectives of the research are assessment of the errors of the FVM modeling and computational issues such as deflation, properties of deflated matrix and acceleration of computations. The forward problem acceleration is especially important in practice, hence alternative approaches for the solution of the forward problem would be interesting. The Finite Volume Method is implemented in such a way that the deflated matrix of the linear system corresponding to the forward problem is symmetric and positive definite. These properties allow the use of the Conjugate Gradient Method with Polynomial Preconditioning and essential acceleration of the computations. The errors of the numerical solution were studied using analytical solutions for three-shell geometry. The realistic three-shell solution derived in this work allows to separate the source and sink of the equivalent dipole. This is essential for the FVM tests, as with this method the source and sink cannot be infinitely close together. As the radial dipole gets closer to the skull, the error of FVM grows. It can be reduced either with the higher resolution grids or with better domain decomposition algorithms. The idea of analytical matrix inversion developed for one, two and thri-dimensional systems of cubic finite volume elements can have potential for a rapid solution of the forward problem provided that it can be extended for deformed and nonuniform cases.

<div align="center">**Thesis Plan.**</div>

Contents

List of Tables

List of Figures

1 Introduction.

1.1 The Forward Problem in EEG.

This work addresses the computational aspects of one of the major problems in Clinical Neurophysiology - the localization of the areas of excessive neural activity in the human brain. These areas of excessive neural firing caused by the external electrical stimulus are associated with possible brain tumors, epilepsy, head injuries, infectious diseases, drug overdoses, etc. Therefore their accurate localization is very important for diagnostic purposes. It is a well known fact [15] that this neural activity can be fairly well approximated by dipole current sources, consisting of closely located "source" and "sink" of the electrical current of the same intensity. The stationary current dipole source (or sometimes the multiple sources) generates the distribution of potential all over the head. In practice, only the potential difference between a given point and a chosen reference point can be measured. This potential difference is collected by a limited number of sensors through the procedure named Electroencephalography or EEG and called the biopotential in EEG literature. Combined with Magnetic Resonance Imaging (MRI), which provides information about the anatomy of the brain system, EEG is a very powerful and informative tool in neural diagnostics.

In EEG literature, the problem of computing the biopotential for such a dipole is called the forward problem of EEG source localization. This problem can be posed as follows: given the geometry of the human head as well as the location and orientation of single or multiple dipole sources, find the potential on the surface of the head. The problem of the source localization itself, given the potential on the head surface only, is called the inverse problem of EEG. One way to solve the inverse problem is to solve the forward problem with a different location and orientation and then try to combine the results in order to

1

fit the boundary data.

1.2 Biophysics of the EEG.

Consider the theoretical aspects of EEG. The electro-magnetic field is governed by the Maxwell equations (macroscopic version)

$$\nabla \cdot \vec{D} = \rho \tag{1.2.1}$$

$$\nabla \times \vec{E} = -\frac{\partial \vec{B}}{\partial t} \tag{1.2.2}$$

$$\nabla \cdot \vec{B} = 0 \tag{1.2.3}$$

$$\nabla \times \vec{H} = \vec{J} - \frac{\partial \vec{D}}{\partial t}, \tag{1.2.4}$$

where $\vec{E}$ - electric field;

$\vec{D} = \varepsilon \vec{E}$ - electric displacement inside the mass of tissue;

ρ - density of electric charge;

$\vec{B}$ - total magnetic field;

$\vec{H}$ - magnetic field due to free currents;

$\vec{J} = \sigma \vec{E}$ - density of the electric current.

Here ε is the permittivity of the brain tissue, σ is the conductivity. The frequency range of the electromagnetic fields in the human brain system is below 100 cycles/second, therefore the electromagnetic field changes slowly. In this case, electric and magnetic fields can be uncoupled in the first approximation [15].

Uncoupling simplifies the equations for the electric field to

$$\nabla \cdot \vec{D} = \rho, \quad \text{(Gauss' Law)} \tag{1.2.5}$$

$$\nabla \times \vec{E} = 0, \tag{1.2.6}$$

$$\vec{J} = \frac{\partial \vec{D}}{\partial t}. \tag{1.2.7}$$

2

By virtue of $\nabla \times \vec{E} = 0$, the electric field is of the form

$$\vec{E} = -\nabla \Psi.$$

Consider a control volume V inside the surface with face $\vec{S}$ containing a current source

$$\vec{J} = \sigma \vec{E} = -\sigma \nabla \Psi.$$

Integration over $\vec{S}$ gives

$$\oint \sigma \nabla \Psi \cdot d\vec{S} = -\oint \vec{J} dS = \int_V I_V dV,$$

where I_V is the current volume source density, i.e. the charge emitted into a unit volume for unit time. If a current source is located at a single point,

$$I_V = I_o \delta(x - x_0, y - y_0, z - z_0),$$

then

$$\oint \sigma \nabla \Psi \cdot d\vec{S} = I_o. \tag{1.2.8}$$

For the domains that do not contain the current sources, the right-hand side is zero. Combination of (1.2.5) and (1.2.7) result in the conservation of charge

$$\nabla \cdot \vec{J} - \frac{\partial \rho}{\partial t} = 0., \tag{1.2.9}$$

or equivalently

$$\vec{\nabla} \cdot (\sigma \vec{E}) - \frac{\partial}{\partial t}(\vec{\nabla} \cdot \varepsilon \vec{E}) = 0. \tag{1.2.10}$$

Dividing the biological volume conductor into smaller domains for which σ and ε can be assumed to be constant and making use of (1.2.7), it is possible to get the equation describing distribution of the potential for every domain,

$$\sigma \Delta \Psi - \varepsilon \frac{(\partial \Delta \Psi)}{\partial t} = 0, \tag{1.2.11}$$

3

where Δ is the Laplacian operator. The current flow normal to the interface between the two adjacent domains does not change, therefore

$$\sigma_{in}\frac{\partial\Psi_{in}}{\partial n} = \sigma_{out}\frac{\partial\Psi_{out}}{\partial n},$$

where n is the normal to the surface of the interface. The first term in (1.2.11) describes the resistive current, whereas the second term describes the capacitive current. Under certain circumstances, namely when the conductivity is high enough and the polarization of tissue is low enough, the second term can be neglected. Assume that the potential is periodic in time with field frequency f,

$$\Psi = \Psi(\vec{x})e^{2\pi i f t}.$$

The condition which determines whether the capacitive effects are negligible [15] is

$$\frac{\text{capacitive current}}{\text{resistive current}} = \frac{2\pi f \varepsilon(f)}{\sigma(f)} \ll 1, \tag{1.2.12}$$

and generally in the case of frequencies below 100 cycles/second this condition is satisfied.

1.3 Solutions to the Forward Problem

.

The main difficulty of the forward EEG problem lies in the complexity of the anatomy of the human head. So far the conventional way of solving the forward problem has been to use the three-shell model of the human head, first introduced in [46]. This allows for the analytical solutions of the forward EEG problem, however it does not reflect the entire complexity of the human head. It was demonstrated in [44] that natural holes in the skull such as the eyes, nose, mouth and ears can already cause errors in the source localization which are significant enough to hinder practical diagnostics.

The finite and boundary element modeling experiments were conducted in order to solve the forward EEG problem numerically ([6], [12], [13], [14], [35], [42]). In these

4

experiments, the three-shell model was used in order to measure the accuracy of the numerical computations. It was found in [35] and [42] that there was a substantial (10-20 %) increase in the error if the dipole got closer to the skull.

The Finite Volume Method (FVM) seems to be the most acceptable way of solving the EEG problem since it allows to take into account the real structure of the human brain, skull and scalp. In order to put it into practice, one must have a three-dimensional map of the human brain of the particular patient. This practical problem of brain mapping by MRI (Magnetic Resonance Imaging) datasets was solved by Koles at al. in [45]. The FVM for three-shell spherical model was done in [5]. However, this implementation does not allow to model the realistic head based on MRI slices with such an approach.

The inverse EEG problem is a well-developed procedure, whereas the forward EEG problem has many aspects that still need thorough study. The source localization given the solution of the forward problem was studied in Koles et al. [2], Mosher et al. [34], as well as Raz et al. [7]. Mosher et al. [34] suggested the *MUSIC* algorithm which localizes several dipoles given the value of potential in a limited number of locations on the head surface. Prior to the *MUSIC* algorithm, spatio-temporal decomposition had to be applied to the data from EEG electrode recordings. The theoretical considerations, implementation and experimental results of this were given in Koles et al. [2]. Besides *MUSIC*, a Frequency Domain Estimation algorithm which does not require spatio-temporal decomposition was developed in [7].

1.4 Objectives of this Research.

1) To accelerate the numerical solution of the forward problem in a realistic head model.

The issue of computational speed is very important, as one needs systems of the order of millions of finite volume elements in order to get the accepted accuracy for source localization.

2) To assess the errors involved in the numerical solution of the forward problem by comparison to the analytical solution of the problem for the spherical head model.

Hence the FVM solution for the three-shell spherical model should be compared with the analytical solution. In the three-shell analytical model one assumes that the distance between a source and a sink is infinitely small, although in reality there is a finite distance (of the order of a few millimeters). Furthermore, the implementation of the FVM brings in a technical obstacle - it is not possible to place both the source and the sink into the same finite volume element. In such a case, the forward problem will have a zero right-hand side. Therefore it would be convenient to have a three-shell model with a finite distance between positive and negative sources of electric current for comparison. Such a model must also be compared with the previous one.

3) To look at alternatives to the numerical approach.

For practical source localization, the iterative methods, even accelerated, are too slow. Linear systems of the order of millions by millions have to be solved for each candidate dipole location and all possible orientations - might be thousands of times. Hence it is worth finding at least some alternative ways of solving the forward problem by FVM. For example, it would be interesting to consider the forward problem for some "good" geometry - a chain, plate or cube consisting of smaller cubes - and see whether the resulting linear system allows the analytical inversion of the matrix rather than the numerical inversion.

2 Background Review.

2.1 Three-shell Spherical Model.

For most of the practical applications so far the forward problem of EEG has been studied with the three-shell spherical head model. The human head is approximated by a sphere surrounded by two concentric spherical shells. The inside sphere corresponds to the brain, the outside shells represent the skull and scalp. With such an approach it is possible to write the analytical solutions for the potential on the surface of the three-layer sphere. The three-shell model is important as it allows one to estimate the errors of the numerical methods if applied to the three-shell geometry.

First, let us consider the point source of the electric current in an infinite homogeneous medium. The potential generated by such a source can be found in a similar way to the potential generated by a single electric charge placed into such a medium. The problem may be stated as follows: given a point source with intensity $I = \frac{dq}{dt}$, find the potential on the surface of the surrounding sphere of radius r. The density $\vec{J}$ of the current through the element of the surface dS will be

$$\vec{J} = Idt\frac{ds}{4\pi r^2}/(dtds) = \frac{I}{4\pi r^2}\frac{\vec{r}}{\|\vec{r}\|}.$$

Since $\vec{J} = \sigma\vec{E}$,

$$\vec{E} = \frac{I}{4\pi\sigma r^2}\frac{\vec{r}}{\|\vec{r}\|},$$

where $\vec{r}$ is a radius-vector which points from the origin to the point on the surface of the sphere with radius r, σ is the conductivity of the medium. Since $\nabla\Psi = -\vec{E}$, integration in one direction gives

$$\Psi = \frac{I}{4\pi\sigma r}. \tag{2.1.1}$$

Now this result will be used in order to obtain the potential of the dipole in the same media. Consider the source and the sink of the same intensity I located at a distance d

7

from each other in order to find the potential on the surface of the sphere that contains the dipole.

First assume that the dipole is oriented radially, i.e. both the source and the sink will be on the line drawn from the center of the sphere of radius R in the radial direction (see Fig. 1). Such a dipole is called radial in EEG literature. b is the distance between the center of the dipole and the center of the sphere, Θ is the latitude. Consider a point P on the surface of the sphere, r is the distance between the dipole and the point. The ratio $\frac{1}{r}$ can be represented as Legendre polynomial expansion ([36], [11]),

$$\frac{1}{r} = \sum_{l=0}^{\infty} \frac{b^l}{R^l} P_l(\cos\Theta). \tag{2.1.2}$$

Here $P_l \equiv P_l^0$ are Legendre polynomials [11, 36] given by Generalized Rodrigues formula,

$$P_l(x) = \frac{1}{2^l l!} \frac{d^l}{dx^l} (x^2 - 1)^l. \tag{2.1.3}$$

By (2.1.1) and (2.1.2), the potential at point P is

$$\Psi = \frac{I}{4\pi\sigma} \sum_{l=0}^{\infty} \left[\frac{(b + \frac{d}{2})^l}{R^{l+1}} - \frac{(b - \frac{d}{2})^l}{R^{l+1}} \right] P_l(\cos\Theta)$$

$$\approx \frac{I}{4\pi\sigma} \sum_{l=0}^{\infty} \frac{b^{l-1} l d}{R^{l+1}} P_l(\cos\Theta) = \frac{m_r}{4\pi\sigma b^2} \sum_{l=1}^{\infty} l \left(\frac{b}{R} \right)^{l+1} l P_l(\cos\Theta), \tag{2.1.4}$$

where $m_r = Id$ is the radial component of the dipole.

8

Figure 1: Radial Dipole.
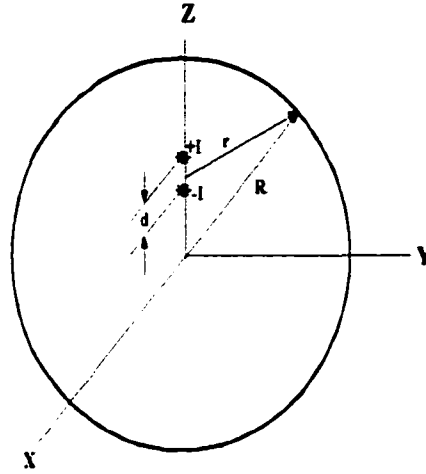
If a line connecting the source and the sink is perpendicular to the radius, then the dipole is called tangential. The dipole of arbitrary orientation can be considered as a vector sum of radial and tangential dipoles. Consider now the dipole which has only a tangential component in the infinite media of conductivity σ. Now $m_t = Id$ is in direction X, and the angles Θ_1 and Θ_2, by Figure 3, are

$$\Theta_1 = \Theta + \frac{d\Theta}{2},$$
$$\Theta_2 = \Theta - \frac{d\Theta}{2},$$

where

$$d\Theta \approx \frac{d\cos\beta}{b}.$$

The potential of the tangential combination of source and sink is

$$\Psi = \sum_{l=1}^{\infty}\left(b + \frac{d}{2}\right)^l \frac{I}{4\pi\sigma R^{l+1}} P_l\left(\cos\left(\Theta + \frac{d\Theta}{2}\right)\right)$$
$$- \sum_{l=0}^{\infty}\left(b + \frac{d}{2}\right)^l \frac{I}{4\pi\sigma R^{l+1}} P_l\left(\cos\left(\Theta - \frac{d\Theta}{2}\right)\right)$$

9

$$= \sum_{l=1}^{\infty} \frac{b^l I}{4\pi\sigma R^{l+1}} \left(P_l \left(\cos(\Theta + \frac{d\Theta}{2}) \right) \right) - P_l \left(\cos\left(\Theta - \frac{d\Theta}{2} \right) \right),$$

using the fact that $P_0(x) \equiv 1$.

$$\Psi = \sum_{l=1}^{\infty} \frac{b^l I}{4\pi\sigma R^{l+1}} \frac{d\cos\beta}{b} \left\{ \frac{P_l \left(\cos(\Theta + \frac{d\Theta}{2}) \right) - P_l \left(\cos(\Theta - \frac{d\Theta}{2}) \right)}{d\Theta} \right\}$$

$$= \sum_{l=1}^{\infty} \frac{b^{l-1} m_t}{4\pi\sigma R^{l+1}} \frac{dP_l(\cos\Theta)}{d\Theta} \cos\beta = - \sum_{l=1}^{\infty} \frac{b^{l-1} m_t}{4\pi\sigma R^{l+1}} P_l^1(\cos\Theta) \cos\beta. \qquad (2.1.5)$$

Here $P_l^1(\cos\Theta)$ is the associated Legendre polynomial ([11], [36])

$$P_l^1(x) = (1 - x^2)^{\frac{1}{2}} \frac{d}{dx} P_l^1(x).$$

If $x = \cos\Theta$, then

$$P_l^1(\cos\Theta) = (1 - \cos^2\Theta)^{\frac{1}{2}} \frac{d}{d\cos\Theta} P_l(\cos\Theta)$$

$$-\frac{\sin\Theta}{\sin\Theta} \frac{dP_l(\cos\Theta)}{d\Theta} = \frac{dP_l(\cos\Theta)}{d\Theta}.$$

Next consider conducting sphere of radius R and conductivity σ surrounded by an air of zero conductivity and find the potential generated by the radial dipole on the surface of such a sphere. It can be written as a solution of Laplace's equation, a function of two spherical coordinates r and Θ with unknown coefficients A_l,

$$\Psi(r, \Theta) = \sum_{l=0}^{\infty} \left[A_l r^l + \frac{m_r}{4\pi\sigma b^2} l \left(\frac{b}{r} \right)^{l+1} \right] P_l(\cos\Theta). \qquad (2.1.6)$$

There is no current through the boundary of the sphere, therefore the boundary condition

$$\left. \frac{\partial\Psi}{\partial r} \right|_{r=R} = 0 \qquad (2.1.7)$$

gives

$$A_l = \frac{b^{l-1}(l + 1)}{4\pi\sigma R^{2l+1}},$$

10

the expression for the potential on the surface of the sphere is

$$\Psi = \sum_{l=1}^{\infty} \frac{(2l+1)m_r}{4\pi\sigma} \frac{b^{l-1}}{R^{l+1}} P_l(\cos\Theta).$$ (2.1.8)

The solution of the three-shell model can be obtained in a similar way by matching the solutions for each shell through boundary conditions. The three-shell idealistic head is shown on Fig. 2. The potentials Ψ_1 for the inside brain, Ψ_2 for the skull, Ψ_3 for the scalp and Ψ_4 for the space outside the three-layer system can be written out as follows:

$$\Psi_1 = \sum_{l=0}^{\infty} \left[A_l r^l + \frac{m_r}{4\pi\sigma_1 b^2} l \left(\frac{b}{r}\right)^{l+1} \right] P_l(\cos\Theta),$$

$$\Psi_2 = \sum_{l=0}^{\infty} \left[C_l r^l + D_l r^{-(l+1)} \right] P_l(\cos\Theta),$$ (2.1.9)

$$\Psi_3 = \sum_{l=0}^{\infty} \left[E_l r^l + F_l r^{-(l+1)} \right] P_l(\cos\Theta).$$

Obviously it can be assumed that the potential of the surrounding air is zero, therefore

$$\Psi_4 = 0.$$

The conductivities of the brain tissue and the scalp can be assumed to be equal, $\sigma_1 = \sigma_3 = \sigma$, and the conductivity of the skull is σ_s. Then the coefficients in (2.1.9) can be obtained from the boundary conditions due to the continuity of radial and tangential components of the current through the boundary,

$$\sigma \frac{\partial \Psi_1}{\partial r}\bigg|_{r=r_1} = \sigma_s \frac{\partial \Psi_2}{\partial r}\bigg|_{r=r_1}, \quad \sigma_s \frac{\partial \Psi_2}{\partial r}\bigg|_{r=r_2} = \sigma \frac{\partial \Psi_3}{\partial r}\bigg|_{r=r_2},$$ (2.1.10)

$$\frac{\partial \Psi_3}{\partial r}\bigg|_{r=R} = 0,$$

$$\frac{\partial \Psi_1}{\partial \Theta}\bigg|_{r=r_1} = \frac{\partial \Psi_2}{\partial \Theta}\bigg|_{r=r_1}, \frac{\partial \Psi_2}{\partial \Theta}\bigg|_{r=r_2} = \frac{\partial \Psi_3}{\partial \Theta}\bigg|_{r=r_2}.$$ (2.1.11)

11

Figure 2: Three-layer Spherical Head Model.

Inside brain, σ

Skull, σ_S

Scalp, σ
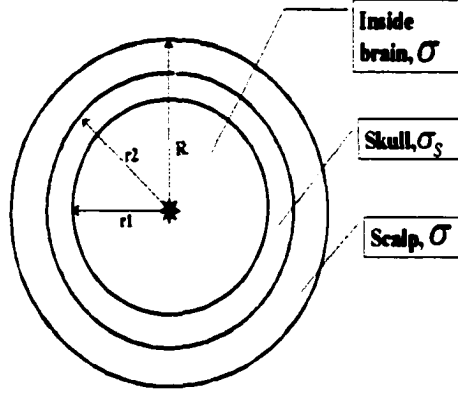
The first three equations due to the boundary conditions (2.1.10) are

$$\sigma\left\{A_l l r_1^{l-1} - \frac{m_r}{4\pi\sigma}b^{l-1}\frac{l(l+1)}{r_1^{l+2}}\right\} = \sigma_S\left\{C_l l r_1^{l-1} - D_l\frac{(l+1)}{r_1^{l+2}}\right\} \tag{2.1.12}$$

$$\sigma_S\left\{C_l l r_2^{l-1} - D_l\frac{(l+1)}{r_2^{l+2}}\right\} = \sigma\left\{E_l l r_2^{l-1} - F_l\frac{(l+1)}{r_2^{l+2}}\right\} \tag{2.1.13}$$

$$E_l l R^{l-1} - F_l\frac{(l+1)}{R^{l+2}} = 0. \tag{2.1.14}$$

Denote $\xi = \frac{\sigma_S}{\sigma}$, than these equations can be more conveniently written as

$$A_l - \frac{m_r(l+1)}{4\pi\sigma}\frac{b^{l-1}}{r_1^{2l+1}} = \xi C_l - \xi D_l\frac{(l+1)}{l r_1^{2l+1}} \tag{2.1.15}$$

$$\xi C_l - \xi D_l\frac{(l+1)}{l r_2^{2l+1}} = E_l - F_l\frac{(l+1)}{l r_2^{2l+1}} \tag{2.1.16}$$

$$E_l = F_l\frac{(l+1)}{l R^{2l+1}}. \tag{2.1.17}$$

The other two equations due to the boundary condition (2.1.11) are

$$A_l r_1^l + \frac{m_r}{4\pi\sigma b^2}l\left(\frac{b}{r_1}\right)^{l+1} = C_l r_1^l + \frac{D_l}{r_1^{l+1}} \tag{2.1.18}$$

$$C_l r_2^l + \frac{D_l}{r_2^{l+1}} = E_l r_2^l + \frac{F_l}{r_2^{l+1}}. \tag{2.1.19}$$

12

Furthermore, equations (2.1.16) and (2.1.19) can be written as

$$C_l + \frac{D_l}{r_2^{2l+1}} = \frac{K_1 F_l}{r_2^l} \tag{2.1.20}$$

$$C_l - \frac{D_l(l+1)}{lr_2^{2l+1}} = \frac{K_1 F_l}{\xi}, \tag{2.1.21}$$

where

$$K_1 = \frac{(l+1)r_2^l}{lR^{2l+1}} + \frac{1}{r_2^{2l+1}}, \tag{2.1.22}$$

$$K_2 = \frac{(l+1)}{l}\left(\frac{1}{R^{2l+1}} - \frac{1}{r_2^{2l+1}}\right). \tag{2.1.23}$$

From equations (2.1.20) and (2.1.21), obtain expressions for D_l and C_l,

$$D_l = \frac{lr_2^{2l+1}}{2l+1}\left\{\frac{K_1 F_l}{r_2^l} - \frac{K_2 F_l}{\xi}\right\}, \tag{2.1.24}$$

$$C_l = \frac{D_l(l+1)}{lr_2^{2l+1}} + \frac{K_2 F_l}{\xi} = \frac{(l+1)}{(2l+1)}\left\{\frac{K_1 F_l}{r_2^l} - \frac{K_2 F_l}{\xi}\right\} + \frac{K_2 F_l}{\xi}. \tag{2.1.25}$$

It is convenient to write

$$C_l = M_C F_l, \quad \text{where} \quad M_C = \frac{(l+1)}{(2l+1)}\left(\frac{K_1}{r_2^l} - \frac{K_2}{\xi}\right) + \frac{K_2}{\xi}, \tag{2.1.26}$$

$$D_l = M_D F_l, \quad \text{where} \quad M_D = \frac{lr_2^{2l+1}}{2l+1}\left(\frac{K_1}{r_2^l} - \frac{K_2}{\xi}\right). \tag{2.1.27}$$

Writing (2.1.15) and (2.1.18) as

$$A_l - \frac{m_r(l+1)}{4\pi\sigma b^2}\frac{b^{l+1}}{r_1^{2l+1}} = \xi M_C F_l - \xi M_D F_l \frac{(l+1)}{lr_1^{2l+1}}$$

$$A_l + \frac{m_r}{4\pi\sigma b^2}l\frac{b^{l+1}}{r_1^{2l+1}} = M_C F_l + \frac{M_D F_l}{r_1^{2l+1}},$$

and combining these expressions, obtain the expressions for F_l and E_l.

$$F_l = \frac{m_r(2l+1)b^{l-1}}{4\pi\sigma}\frac{1}{M_C r_1^{2l+1}(1-\xi) + M_D\left(1 + \frac{\xi(l+1)}{l}\right)} \tag{2.1.28}$$

$$E_l = \frac{m_r(l+1)}{lR^{2l+1}}\frac{(2l+1)b^{l-1}}{4\pi\sigma}\frac{1}{M_C r_1^{2l+1}(1-\xi) + M_D\left(1 + \frac{\xi(l+1)}{l}\right)}. \tag{2.1.29}$$

13

Hence the potential on the surface of the sphere will be

$$\Psi = \sum_{l=0}^{\infty} \left\{ E_l R^l + \frac{F_l}{R^{l+1}} \right\} P_l(\cos\Theta) =$$

$$\sum_{l=0}^{\infty} \frac{m_r b^{l-1}(2l+1)^2}{4\pi\sigma R^{l+1} l} \frac{1}{M_C r_1^{2l+1}(1-\xi) + M_D\left(1 + \frac{\xi(l+1)}{l}\right)} P_l(\cos\Theta). \qquad (2.1.30)$$

Writing out the denominator in the last expression, $f_1 = \frac{r_1}{R}$, $f_2 = \frac{r_2}{R}$

$$M_C r_1^{2l+1}(1-\xi) + M_D\left(1 + \frac{\xi(l+1)}{l}\right) = \left(\frac{r_1}{R}\right)^{2l+1}(1-\xi)\frac{(l+1)}{(2l+1)}\left(\frac{\xi(l+1)+l}{l\xi}\right)$$

$$+ \frac{(l+1)}{(2l+1)}\left(1 - \frac{1}{\xi}\right)\left(\frac{r_1}{r_2}\right)^{2l+1}(1-\xi) + \frac{(l+1)}{(2l+1)}\left(\frac{r_2}{R}\right)^{2l+1}\left(1 - \frac{1}{\xi}\right)\left(1 + \frac{\xi(l+1)}{l}\right)$$

$$+ \frac{\xi l + (l+1)}{\xi(2l+1)}\left(1 + \frac{\xi(l+1)}{l}\right)$$

$$= \frac{(l+1)}{\xi l(2l+1)}\left\{ f_1^{2l+1}(1-\xi)\frac{\xi(l+1)+l}{l} + (\xi-1)\left(\frac{f_1}{f_2}\right)^{2l+1}(1-\xi)l \right.$$

$$\left. + f_2^{2l+1}(\xi-1)(\xi(l+1)+l) + \left(\frac{\xi l}{l+1} + 1\right)(\xi(l+1)+l) \right\}.$$

Finally

$$\Psi = \frac{1}{4\pi\sigma} \sum_{l=0}^{\infty} \frac{b^{l-1}}{R^{l+1}} \left[\frac{\xi(2l+1)^3}{d_\xi(l+1)} \right] m_r P_l(\cos\Theta), \qquad (2.1.31)$$

where

$$d_\xi = \left(f_1^{2l+1} + f_2^{2l+1} \right)(1-\xi)(l+\xi(l+1))$$

$$+ l(1-\xi)^2 \left(\frac{f_1}{f_2}\right)^{2l+1} + \left(\frac{\xi l}{l+1} + 1\right)(l+\xi(l+1)). \qquad (2.1.32)$$

Now conduct the similar calculations for tangential dipole. It is shown on Fig. 3. For the uniform conducting sphere of radius R and conductivity σ, the potential inside the sphere will be

$$\Psi = \sum_{l=1}^{\infty} \left(A_l r^l + \frac{m_t b^{l-1}}{4\pi\sigma r^{l+1}} \right) P_l^1(\cos\Theta)\cos\beta. \qquad (2.1.33)$$

Due to the boundary condition

$$\left.\frac{\partial\Psi}{\partial r}\right|_{r=R} = 0, \qquad (2.1.34)$$

14

$$A_l = \frac{l+1}{l} \frac{m_t}{4\pi\sigma R^{2l+1}}.$$

Therefore,

$$\Psi = \sum_{l=1}^{\infty} \frac{m_t}{4\pi\sigma} \frac{2l+1}{l} \frac{b^{l-1}}{R^{2l+1}} P_l^1(\cos\Theta)\cos\beta. \tag{2.1.35}$$

Hence for the three-shell model, the potentials Ψ_1, Ψ_2, Ψ_3 and Ψ_4 can be described by equations

$$
\begin{aligned}
\Psi_1 &= \sum_{l=1}^{\infty} \left[A_l r^l + \frac{m_t}{4\pi\sigma b^2} \left(\frac{b}{r}\right)^{l+1} \right] P_l^1(\cos\Theta)\cos\beta, \\
\Psi_2 &= \sum_{l=1}^{\infty} \left[C_l r^l + D_l r^{-(l+1)} \right] P_l^1(\cos\Theta)\cos\beta, \\
\Psi_3 &= \sum_{l=1}^{\infty} \left[E_l r^l + F_l r^{-(l+1)} \right] P_l^1(\cos\Theta)\cos\beta.
\end{aligned}
\tag{2.1.36}
$$

The boundary conditions are the same therefore the equations due to these boundary conditions will be the same, except (2.1.12) and (2.1.18),

$$\sigma\left\{ A_l l r_1^{l-1} - \frac{m_t}{4\pi\sigma b^2} b^{l+1} \frac{(l+1)}{r_1^{l+2}} \right\} = \sigma_S \left\{ C_l l r_1^{l-1} - D_l \frac{(l+1)}{r_1^{l+2}}, \right\} \tag{2.1.37}$$

$$A_l r_1^l + \frac{m_t}{4\pi\sigma b^2} \left(\frac{b}{r_1}\right)^{l+1} = C_l r_1^l + \frac{D_l}{r_1^{l+1}}. \tag{2.1.38}$$

Again the above two equations can be more conveniently written as

$$A_l - \frac{m_t b^{l+1}(l+1)}{4\pi\sigma l r_1^{2l+1}} = \xi C_l - \xi \frac{D_l(l+1)}{r_1^{2l+1} l}, \tag{2.1.39}$$

$$A_l + \frac{m_t b^{l-1}}{4\pi\sigma l r_1^{2l+1}} = C_l + \frac{D_l}{r_1^{2l+1}}. \tag{2.1.40}$$

As before

$$C_l = M_C F_l,$$

$$D_l = M_D F_l,$$

where M_C and M_D are defined by the formulas (2.1.26) and (2.1.27). The expressions for coefficients K_1 and K_2 in these formulas also remain the same.

15

Thus

$$A_l - \frac{m_t b^{l+1}(l+1)}{4\pi\sigma l r_1^{2l+1}} = \xi M_C F_l - \xi \frac{M_D F_l(l+1)}{r_1^{2l+1}l},$$

$$A_l + \frac{m_t b^{l-1}}{4\pi\sigma l r_1^{2l+1}} = M_C F_l + \frac{M_D F_l}{r_1^{2l+1}},$$

and the new formulas for F_l and E_l will be

$$F_l = \frac{m_t(2l+1)b^{l-1}}{4\pi\sigma l r_1^{2l+1}} \frac{1}{M_C r_1^{2l+1}(1-\xi) + M_D\left(1 + \frac{\xi(l+1)}{l}\right)}, \qquad (2.1.41)$$

$$E_l = \frac{m_t(l+1)}{l^2 R^{2l+1}} \frac{(2l+1)b^{l-1}}{4\pi\sigma} \frac{1}{M_C r_1^{2l+1}(1-\xi) + M_D\left(1 + \frac{\xi(l+1)}{l}\right)}. \qquad (2.1.42)$$

The potential on the surface of the three-shell sphere due to the tangential dipole will be

$$\Psi_3 = \sum_{l=1}^{\infty}\left[E_l r^l + F_l r^{-(l+1)}\right] P_l^1(\cos\Theta)\cos\beta$$

$$= \sum_{l=1}^{\infty} \frac{m_t b^{l-1}}{4\pi\sigma R^{l+1}} \frac{\xi(2l+1)^3}{l(l+1)d_\xi} P_l^1(\cos\Theta)\cos\beta. \qquad (2.1.43)$$

Finally the following expression describes the potential on the surface of the three-shell sphere of radius R

$$V(\Theta,\beta) = \frac{1}{4\pi\sigma_1} \sum_{l=1}^{\infty} \frac{b^{l-1}}{R^{l+1}}\left[\frac{\xi_2(2l+1)^3}{d_{\xi_1\xi_2}l(l+1)}\right](lm_r P_l(\cos\Theta) - m_t P_l^1(\cos\Theta)\cos\beta). \quad (2.1.44)$$

Of course the tangential component of the dipole does not necessary need to be oriented in direction X. If it has a component in direction Y as well, then by the appropriate rotation of the coordinates the problem can be reduced to the one described above. In the case of multiple dipoles, the forward problem is a superposition of the solutions for each dipole.

The three-shell model cannot adequately describe the complexity of the realistic head. Therefore the numerical models as well as advanced brain mapping techniques are needed in order to make the source localization procedures applicable for clinical purposes.

16

2.2 Finite and Boundary Element Methods.

The Boundary Element (BEM) and Finite Element (FEM) Methods are already widely used in literature ([6], [12], [13],[14]) for the solution of the forward problem. For the sake of consistency a brief overview of these methods will be given in this work, although the Finite Volume Method will be used for practical computations.

With BEM the governing differential equations are transferred into equivalent boundary integral equations which contain no volume integrals. This is done by using certain well known integral identities. Among them are:

1) Gauss-Green Theorem

$$\int_V \frac{\partial f}{\partial x} dV = \int_V f n_x dS, \qquad (2.2.1)$$

where n_x is the x-component of the unit normal $\vec{n}$ to the boundary surface S of the domain V;

2) Divergence Theorem,

$$\int_V (\nabla \cdot \mathbf{f}) \, dV = \int_S (\mathbf{f} \cdot \mathbf{n}) dS, \qquad (2.2.2)$$

where $\mathbf{f}$ is defined on the domain V;

3) Green's First Identity

$$\int_V (\nabla a \cdot \nabla b + b \Delta a) dV = \int_S (b \nabla a \cdot n) dS \qquad (2.2.3)$$

4) Green's Secon$\int_V (b\Delta a - a\Delta b) dV = \int_S (b\nabla a - a\nabla b) \cdot \vec{n} dS,$

$$\int_V (b\Delta a - a\Delta b) dV = \int_S (b\nabla a - a\nabla b) \cdot \vec{n} dS, \qquad (2.2.4)$$

where a and b are scalar functions.

Sometimes depending on the partial differential equation the transformation to the boundary integral equation involves certain known solutions, usually called the fundamental solutions to the original differential equation. The boundary of the 3D volume is

17

Figure 3: Tangential Dipole.

18
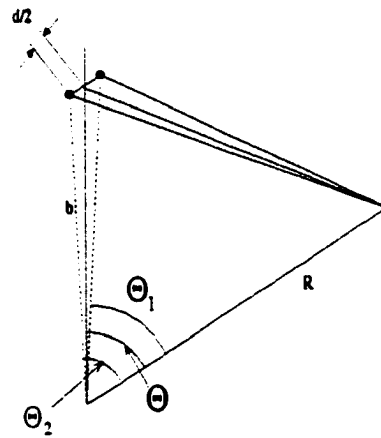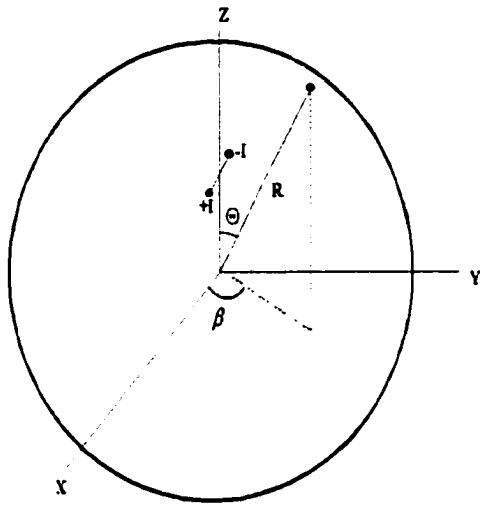
triangularized, the discrete integration is performed over the boundary elements (triangles), which results in a linear system from which the values of the biopotential at any location within the volume can be determined. For further details on BEM, see [37]. The BEM allows to model boundaries and boundary conditions very naturally, it doesn't require grids over the entire volume, surface grids are sufficient. BEM also gives rise to quite sparse matrices.

Unfortunately the BEM sometimes gives rise to very complicated formulations; since it requires integral relation as well as transformation to boundary formulation using the fundamental solutions, it also requires substantial integration of complex functions. For BEM, nonhomogeneity within the domain causes serious errors, and this is exactly the case of the forward problem of the EEG source localization. The matrices obtained by BEM are not usually symmetric.

The Finite Element Method envisions the solution as being built up of many small, interconnected subregions or elements. The basic idea of FEM is that a solution region can be analytically modeled or approximated by replacing it with an assemblage of discrete elements. Since these elements can be put together in a variety of ways, they can be used to represent exceedingly complex shapes.

The boundary value problem for the biopotential Ψ in tri-dimensional domain V bounded by the surface S can be written in the functional form

$$L(\Psi) - f = 0. \tag{2.2.5}$$

We assume that the proper boundary conditions are prescribed in S. The variable Ψ is being approximated by the linear combination of certain functions

$$\Psi \approx \tilde{\Psi} = \sum_{i=1}^{m} N_i C_i,$$

where C_i are the unknown parameters and the N_i are functions such that they satisfy the boundary conditions.

19

Define the residual or error which results from approximating Ψ by $\tilde{\Psi}$ as

$$R = L(\tilde{\Psi}) - f. \tag{2.2.6}$$

The m unknowns C_i are determined in such a way that the error R over the entire solution domain is small. This is accomplished by forming a weighted average of the error and requiring that this weighted average vanishes over the solution domain.

Therefore one chooses m linearly independent weighting functions W_i and then insists that

$$\int_V [L(\tilde{\Psi}) - f] W_i dV = \int_V R W_i dV = 0 \qquad i = 1, 2, ..., m. \tag{2.2.7}$$

There are quite a variety of weighted residual techniques because of the broad choice of weighting functions (see, p.e., Collatz [2]). The choice of the weighting functions is commonly referred to as the error distribution principle. The error distribution principle most often used is known as the Galerkin criterion, or Galerkin's method. According to Galerkin's method, the weighting functions are chosen to be the same as the approximating functions used to represent Ψ, that is, $W_i = N_i$ for $i = 1, 2, ..., m$. Thus Galerkin's method requires that

$$\int_V [L(\tilde{\Psi}) - f] N_i dV = 0, \qquad i = 1, 2, ..., m. \tag{2.2.8}$$

Since (2.2.8) holds for any point in the solution domain, it also holds for any arbitrary subdomain or element of the smaller domain. In practice the functions N_i are defined in a way that they are nonzero only on a certain subdomain $V_i^{(e)}$ of the domain V, the finite element. Hence for each element $V_i^{(e)}$ there is one interpolating function N_i, and C_i are the nodal values of Ψ at the center of each finite element. In the simplest case $N_i = 1$ if they are within $V_i^{(e)}$, and zero everywhere else, although in practice N_i can be defined in other ways. The m equations

$$\int_{V_i^{(e)}} [L(\Psi^{(e)}) - f^{(e)}] N_i^{(e)} dV_i^{(e)} = 0, \qquad i = 1, 2, ...m, \tag{2.2.9}$$

20

will result in the linear system from which the biopotential will be determined at chosen m locations.

The obvious advantage of the Finite Element Method is its natural way of modeling the boundaries and the boundary conditions. FEM does not require structured grids, it can accomodate a broad range of elements of different geometries. Unlike BEM, FEM requires the integration of simple functions only, which leads to quite sparse, usually symmetric matrices. It also allows good enough handling of nonhomogenuities. The technology of FEM is quite mature. Those who want to apply the FEM for practical purposes will have to face certain difficulties however. They will have to generate volume grids, which can be quite arduous in the case of complex geometries. Writing out the discrete relations from the weighted residual formulation may be a rather complicated and tedious matter. The resolution of the response gradient, if needed, will be tied to the volume mesh refinement.

2.3 Finite Volume Method.

In this work the Finite Volume Method (FVM)[1] was applied for the EEG forward problem. For this approach the biological volume conductor is decomposed into smaller finite volume elements. For each element the conservation laws of charge equation

$$\oint \sigma \nabla \Psi \cdot d\vec{S} = I_o$$

is written in the form of finite difference equations. The boundary condition of no current into the surrounding air is $\sigma \frac{\partial \Psi}{\partial n} = 0$, where n is normal to the boundary. The discretization can be done for a generalized curvilinear coordinate system (ξ, η, ζ). The centers of the finite volume elements or cells inside the biological volume conductor are indexed with respect to each curvilinear coordinate as (i, j, k), whereas the eight vertices correspond to $(i \pm \frac{1}{2}, j \pm \frac{1}{2}, k \pm \frac{1}{2})$, and the centers of faces are indexed as $(i \pm \frac{1}{2}, j, k)$, or $(i, j \pm \frac{1}{2}, k)$, or $(i, j, k \pm \frac{1}{2})$. The faces of cells are given by the normal area vectors S^l, where $l = (\xi, \eta, \text{or } \zeta)$. The values of potential $\Psi_{i,j,k}$ are defined at the cell's centers. Each cell is a hexahedron of arbitrary shape. The area vectors, for example $\vec{S}^\xi$ are calculated as

$$\vec{S}^\xi_{i+\frac{1}{2},j,k} = \frac{1}{2}\left((\vec{r}_{j+\frac{1}{2},k+\frac{1}{2}} - \vec{r}_{j-\frac{1}{2},k-\frac{1}{2}}) \times (\vec{r}_{j-\frac{1}{2},k+\frac{1}{2}} - \vec{r}_{j+\frac{1}{2},k-\frac{1}{2}}) \right)_{i+\frac{1}{2}}, \qquad (2.3.1)$$

where $\vec{r}$ is the position vector. The volume of each hexahedron cell is calculated by dividing it into three pyramids, each one having the main diagonal of the hexahedron cell in common

$$V_{i,j,k} = \frac{1}{3}\left(\vec{S}^\xi_{i-\frac{1}{2},j,k} + \vec{S}^\eta_{i,j-\frac{1}{2},k} + \vec{S}^\zeta_{i,j,k-\frac{1}{2}} \right) \cdot \left(\vec{r}_{i+\frac{1}{2},j+\frac{1}{2},k+\frac{1}{2}} - \vec{r}_{i-\frac{1}{2},j-\frac{1}{2},k-\frac{1}{2}} \right). \qquad (2.3.2)$$

22

For each finite volume the integral equation (1.14) is discretized by the second order accuracy scheme

$$
\begin{aligned}
& (\sigma \nabla \Psi \cdot \vec{S}^\xi)_{i+\frac{1}{2},j,k} - (\sigma \nabla \Psi \cdot \vec{S}^\xi)_{i-\frac{1}{2},j,k} \\
+ \quad & (\sigma \nabla \Psi \cdot \vec{S}^\eta)_{i,j+\frac{1}{2},k} - (\sigma \nabla \Psi \cdot \vec{S}^\eta)_{i,j-\frac{1}{2},k} \\
+ \quad & (\sigma \nabla \Psi \cdot \vec{S}^\zeta)_{i,j,k+\frac{1}{2}} - (\sigma \nabla \Psi \cdot \vec{S}^\zeta)_{i,j,k-\frac{1}{2}} = I_0.
\end{aligned}
\tag{2.3.3}
$$

Each term on the left-hand side represents the current flow through the relevant face, while the right-hand side equals the total current volume source in the cell. The gradient for each primary cell is calculated from the integral definition

$$
\nabla \Psi = \frac{1}{V} \int_S \Psi d\vec{S}.
\tag{2.3.4}
$$

Such a definition has advantages over the differential form, as it imposes fewer restrictions on the smoothness of the mesh than the finite difference approximation based on the differential form of the equation. Discretization yields

$$
\nabla \Psi = \frac{1}{V} \sum_l \Psi_l \vec{S}^l,
\tag{2.3.5}
$$

where l denotes the face of the secondary cell and Ψ_l is the potential at the corresponding centers of the face. For example the approximation for the $(i+1,j,k)$ face of the hexahedron is

$$
\begin{aligned}
(V\nabla \Psi)_{i+\frac{1}{2},j,k} = \quad & (\Psi S^\xi)_{i+1,j,k} - (\Psi S^\xi)_{i,j,k} \\
+ & \left((\Psi S^\eta)_{j+\frac{1}{2}} - (\Psi S^\eta)_{j-\frac{1}{2}} \right)_{i+\frac{1}{2},k} \\
+ & \left((\Psi S^\zeta)_{k+\frac{1}{2}} - (\Psi S^\zeta)_{k-\frac{1}{2}} \right)_{i+\frac{1}{2},j}.
\end{aligned}
\tag{2.3.6}
$$

23

The corresponding flow term in (2.3.3) will be

$$
(\sigma \nabla \Psi \cdot S^{\xi})_{i+\frac{1}{2},j,k} = \left(\frac{\sigma}{V}\right)_{i+\frac{1}{2},j,k} \times \left((\Psi S^{\xi})_{i+1,j,k} - (\Psi S^{\xi})_{i,j,k} \right.
$$

$$
+ \left((\Psi S^{\eta})_{j+\frac{1}{2}} - (\Psi S^{\eta})_{j-\frac{1}{2}} \right)_{i+\frac{1}{2},k} \qquad (2.3.7)
$$

$$
+ \left. \left((\Psi S^{\zeta})_{k+\frac{1}{2}} - (\Psi S^{\zeta})_{k-\frac{1}{2}} \right)_{i+\frac{1}{2},j} \right) \times S^{\xi}_{i+\frac{1}{2},j,k}.
$$

Similar expressions can be applied for the calculation of fluxes through the other faces. Finally one has to work with a discrete equation involving the potential $\Psi_{i,j,k}$ in the center of the cell under consideration and the potentials at 18 neighboring points, with coefficients dependent on the geometry and conductivity only. The conductivities of the neighboring hexahedrons may vary, hence one has to take into account the abrupt changes in conductivities.

In such a case for the face indexed as $(i + \frac{1}{2}, j, k)$, the effective conductivity can be defined as

$$
\left(\frac{\sigma}{V}\right)_{\text{eff}} = \frac{2\left(\frac{\sigma}{V}\right)_{i,j,k}\left(\frac{\sigma}{V}\right)_{i+1,j,k}}{\left(\frac{\sigma}{V}\right)_{i,j,k} + \left(\frac{\sigma}{V}\right)_{i+1,j,k}}. \qquad (2.3.8)
$$

$\left(\frac{\sigma}{V}\right)_{\text{eff}}$ must be used instead of $\left(\frac{\sigma}{V}\right)_{i+\frac{1}{2},j,k}$ in the formula (2.3.7). It is easy to see that if $\sigma_{i,j,k} = \sigma_{i+1,j,k}$ and $V_{i,j,k} = V_{i+1,j,k}$, then $\left(\frac{\sigma}{V}\right)_{\text{eff}} = \left(\frac{\sigma}{V}\right)_{i+1,j,k}$ and $\left(\frac{\sigma}{V}\right)_{\text{eff}} = \left(\frac{\sigma}{V}\right)_{i,j,k}$. Otherwise if $\sigma_{i+1,j,k}$ differs from $\sigma_{i,j,k}$, then $\left(\frac{\sigma}{V}\right)_{\text{eff}}$ gives some intermediate value between $\left(\frac{\sigma}{V}\right)_{i,j,k}$ and $\left(\frac{\sigma}{V}\right)_{i+1,j,k}$ for $\left(\frac{\sigma}{V}\right)_{i+\frac{1}{2},j,k}$. Without effective conductivity the resulting distribution of the potential may be distorted. This formula can be trivially generalized for the fluxes through the other faces.

The FVM described here is a particular case of the FEM. In order to see this consider

24

the Method of Weighted Residuals. Recall that for this method

$$\int_{\mathcal{D}} [\mathcal{L}(\tilde{\Phi}) - f] W_i d\mathcal{D} = \int_{\mathcal{D}} \mathcal{R} W_i d\mathcal{D} = 0 \quad i = 1, \ldots, m,$$

where $\tilde{\Phi} = \sum_{i=1}^{m} C_i N_i$ is an approximation to the solution of the differential equation $\mathcal{L}(\Phi) - f = 0$;

$\mathcal{R} = \mathcal{L}(\tilde{\Phi}) - f$ is the residual,

$\mathcal{D}$ is the three-dimensional domain bounded by the surface Σ.

Suppose that V_i are three-dimensional finite elements obtained as a result of decomposition of the domain $\mathcal{D}$. Require N_i to be

$$N_i = \begin{cases} 1, & (x, y, z) \in V_i \\ 0, & \text{otherwise.} \end{cases} \tag{2.3.9}$$

The Galerkin Method requires that $W_i = N_i$, so

$$\int_{\mathcal{D}} [\mathcal{L}(\tilde{\Phi}) - f] N_i d\mathcal{D} = \int_{V_i} [\mathcal{L}(\tilde{\Phi}) - f] dV_i = 0,$$

hence there are m equations, one for each finite element. If

$$\mathcal{L}(\Psi) = \nabla \cdot \sigma \nabla \Psi, \quad f = -\nabla \cdot \vec{j}, \text{where} \vec{j} = -\sigma \nabla \Psi,$$

then by the Divergence Theorem

$$\int_{V_i} (\nabla \cdot \sigma \nabla \Psi) dV_i = \oint_{S_i} \sigma \nabla \Psi \cdot d\vec{S_i} \tag{2.3.10}$$

where S_i is a surface of three-dimensional finite element V_i. For the right-hand side

$$-\int_{V_i} \nabla \cdot \vec{j} dV_i = -\oint_{S_i} \vec{j} d\vec{S_i} = -I_0,$$

where I_0 is the charge emitted by the point source into a unit volume for the unit time. Since the FVM is a particular case of Galerkin FEM, the matrices for the FVM will be symmetric and as sparse as those resulting from FEM formulation. Due to effective

25

conductivity $\left(\frac{\sigma}{\mathcal{V}}\right)_{\text{eff}}$, the non-diagonal elements of the resulting matrix differ less, hence the condition number of that matrix decreases. Unlike [5], the implementation of FVM which will be presented further in this work does not require any singularities, i.e. the hexahedrons that have a common boundary with more then 6 neighboring hexahedrons, which can worsen the conditioning of the matrix. Futhermore the question of deflation of the resulting linear system was not studied in [5], but is discussed in this work.

26

2.4 Conjugate Gradient Method.

The Conjugate Gradient Method (CGM) [43, 37, 40, 31] was first introduced by Hestenes and Steiffel in 1952. Combined with preconditioning strategies it remains one of the most efficient iterative methods of solving the linear systems $A\mathbf{x} = \mathbf{b}$, where A is Hermitian positive definite matrix (hpd), $A \in M_{n,n}(\mathbf{C})$. The basic idea of the conjugate directions as a whole is to represent the solution $\mathbf{x}$ as a linear combination of vectors $\mathbf{p}_1, ..., \mathbf{p}_n$ orthogonal in the metric called A-norm,

$$(A\mathbf{p}_i, \mathbf{p}_j) = \delta_{ij}. \tag{2.4.1}$$

The solution can be written out as

$$\mathbf{x} = \mathbf{x}_0 + \sum_{i=1}^{n} a_i \mathbf{p}_i. \tag{2.4.2}$$

The coefficients a_i can be written out explicitly due to the A-orthogonality of $\mathbf{p}_i$. Multiplying (2.4.2) by A,

$$A \sum_{i=1}^{n} a_i \mathbf{p}_i = \mathbf{b} - A\mathbf{x}_0 = \mathbf{r}_0,$$

$$a_i = \frac{(\mathbf{r}_0, \mathbf{p}_i)}{(A\mathbf{p}_i, \mathbf{p}_i)}. \tag{2.4.3}$$

In practice there is no need to compute all the vectors $\mathbf{p}_i$ and all the coefficients a_i. Only the approximate solution $\mathbf{x}_i$ is computed, it can be represented as a last element in the sequence of the successive approximations to the solution

$$\mathbf{x}_0, \mathbf{x}_1, ..., \mathbf{x}_i,$$

where $\mathbf{x}_0$ is an initial vector,

$$\mathbf{x}_i = \mathbf{x}_0 + \sum_{k=1}^{i} a_k \mathbf{p}_k = \mathbf{x}_{i-1} + a_i \mathbf{p}_i. \tag{2.4.4}$$

27

For each successive approximation, the corresponding residuals $r_0, r_1, ...$ are computed

$$r_0 = b - Ax_0 \qquad (2.4.5)$$

$$r_i = b - Ax_i = b - Ax_{i-1} - a_i Ap_i = r_{i-1} - a_i Ap_i. \qquad (2.4.6)$$

The approximation x_i is best in the sense that of all vectors of the form $u = x_0 + v, \quad v \in$ span$\{p_1, ..., p_i\}$, the generalized error function $f_A(u) = (A(x - u), (x - u))$, where x is the exact solution, will take its least value for x_i. Indeed consider $u = x_0 + \sum_{k=1}^{i} \beta_k p_k$.

$$f_A(u) = \left(A(\sum_{k=1}^{n} a_k p_k - \sum_{k=1}^{i} \beta_k p_k), (\sum_{k=1}^{n} a_k p_k - \sum_{k=1}^{i} \beta_k p_k) \right) =$$

$$\sum_{k=1}^{i} (a_k - \beta_k)^2 (Ap_k, p_k) + \sum_{k=i+1}^{n} a_k^2 (Ap_k, p_k) \geq \sum_{k=i+1}^{n} a_k^2 (Ap_k, p_k),$$

the equality can be attained only for $a_k = \beta_k$. Therefore the generalized error function decreases with increasing index i. The two lemmas below summarize the properties of the direction vectors p_i.

Lemma 1.

$$(r_i, p_j) = 0, \qquad (j = 1, ..., i). \qquad (2.4.7)$$

Proof.

$$r_i = b - Ax_i = A(x - x_i) = \sum_{k=i+1}^{n} \frac{(r_0, p_k)}{(Ap_k, p_k)} Ap_k.$$

Hence $(r_i, p_j) = 0$ if $j < i + 1$. $\qquad \qquad \square$

Lemma 2.

$$(r_i, p_j) = (r_0, p_j), \qquad (i = 1, ..., j - 1). \qquad (2.4.8)$$

Proof.

$$(r_i, p_j) = \frac{(r_0, p_j)}{(Ap_j, p_j)} (Ap_j, p_j) = (r_0, p_j).$$

$\qquad \qquad \square$

28

The direction vectors $\mathbf{p}_1, ..., \mathbf{p}_{k+1}$ are constructed successively together with the residuals $\mathbf{r}_0, ..., \mathbf{r}_i$,

$$\mathbf{p}_{i+1} = \mathbf{r}_i - b_i \mathbf{p}_i, \tag{2.4.9}$$

$$b_i = \frac{(\mathbf{r}_i, A\mathbf{p}_i)}{(\mathbf{p}_i, A\mathbf{p}_i)}. \tag{2.4.10}$$

The residuals $\mathbf{r}_0, ..., \mathbf{r}_i$ are mutually orthogonal. In order to see this, consider $(\mathbf{r}_i, \mathbf{r}_j)$, where $i > j$. By (2.4.9),

$$\mathbf{r}_i = \mathbf{p}_{i+1} - b_i \mathbf{p}_i$$

Therefore

$$(\mathbf{r}_i, \mathbf{r}_j) = (\mathbf{p}_{i+1}, \mathbf{r}_j) - b_i(\mathbf{p}_i, \mathbf{r}_j),$$

and both terms are equal to zero by (2.1.13). Each successive vector $\mathbf{p}_{i+1}$ will be A-orthogonal to $\mathbf{p}_1, ..., \mathbf{p}_i$, which are already mutually A-orthogonal.

$$(\mathbf{p}_{i+1}, A\mathbf{p}_i) = (\mathbf{r}_i, A\mathbf{p}_i) - \frac{(\mathbf{r}_i, A\mathbf{p}_i)}{(\mathbf{p}_i, A\mathbf{p}_i)}(\mathbf{p}_i, A\mathbf{p}_i) = 0. \tag{2.4.11}$$

Consider $(\mathbf{p}_{i+1}, A\mathbf{p}_j)$, $j = 1, 2, ..., i - 1$.

$$(\mathbf{p}_{i+1}, A\mathbf{p}_j) = (\mathbf{r}_i, A\mathbf{p}_j) + b_i(\mathbf{p}_i, A\mathbf{p}_j) = (\mathbf{r}_i, A\mathbf{p}_j),$$

by A-orthogonality of $\mathbf{p}_1, ..., \mathbf{p}_i$. Since

$$A\mathbf{p}_j = \frac{1}{a_j}(\mathbf{r}_{j-1} - \mathbf{r}_j),$$

$$(\mathbf{p}_{i+1}, A\mathbf{p}_j) = \frac{1}{a_j}(\mathbf{r}_i, \mathbf{r}_{j-1}) - \frac{1}{a_j}(\mathbf{r}_i, \mathbf{r}_j) = 0, \tag{2.4.12}$$

since $j - 1 < i$, $j < i$. It is also possible to derive the recurrent formula for $\mathbf{r}_i$. By (2.1.14),

$$\mathbf{b} - A\mathbf{x}_i = \mathbf{b} - A\mathbf{x}_{i-1} - a_i A\mathbf{p}_i$$

$$\mathbf{r}_i = \mathbf{r}_{i-1} - a_i A\mathbf{p}_i. \tag{2.4.13}$$

Two more useful lemmas will be proved below.

29

Lemma 3.

$$a_i = \frac{(\mathbf{p}_i, \mathbf{r}_{i-1})}{(\mathbf{p}_i, A\mathbf{p}_i)} = \frac{(\mathbf{r}_{i-1}, \mathbf{r}_{i-1})}{(\mathbf{p}_i, A\mathbf{p}_i)}.$$ (2.4.14)

Proof.

$$(\mathbf{p}_i, \mathbf{r}_{i-1}) = (\mathbf{r}_{i-1}, \mathbf{r}_{i-1}) + b_{i-1}(\mathbf{p}_{i-1}, \mathbf{r}_{i-1}) = (\mathbf{r}_{i-1}, \mathbf{r}_{i-1}) \text{ by } (2.1.13).$$

□

Lemma 4.

$$b_i = -\frac{(\mathbf{r}_i, \mathbf{r}_i)}{(\mathbf{r}_{i-1}, \mathbf{r}_{i-1})}$$ (2.4.15)

Proof.

$$A\mathbf{p}_i = \frac{1}{a_i}(\mathbf{r}_{i-1} - \mathbf{r}_i),$$

hence

$$(\mathbf{r}_i, A\mathbf{p}_i) = -\frac{1}{a_i}(\mathbf{r}_i, \mathbf{r}_i).$$

Furthermore

$$(\mathbf{p}_i, A\mathbf{p}_i) = (\mathbf{r}_{i-1}, A\mathbf{p}_i) + b_{i-1}(\mathbf{p}_{i-1}, A\mathbf{p}_i) =$$

$$(\mathbf{r}_{i-1}, A\mathbf{p}_i) = \frac{1}{a_i}(\mathbf{r}_{i-1}, \mathbf{r}_{i-1} - \mathbf{r}_i) = \frac{1}{a_i}(\mathbf{r}_{i-1}, \mathbf{r}_{i-1}).$$

Finally,

$$b_i = \frac{(\mathbf{r}_i, A\mathbf{p}_i)}{(\mathbf{p}_i, A\mathbf{p}_i)} = -\frac{(\mathbf{r}_i, \mathbf{r}_i)}{(\mathbf{r}_{i-1}, \mathbf{r}_{i-1})}.$$

□

30

The above considerations result in a classical algorithm of Hestenes and Steiffel. The Matlab program *pcg.m* is based on this algorithm.

$$\mathbf{p}_0 = \mathbf{r}_0, \quad \rho_0 = 1,$$

for   k = 1:maxit

$$\rho_1 = (\mathbf{r}_{k-1}, \mathbf{r}_{k-1}) \tag{2.4.16}$$

$$b_{k-1} = \frac{\rho_1}{\rho_0} \tag{2.4.17}$$

$$\mathbf{p}_k = \mathbf{r}_{k-1} + b_{k-1}\mathbf{p}_{k-1} \tag{2.4.18}$$

$$a_k = \frac{(\mathbf{r}_{k-1}, \mathbf{r}_{k-1})}{(\mathbf{p}_k, A\mathbf{p}_k)} \tag{2.4.19}$$

$$\mathbf{x}_k = \mathbf{x}_{k-1} + a_k\mathbf{p}_k \tag{2.4.20}$$

$$\mathbf{r}_k = \mathbf{r}_{k-1} - a_k A\mathbf{p}_k \tag{2.4.21}$$

$$\rho_0 = \rho_1 \tag{2.4.22}$$

end

So far the forward EEG problem is being solved with the use of a three-shell idealistic model. This is then combined with the MUSIC algorithm [35] in order to solve the inverse problem. For practical applications the geometry of the head must be taken into account, so the Finite Element and Boundary Element methods have been used for the experimental modeling. In this work the Finite Volume Method is applied. It allows one to take into account the realistic distibution of the conductivities in a natural way. The Conjugate Gradient Method is an efficient way of getting the iterative solution of large sparse linear systems, provided that the matrix is symmetric and positive definite. The properties of the matrix resulting from the FVM implementation will be considered in the next chapter.

3 Numerical Implementation and Acceleration.

3.1 Formulation of the Thesis Problem.

In this work the forward problem of EEG source localization is posed in the following way: given the intensity and location of the positive and negative sources of electric current, find the potential distribution inside the biological volume conductor, as well as on its surface. This problem has to be solved both for the three-shell spherical head model and for the head of realistic shape obtained by means of the MRI scans. It is natural to apply the Finite Volume Method in this case, since this will allow one to take into account the geometry of the realistic head and the conductivity distribution. In this respect it is important to study the properties of the matrix of the resulting linear system and to determine how the system can be deflated in order to avoid semidefiniteness.

The inverse problem of EEG source localization can be posed as follows: given the value of potential for a limited number of surface points, find the location and orientation of the dipole source. In order to do this the forward problem has to be solved for all the candidate dipole locations. The potential for each particular location has to be computed for each of three spatial directions. Therefore it is very important for practical purposes to reduce as much as possible the computational time needed for the forward problem solution. Below The preconditioning technique will be discussed below.

In fact the three-shell model described above has quite a serious drawback. It assumes that the positive and negative sources are infinitely close, which is too idealistic from a brain anatomy point of view. Therefore it is important to develop a more realistic three-shell model which would allow the comparison of the performance of FVM with theory.

3.2 Realization of the Finite Volume Method for a Realistic Head. Discretization, Deflation and Positive Definiteness.

Until recently the Finite Volume Method did not have applications in EEG Source Localization, although this method was widely used in Fluid Mechanics [1]. There are quite a few technical difficulties one can face while implementing the inverse problem algorithms combined with the FVM. While implementing the BEM only the surface of the biological volume conductor is triangularized. For the FVM the entire three-dimensional domain of the biological volume conductor has to be decomposed. Moreover such a domain decomposition algorithm has to take into account the differences in conductivities for different layers. In order to solve the inverse problem of source localization a regular and dense grid is needed. Such a grid has to be adjusted to the real geometry of the human head.

Rosenfeld et al.[5] implemented a forward problem by mapping the sphere onto the real volume. The basic idea is the decomposition of the sphere by meridians and parallels and then mapping the surfaces of the layers of the realistic head. This approach works reasonably well for spherical or ellipsoidal head models, the distribution of potential obtained matched quite well the results for the analytical three-layer head models. However there is no indication in the literature that such an approach can work well for a more realistic head. First mapping the sphere onto the real head surface is a very complex task if we take into consideration the ears, nose, lips, etc. Second such an approach assumes the existence of the so-called singularities, i.e. points common to more than 8 neighboring finite volume elements. The singularity is shown on Fig. 4. For such a singularity additional cells must be constructed and additional equations must be written, which makes the resulting matrix less sparse and poorly conditioned.

In this work a more simple approach based on the decomposition of the cube is adopted. An algorithm which was used for the code generation will now be considered in detail.

33

Suppose that the dipole of intensity I is located somewhere inside the biological volume conductor. First the biological volume conductor is enclosed into the cube. Without loss of generality we may assume that the length of a side is 2, so the sphere with unit radius can be enclosed into such a cube. Divide such a cube into a number of smaller cubes with side h. These smaller cubes will form a system of $(2l + 1)^3$ finite volume elements, where l is defined as

$$l = \left[\frac{1}{h}\right], \tag{3.2.1}$$

$[\cdot]$ means the operation of taking the integer part of a number. The coordinates of the cubes' centers can be written as a product of the cube's size h and the indexes i, j, k for each spatial direction

$$x = ih, \quad y = jh, \quad z = kh, \tag{3.2.2}$$

$$i, j, k = -l, -l + 1, ..., -1, 0, 1, ..., l - 1, l.$$

The finite volume elements are numbered with index s

$$s = (i + l)(2l + 1)^2 + (j + l)(2l + 1) + k + l + 1, \tag{3.2.3}$$

$$s = 1, ..., (2l + 1)^3.$$

However only the cubes with centers inside the biological volume conductor are of interest for the forward problem computation, since for all other cubes the conductivity is assumed to be zero. Hence one more index is needed for the cubes with nonzero conductivity, and the indexing is done in the following way:

34

$$n = 0$$

for i starting from $-l$ up to l with step 1

　for j starting from $-l$ up to l with step 1

　　for k starting from $-l$ up to l with step 1

> if cube with indexes i, j, k
>
> has nonzero conductivity, then
>
> $n = n + 1;$
>
> otherwise n does not change

　　end;

　end;

end.

The procedures for assigning the values of $\sigma_{i,j,k}$ for each cube will be described later on, as they depend on a particular experiment. There are five important parameters in these codes:

s - parameter indexing all the cubes;

n - parameter indexing only the cubes with nonzero conductivity;

i, j, k - parameters defining the spatial coordinates of the center of the cube.

The computational scheme (2.3.3)

$$(\sigma \nabla \Psi \cdot \vec{S}^\xi)_{i+\frac{1}{2},j,k} - (\sigma \nabla \Psi \cdot \vec{S}^\xi)_{i-\frac{1}{2},j,k}$$

$$+ \quad (\sigma \nabla \Psi \cdot \vec{S}^\eta)_{i,j+\frac{1}{2},k} - (\sigma \nabla \Psi \cdot \vec{S}^\eta)_{i,j-\frac{1}{2},k}$$

$$+ \quad (\sigma \nabla \Psi \cdot \vec{S}^\zeta)_{i,j,k+\frac{1}{2}} - (\sigma \nabla \Psi \cdot \vec{S}^\zeta)_{i,j,k-\frac{1}{2}} \quad = I_0$$

is discretized in the following way. Change $\xi \to x$, $\eta \to y$, $\zeta \to z$,

$$\vec{S}^\xi = \vec{S}^\xi_{i,j,k} = \vec{S}^\xi_{i\pm\frac{1}{2},j,k} = \vec{S}^x = h^2 \vec{i},$$

$$\vec{S}^\eta = \vec{S}^\eta_{i,j,k} = \vec{S}^\eta_{i,j\pm\frac{1}{2},k} = \vec{S}^y = h^2 \vec{j},$$

$$\vec{S}^\zeta = \vec{S}^\zeta_{i,j,k} = \vec{S}^\zeta_{i,j,k\pm\frac{1}{2}} = \vec{S}^z = h^2\vec{k},$$

$$V_{i,j,k} = V_{i\pm\frac{1}{2},j\pm\frac{1}{2},k\pm\frac{1}{2}} = h^3.$$

Here $\vec{i},\vec{j},\vec{k}$ are unit vectors in three spatial directions. One shouldn't confuse them with the scalar indexes i,j,k.

Therefore the expression for the current flow through the face $(i+\frac{1}{2},j,k)$ is

$$(\sigma\nabla\Psi\cdot S^x)_{i+\frac{1}{2},j,k} = \sigma_{i+\frac{1}{2},j,k}(\Psi_{i+1,j,k} - \Psi_{i,j,k})h, \tag{3.2.4}$$

and it was already discussed in the previous chapter that

$$\sigma_{i+\frac{1}{2},j,k} = \frac{2\sigma_{i+1,j,k}\sigma_{i,j,k}}{\sigma_{i+1,j,k} + \sigma_{i,j,k}}.$$

It is straightforward now to write the expressions for the fluxes through the other faces of the cube. Finally

$$\frac{2\sigma_{i+1,j,k}\sigma_{i,j,k}}{\sigma_{i+1,j,k}+\sigma_{i,j,k}}\left(\Psi_{i+1,j,k}-\Psi_{i,j,k}\right) - \frac{2\sigma_{i,j,k}\sigma_{i-1,j,k}}{\sigma_{i,j,k}+\sigma_{i-1,j,k}}\left(\Psi_{i,j,k}-\Psi_{i-1,j,k}\right)$$
$$+\frac{2\sigma_{i,j+1,k}\sigma_{i,j,k}}{\sigma_{i,j+1,k}+\sigma_{i,j,k}}\left(\Psi_{i,j+1,k}-\Psi_{i,j,k}\right) - \frac{2\sigma_{i,j,k}\sigma_{i,j-1,k}}{\sigma_{i,j,k}+\sigma_{i,j-1,k}}\left(\Psi_{i,j,k}-\Psi_{i,j-1,k}\right) \tag{3.2.5}$$
$$+\frac{2\sigma_{i,j,k+1}\sigma_{i,j,k}}{\sigma_{i,j,k+1}+\sigma_{i,j,k}}\left(\Psi_{i,j,k+1}-\Psi_{i,j,k}\right) - \frac{2\sigma_{i,j,k}\sigma_{i,j,k-1}}{\sigma_{i,j,k}+\sigma_{i,j,k-1}}\left(\Psi_{i,j,k}-\Psi_{i,j,k-1}\right) = \frac{I_{i,j,k}}{h}.$$

Singularities and additional equations are no longer needed. Now the computational scheme needs to be transferred into the matrix equation

$$A\mathbf{u} = \mathbf{b}.$$

The dimension of the matrix A is $N \times N$, where N is the maximum value of the parameter n. For each value of n there is only one combination of indexes i,j,k. Such a transformation can be represented as a function of i,j,k.

$$n = f(i,j,k).$$

36

. Denote $n_1 - n_6$ as the indexes of the adjacent cubes,

$$n_1 = f(i+1,j,k), \quad n_2 = f(i-1,j,k),$$

$$n_3 = f(i,j+1,k), \quad n_4 = f(i,j-1,k),$$

$$n_5 = f(i,j,k+1), \quad n_6 = f(i,j,k-1).$$

If the sign of the left and right-hand-side is changed to the opposite the equation (3.2.5) has the form

$$\frac{2\sigma_{n_1}\sigma_n}{\sigma_{n_1}+\sigma_n}(\Psi_n - \Psi_{n_1}) + \frac{2\sigma_{n_2}\sigma_n}{\sigma_{n_2}+\sigma_n}(\Psi_n - \Psi_{n_2})$$

$$+ \quad \frac{2\sigma_{n_3}\sigma_n}{\sigma_{n_3}+\sigma_n}(\Psi_n - \Psi_{n_3}) + \frac{2\sigma_{n_4}\sigma_n}{\sigma_{n_4}+\sigma_n}(\Psi_n - \Psi_{n_4}) \tag{3.2.6}$$

$$+ \quad \frac{2\sigma_{n_5}\sigma_n}{\sigma_{n_5}+\sigma_n}(\Psi_n - \Psi_{n_5}) + \frac{2\sigma_{n_6}\sigma_n}{\sigma_{n_6}+\sigma_n}(\Psi_n - \Psi_{n_6}) \quad = -\frac{I_n}{h}.$$

For each value of n the elements of the n-th row of the matrix A are

$$A_{nn} = 2\sigma_n \left(\sum_{t=1}^{6} \frac{\sigma_{n_t}}{\sigma_{n_t} + \sigma_n} \right), \quad A_{nn_t} = -\frac{2\sigma_n\sigma_{n_t}}{\sigma_n + \sigma_{n_t}}, \quad t = 1,...,6. \tag{3.2.7}$$

Since the normal component of the current flux does not change at the interface of the biological volume conductor,

$$\sigma_{in}\frac{\partial \Psi}{\partial n}\bigg|_{in} = \sigma_{out}\frac{\partial \Psi}{\partial n}\bigg|_{out}.$$

The conductivity of the surrounding air is zero, therefore the current flux at the interface is zero. For the computational scheme it means that if the center of the adjacent cube with indexes $i+1,j,k$ is located outside the biological volume conductor, then

$$\sigma_{i+1,j,k} = 0,$$

therefore the correspondent terms in (3.2.6) and (3.2.7) become zeros as well.

The matrix A is symmetric since for two cubes with n-indexes p and t,

$$A_{pt} = A_{tp} = -\frac{2\sigma_p\sigma_t}{\sigma_p + \sigma_t}. \tag{3.2.8}$$

Now we will study the question of positive definiteness of the matrix A.

37

Definition 1. *A positive definite matrix $A \in M_n$ is a nonsingular Hermitian matrix such that $(A\mathbf{x}, \mathbf{x}) > 0$ for all nonzero $\mathbf{x} \in C^n$.*

Here M_n is a set of all n-by-n complex matrixes, C^n is a complex vector space of the complex n-vectors [25]. If for some nonzero $\mathbf{x}^* \in C^n$, $(A\mathbf{x}^*, \mathbf{x}^*) = 0$, then the nonsingular Hermitian matrix A is called *positive semidefinite*. In our case matrix A is Hermitian, since it is symmetric and it has only real entries. It is easy to see that for N-dimensional vector $\mathbf{u} = [c, ..., c]^T$, where c is a constant, $(A\mathbf{u}, \mathbf{u}) = 0$, hence matrix A is positive semidefinite. In such a case vector $\mathbf{v} = [c, ..., c]^T \in \ker(A)$, and $\text{rank}(A) \leq N - 1$.

Lemma 5. *rank $(A) = N - 1$.*

Proof.

Assume that the opposite is true, i.e. there is another vector $\mathbf{w} = [\Psi_1, \Psi_2, ..., \Psi_N]^T \in \ker(A)$ such that for some indices i and j, $\Psi_i \neq \Psi_j$. This means that for at least one of the finite volume elements with index n at least one of its adjacent elements indexed as n_t^* has a different potential. Without loss of generality we assume that $\Psi_{n_t^*} > \Psi_n$. Define new indexes n^0 and n^1 as $n^0 = n, n^1 = n_t^*$. Since

$$(A\mathbf{w})_{n^1} = \sum_{\substack{t = 1 \\ n_t^1 \neq n^0}}^{6} \frac{2\sigma_{n^1}\sigma_{n_t^1}}{\sigma_{n^1} + \sigma_{n_t^1}}(\Psi_{n^1} - \Psi_{n_t^1}) + \frac{2\sigma_{n^1}\sigma_{n^0}}{\sigma_{n^1} + \sigma_{n^0}}(\Psi_{n^1} - \Psi_{n^0}) = 0, \quad (3.2.9)$$

then there is at least one index n_t^{1*} such that $\Psi_{n_t^{1*}} > \Psi_{n^1}$. Denote $n^2 = n_t^{1*}$. In such a way it is possible to construct a sequence $n^0, n^1, n^2, ...$ of indexes such that $\Psi_{n^0} < \Psi_{n^1} < \Psi_{n^2} < ...$ Since the set of the finite volume elements is finite, this sequence must end with an index m. For such a finite volume element there are adjacent elements with lower potential, however there are no elements with higher potential.

38

For this index

$$(A\mathbf{w})_{n^m} = \frac{2\sigma_{n^m}\sigma_{n^{m-1}}}{\sigma_{n^m} + \sigma_{n^{m-1}}}(\Psi_{n^m} - \Psi_{n^{m-1}})$$

$$+ \sum_{t=1}^{6} \frac{2\sigma_{n^m}\sigma_{n_t^m}}{\sigma_{n^m} + \sigma_{n_t^m}}(\Psi_{n^m} - \Psi_{n_t^m}). \qquad (3.2.10)$$

$$n_t^m \neq n^{m-1}$$

The first term is greater than zero, the second is greater or equal to zero. Hence $(A\mathbf{w})_n > 0$ and there is a contradiction, $\mathbf{w} \notin \ker(A)$. There is no vector $\mathbf{w}$ linearly independent from $\mathbf{v}$ such that $\mathbf{w} \in \ker(A)$. Therefore $\dim(\ker(A)) = 1$, $\text{rank}(A) = N - 1$.

This property of matrix A has a clear physical sense. In the absence of the sources or sinks of the current the potential is the same everywhere within the biological volume conductor.

Consider

$$(A\mathbf{u}, \mathbf{u}) = \sum_{n=1}^{N}\sum_{t=1}^{6}(\Psi_n - \Psi_{n_t})\Psi_n \frac{2\sigma_n\sigma_{n_t}}{\sigma_n + \sigma_{n_t}}. \qquad (3.2.11)$$

It is easy to see that for each term with indexes n, n_t there is a term

$$(\Psi_{n_t} - \Psi_n)\Psi_{n_t}\frac{2\sigma_n\sigma_{n_t}}{\sigma_n + \sigma_{n_t}}.$$

The sum of the two results in

$$\frac{2\sigma_n\sigma_{n_t}}{\sigma_n + \sigma_{n_t}}\left\{(\Psi_n - \Psi_{n_t})\Psi_n + (\Psi_{n_t} - \Psi_n)\Psi_{n_t}\right\} = \frac{2\sigma_n\sigma_{n_t}}{\sigma_n + \sigma_{n_t}}(\Psi_n - \Psi_{n_t})^2.$$

Finally the expression (3.2.11) can be written out as a sum with respect to all the sides of the finite volume elements,

$$(A\mathbf{u}, \mathbf{u}) = \sum_{n=1}^{N}\sum_{t=1}^{6}\frac{2\sigma_n\sigma_{n_t}}{\sigma_n + \sigma_{n_t}}(\Psi_n - \Psi_{n_t})^2 H(n_t - n), \qquad (3.2.12)$$

where H is a Heaviside function,

$$H(n_t - n) = \begin{cases} 1, & n_t > n, \\ 0, & n_t < n. \end{cases}$$

39

It is also possible to prove that any row of the matrix A is a sum of all the other rows, taken with the opposite sign. Indeed for the n-th row of A,

$$A_{nn} = \sum_{t=1}^{6} \frac{2\sigma_{n_t}\sigma_n}{\sigma_{n_t} + \sigma_n} = -\sum_{t=1}^{6} A_{n_t n} = -\sum_{\substack{m=1 \\ m \neq n}}^{N} A_{mn}. \qquad (3.2.13)$$

$$A_{nn_t} = -\frac{2\sigma_{n_t}\sigma_n}{\sigma_{n_t} + \sigma_n} = -\left\{ A_{n_t n_t} - \sum_{\substack{s=1 \\ n_s \neq n_t}}^{6} \frac{2\sigma_{n_t}\sigma_{n_s}}{\sigma_{n_t} + \sigma_{n_s}} \right\} =$$

$$-\left\{ \sum_{s=1}^{6} \frac{2\sigma_{n_t}\sigma_{n_s}}{\sigma_{n_t} + \sigma_{n_s}} - \sum_{\substack{s=1 \\ n_s \neq n_t}}^{6} \frac{2\sigma_{n_t}\sigma_{n_s}}{\sigma_{n_t} + \sigma_{n_s}} \right\} = -\sum_{m=1}^{N} A_{mn_t}. \qquad (3.2.14)$$

For all other entries with $k \neq n, k \neq n_t, \sum_{m=1}^{N} A_{mk} = 0$.

Apparently the linear system will have multiple solutions. However if a certain value of the potential is ascribed to one of the finite volumes, then the linear system will have a unique solution. Such a practice is called deflation of the matrix A. Without the loss of generality the biopotential in the center of the finite volume element with n-index 1 can be ascribed the value a, then all the other potentials will be measured with respect to that potential. It is well known that not just the value of the potential but the potential difference makes physical sense. In practice one measures the potential difference with respect to the so-called reference electrode. Therefore we can assume that $\Psi_1 = a$. Instead of $A\mathbf{u} = \mathbf{b}$, there is a system

$$A_d \mathbf{u}_d = \mathbf{b}_d, \qquad (3.2.15)$$

40

$$
\text{where} \quad A_d = \begin{bmatrix} A_{22} & \cdot & \cdot & \cdot & A_{2N} \\ & \cdot & & & \cdot \\ & \cdot & & & \cdot \\ & \cdot & & & \cdot \\ A_{N2} & \cdot & \cdot & \cdot & A_{NN} \end{bmatrix}, \tag{3.2.16}
$$

$$
\mathbf{u}_d = \begin{bmatrix} \Psi_2 \\ \cdot \\ \cdot \\ \cdot \\ \Psi_N \end{bmatrix}, \quad \mathbf{b}_d = \begin{bmatrix} b_2 \\ \cdot \\ \cdot \\ \cdot \\ b_N \end{bmatrix} - a \begin{bmatrix} A_{21} \\ \cdot \\ \cdot \\ \cdot \\ A_{N1} \end{bmatrix}. \tag{3.2.17}
$$

The deflated matrix A_d is positive definite. Assume that i_1, j_1, k_1 are the indexes that correspond to $n = 1$,

$$
s_1 = f(i+1, j, k), \quad s_2 = f(i, j+1, k), \quad , s_3 = f(i, j, k+1).
$$

For any nonzero $\mathbf{u}_d$,

$$
(A_d \mathbf{u}_d, \mathbf{u}_d) = \sum_{t=1}^{3} \frac{2\sigma_1 \sigma_{s_t}}{\sigma_1 + \sigma_{s_t}} \Psi_{1_t}^2 +
$$

$$
\sum_{n=2}^{N} \sum_{\substack{t=1 \\ n_t \neq 1}}^{6} \frac{2\sigma_{n_t} \sigma_n}{\sigma_{n_t} + \sigma_n} (\Psi_n - \Psi_{n_t})^2 H(n_t - n) > 0. \tag{3.2.18}
$$

This sum is greater than zero unless $\Psi_2 = \Psi_3 = \ldots = \Psi_N = 0$.

It is further assumed that the human head has three major domains with the same anisotropic conductivity - the inside brain, skull and scalp. The brain tissue and scalp have the same conductivity of value $0.0029 \ (\Omega m)^{-1}$. It is quite realistic to assume that the conductivity of the skull is much lower. For the numerical experiments it is considered to be $3.6 \cdot 10^{-5} (\Omega m)^{-1}$. If the center of the finite volume element is within the domain of

41

the brain, the conductivity of the brain is attributed to the entire element, similarly for the skull and the scalp. It is assumed that the brain, skull and scalp have clearly outlined shapes, so it is possible to determine the conductivity for each particular center.

42

3.3 Preconditioning of the Conjugate Gradient Method.

3.3.1 The Idea of Preconditioning.

In order to reduce the computational time for the CGM, one applies preconditioning strategies. The basic idea of preconditioning ([30], [39], [40]) can be described in the following way. Instead of the system $A_d \mathbf{x}_d = \mathbf{b}_d$, consider the linear system $C_L A_d C_R \tilde{\mathbf{x}} = C_L \mathbf{b}_d$. Such a system can be written out as

$$\tilde{A}\tilde{\mathbf{x}} = \tilde{\mathbf{b}}, \tag{3.3.1}$$

$$\text{where} \quad \tilde{A} = C_L A_d C_R, \quad \tilde{\mathbf{b}} = C_L \mathbf{b}_d.$$

The matrixes C_L and C_R are called left and right preconditioners. The choice of these matrices depends on the particular preconditioning strategy. The matrix $C_L A_d C_R$ is supposed to have better spectral properties than the original A_d, the details will be given below. Such an approach does not require matrix inversion, it does not reduce the sparsity of the matrix of the system.

Consider the classical CGM, described in the previous chapter

$$\tilde{\mathbf{x}}_0 \quad - \quad \text{initial approximation;} \quad \tilde{\mathbf{r}}_0 = \tilde{\mathbf{b}} - \tilde{A}\tilde{\mathbf{x}}_0, \quad \tilde{\mathbf{p}}_0 = \tilde{\mathbf{r}}_0, \quad \rho_0 = 1.$$

for $k = 1{:}\text{maxit}$

$$\rho_1 = (\tilde{\mathbf{r}}_{k-1}, \tilde{\mathbf{r}}_{k-1}),$$

$$b_{k-1} = \frac{\rho_1}{\rho_0}$$

$$\tilde{\mathbf{p}}_k = \tilde{\mathbf{r}}_{k-1} + b_{k-1}\tilde{\mathbf{p}}_{k-1}$$

$$a_k = \frac{(\tilde{\mathbf{r}}_{k-1}, \tilde{\mathbf{r}}_{k-1})}{(\tilde{\mathbf{p}}_k, \tilde{A}\tilde{\mathbf{p}}_k)}$$

$$\tilde{\mathbf{x}}_k = \tilde{\mathbf{x}}_{k-1} + a_k\tilde{\mathbf{p}}_k$$

$$\tilde{\mathbf{r}}_k = \tilde{\mathbf{r}}_{k-1} - a_k\tilde{A}\tilde{\mathbf{p}}_k$$

$$\rho_0 = \rho_1$$

43

end

The successive approximation vectors $\mathbf{x}_k$ and direction vectors $\mathbf{p}_k$ of the CGM for the system $A_d\mathbf{x}_d = \mathbf{b}_d$ are related to the corresponding vectors $\tilde{\mathbf{x}}_k$ and $\tilde{\mathbf{p}}_k$ of the preconditioned linear system (3.3.1) in the following way

$$\mathbf{x}_{dk} = C_R\tilde{\mathbf{x}}_k, \quad \mathbf{p}_k = C_R\tilde{\mathbf{x}}_k. \tag{3.3.2}$$

For the new residual vectors $\tilde{\mathbf{r}}_k$,

$$\tilde{\mathbf{r}}_k = \tilde{\mathbf{b}} - \tilde{A}\tilde{\mathbf{x}}_k = C_L\mathbf{b} - C_LA_dC_R\tilde{\mathbf{x}}_k = C_L(\mathbf{b} - A_d\mathbf{x}_{dk}) = C_L\mathbf{r}_k. \tag{3.3.3}$$

Now one can derive all the intermediate parameters and vectors for the preconditioned CGM,

$$b_{k-1} = \frac{(\tilde{\mathbf{r}}_{k-1}, \tilde{\mathbf{r}}_{k-1})}{(\tilde{\mathbf{r}}_{k-2}, \tilde{\mathbf{r}}_{k-2})} = \frac{(C_L\mathbf{r}_{k-1}, C_L\mathbf{r}_{k-1})}{(C_L\mathbf{r}_{k-2}, C_L\mathbf{r}_{k-2})}. \tag{3.3.4}$$

$$\tilde{\mathbf{p}}_k = \tilde{\mathbf{r}}_{k-1} + b_{k-1}\tilde{\mathbf{p}}_{k-1},$$

$$C_R\tilde{\mathbf{p}}_k = C_R\tilde{\mathbf{r}}_{k-1} + b_{k-1}C_R\tilde{\mathbf{p}}_{k-1},$$

$$\mathbf{p}_k = C_RC_L\mathbf{r}_{k-1} + b_{k-1}\mathbf{p}_{k-1}.$$

If $C = C_RC_L$, then

$$\mathbf{p}_k = C\mathbf{r}_{k-1} + b_{k-1}\mathbf{p}_{k-1}. \tag{3.3.5}$$

Since

$$(\tilde{\mathbf{p}}_k, \tilde{A}\tilde{\mathbf{p}}_k) = (C_R^{-1}\mathbf{p}_k, C_LA_dC_RC_R^{-1}\mathbf{p}_k)$$

$$= (C_R^{-1}\mathbf{p}_k, C_LA_d\mathbf{p}_k) = (\mathbf{p}_k, CA_d\mathbf{p}_k),$$

$$a_k = \frac{(\tilde{\mathbf{r}}_{k-1}, \tilde{\mathbf{r}}_{k-1})}{(\tilde{\mathbf{p}}_k, \tilde{A}\tilde{\mathbf{p}}_k)} = \frac{(C_L\mathbf{r}_{k-1}, C_L\mathbf{r}_{k-1})}{(\mathbf{p}_k, CA_d\mathbf{p}_k)}. \tag{3.3.6}$$

$$\mathbf{x}_k = \mathbf{x}_{k-1} + a_k\mathbf{p}_k \tag{3.3.7}$$

44

$$\tilde{\mathbf{r}}_k = \tilde{\mathbf{r}}_{k-1} - a_k \tilde{A}\tilde{\mathbf{p}}_k,$$

$$C_L\mathbf{r}_k = C_L\mathbf{r}_{k-1} - a_k C_L A_d C_R C_R^{-1}\mathbf{p}_k.$$

Therefore

$$\mathbf{r}_k = \mathbf{r}_{k-1} - a_k A_d\mathbf{p}_k. \tag{3.3.8}$$

Hence for the preconditioned CGM there is a following set of equations,

$\mathbf{x}_0$ $-$ initial approximation;

$$\mathbf{r}_0 = C_L(\mathbf{b}_d - A_d\mathbf{x}_0),$$

$$\mathbf{p}_0 = \mathbf{r}_0, \quad \rho_0 = 1,$$

for   k = 1:maxit

$$\rho_1 = (C_L\mathbf{r}_{k-1}, C_L\mathbf{r}_{k-1})$$

$$b_{k-1} = \frac{\rho_1}{\rho_0}$$

$$\mathbf{p}_k = C\mathbf{r}_{k-1} + b_{k-1}\mathbf{p}_{k-1}$$

$$a_k = \frac{(C_L\mathbf{r}_{k-1}, C_L\mathbf{r}_{k-1})}{(\mathbf{p}_k, CA_d\mathbf{p}_k)}$$

$$\mathbf{x}_k = \mathbf{x}_{k-1} + a_k\mathbf{p}_k$$

$$\mathbf{r}_k = \mathbf{r}_{k-1} - a_k A_d\mathbf{p}_k$$

$$\rho_0 = \rho_1$$

end

3.3.2 Polynomial Preconditioning.

For the problem under consideration the polynomial preconditioning ([30], [39])was applied. Consider the basic ideas underlying this approach. The left preconditioner C_L is

45

chosen to be a matrix polynomial,

$$C_L(A_d) = a_0 I + a_1 A_d + a_2 A_d^2 + a_3 A_d^3 + ..., \tag{3.3.9}$$

such that the product $C_L(\lambda)\lambda$ will be close to 1 in l_∞ norm on some set $S \subset \sigma(A_d)$, where $\sigma(A_d)$ is the spectrum of matrix A_d. Since A_d is symmetric and nonsingular, it can be assumed that S is a subset of the real line that excludes the origin. Next let S be a compact set, and for f a continuous function on S, define

$$\|f\|_S = \max_{\lambda \in S} |f(\lambda)|. \tag{3.3.10}$$

This norm is also called the *uniform norm*; note its dependence on the set S. We shall seek the polynomial which minimizes $\|1 - C_L(\lambda)\lambda\|_S$, i.e. the best polynomial approximation to 1 from among all polynomials of degree m or less having a root at zero. If $p_m \equiv C_L(\lambda)\lambda$ is such a polynomial, the problem may be recast as a constrained minimax approximation problem

$$\min_{p \in \pi_m,\ p(0)=0} \|1 - p\|_S, \tag{3.3.11}$$

where $\pi_m = \{p : p \text{ is a real polynomial of degree m or less}\}$. Therefore it is desirable to choose such p_m that the eigenvalues of the preconditioned matrix $p_m(A_d)$ are as tightly clustered around 1 as possible. In this way the convergence of the Conjugate Gradient Method can be accelerated. Since $p_m(A_d)$ is a preconditioned matrix, $p_m(\lambda)$ is called the *preconditioning polynomial*. In order to find a_i, we need Chebyshev polynomials of the first kind [42], orthogonal on the interval [-1,1] with weight function

$$h_1 = \frac{1}{\sqrt{1 - x^2}}, \quad x \in (-1, 1),$$

which provide the solution for the minimax problem [47].

The explicit form for m-th Chebyshev polynomial is $T_m = \cos(m \arccos x)$. In practice Chebyshev polynomials are generated by the recurrent formulas

$$T_0(x) = 1, \quad T_1(x) = x,$$

46

$$T_{n+1}(x) = 2xT_n(x) - T_{n-1}(x). \tag{3.3.12}$$

The leading coefficient of $T_n(x)$, for $n \geq 1$, is 2^{n-1}. Therefore the Chebyshev polynomials with leading coefficient 1 are defined by the formula

$$\tilde{T}_m(x) = \frac{1}{2^{m-1}} T_m(x) = \frac{1}{2^{m-1}} \cos(m \arccos x), \quad m \geq 1. \tag{3.3.13}$$

The polynomials $\tilde{T}_m(x)$ deviate as little as possible from zero on the interval $[-1,1]$, in the sense that for any other polynomial $\tilde{F}_m(x)$ of degree m with leading coefficient 1 the following is true,

$$\max_{x \in (-1,1)} |\tilde{F}_m(x)| > \max_{x \in (-1,1)} |\tilde{T}_m(x)| = \frac{1}{2^{m-1}}. \tag{3.3.14}$$

Proof of this fact can be found in [47] or [48]. Suppose that $[c,d] = \sigma(A_d)$ for a known positive c and d. Introduce the following coordinate transform,

$$\hat{x} = \frac{2x - (c+d)}{d-c}, \tag{3.3.15}$$

then $\hat{x} \in [-1, 1]$. The Chebyshev polynomial $T_m\left(\frac{2\lambda - (c+d)}{d-c}\right)$ will minimize $\|f\|_S = \|1 - p\|_S$. In order to satisfy the condition $f(0) = 1$ one should divide $T_m\left(\frac{2\lambda - (c+d)}{d-c}\right)$ by T_m taken at $\lambda = 0$, i.e.

$$f_m = \frac{T_m\left(\frac{c+d-2\lambda}{d-c}\right)}{T_m\left(\frac{c+d}{d-c}\right)}, \tag{3.3.16}$$

$$p_m = 1 - \frac{T_m\left(\frac{c+d-2\lambda}{d-c}\right)}{T_m\left(\frac{c+d}{d-c}\right)}. \tag{3.3.17}$$

Now the explicit form of $C_L(A_d)$ can be obtained. Since $p(A_d) = C_L(A_d)A_d = A_d C_L(A_d)$,

$$C_L(A_d) = A_d^{-1}\left\{I - \frac{T_m\left(\frac{(c+d)I - 2A_d}{d-c}\right)}{T_m\left(\frac{c+d}{d-c}\right)}\right\} = A_d^{-1}\left\{I - \frac{T_m(aI - bA)}{T_m(a)}\right\}, \tag{3.3.18}$$

$$\text{where} \quad a = \frac{c+d}{d-c}, \quad b = \frac{2}{d-c}.$$

47

The minimax preconditioning polynomial is attractive for application to large sparse systems for several reasons. First the minimax preconditioning polynomial $p_m(\lambda)$ equioscillates about 1 over the set S, therefore the preconditioning polynomial $C_L(\lambda)$ is unbiased in its suppression of the error: no portion of the set S is preferred over another. Second if $\sigma(A_d) \subset S$, then $\sigma(p_m(A_d)) \subset [1 - \epsilon_m, 1 + \epsilon_m]$, where $\epsilon_m = \|1 - p_m\|_S$. The original matrix may even be indefinite, but the minimax preconditioned matrix is positive definite, since $\epsilon_m < 1$.

Define the spectral condition number $k(A_d) = \|A_d^{-1}\|_2\|A_d\|_2 = \frac{\lambda_n}{\lambda_1}$. The spectral condition number of $p_m(A_d)$, $k(p_m(A_d))$, satisfies

$$k(p_m(A_d)) \leq \frac{1 + \epsilon_m}{1 - \epsilon_m}, \tag{3.3.19}$$

when $\sigma(A_d) \subset S$. This bound yields an estimate of the number of steps the Conjugate Gradient Method requires for convergence. One needs approximately

$$\frac{ln(\frac{\delta}{2})}{ln(C_F)} \tag{3.3.20}$$

steps to reduce the errors by an amount δ [31], where

$$C_F = C_F(p_m(A_d)) = \frac{\sqrt{k(p_m(A_d))} - 1}{\sqrt{k(p_m(A_d))} + 1} \tag{3.3.21}$$

is the *convergence factor* for the Hermitian positive definite matrix $p_m(A_d)$. The estimate (3.3.21) is fairly accurate if the eigenvalues of $p_m(A_d)$ are uniformly distributed throughout $[1 - \epsilon_m, 1 + \epsilon_m]$. Since A_d^{-1} is not known a different formula for the polynomial preconditioner is needed, which would be suitable for practice. Now consider

$$T_m(aI) - T_m(aI - bA).$$

Here a well known formula can be used,

$$x^n - y^n = (x - y)(x^{n-1} + x^{n-2}y + \ldots + xy^{n-2} + y^{n-1}) = (x - y)\sum_{k=0}^{n-1} x^{n-1-k}y^k \tag{3.3.22}$$

48

Hence taking aI instead of x and $aI - bA$ instead of y,

$$(aI)^n - (aI - bA)^n = bA \sum_{k=0}^{n-1} a^{n-1-k}(aI - bA)^k. \tag{3.3.23}$$

Now consider

$$T_m(x) = t_0 + t_1 x + t_2 x^2 + \ldots + t_m x^m, \tag{3.3.24}$$

the m-th order Chebyshev polynomial.

$$T_m(aI) - T_m(aI - bA) = \sum_{n=1}^{m} t_n \left((aI)^n - (aI - bA)^n \right) = bA \sum_{n=1}^{m} t_n \sum_{k=0}^{n-1} a^{n-1-k}(aI - bA)^k$$

$$= bA \sum_{n=1}^{m} t_n \sum_{k=0}^{n-1} a^{n-1-k} \sum_{s=0}^{k} C_s^k (-1)^s a^{k-s} b^s A^s, \tag{3.3.25}$$

where $C_s^k = \dfrac{k!}{(k-s)!s!}$ are binomial coefficients.

Finally the expression for the m-th order polynomial preconditioner is

$$C_{Lm}(A) = \frac{b}{T_m(a)} \sum_{n=1}^{m} t_n \sum_{k=0}^{n-1} a^{n-1-k}(aI - bA)^k$$

$$= \frac{2}{(d-c)\cos\left(m \arccos\left(\frac{c+d}{d-c}\right)\right)} \sum_{n=1}^{m} t_n \sum_{k=0}^{n-1} \left(\frac{c+d}{d-c}\right)^{n-1-k} \sum_{s=0}^{k} (-1)^s C_s^k \frac{(c+d)^s 2^{k-s}}{(d-c)^k} A^s$$

$$= \sum_{n=0}^{m-1} \alpha_n A^n. \tag{3.3.26}$$

By formulas (3.3.12), the coefficients t_n should be defined as follows: consider the array of coefficients

$$f_0^0 = 1, f_1^0 = 0 = f_2^0 = \ldots = f_m^0 = 0.$$

These coefficients correspond to $T_0(x) = 1$. The coefficients which correspond to $T_1(x) = x$ will be

$$f_0^1 = 0, f_1^1 = 1, f_2^1 = f_3^1 = \ldots = f_m^1 = 0.$$

49

Then the coefficients f_i^m which correspond to $T_m(x)$ can be obtained in the following way

for $k = 2 : m$

    for $i = 0 : m$

$$\boxed{f_i^{k+1} = 2f_{i-1}^k - f_i^{k-1}}$$

    end;

end.

Finally,

$$t_1 = f_1^m, t_2 = f_2^m, ..., t_n = f_n^m.$$

One more advantage of the Polynomial Preconditioning approach stems from the fact that there is no need to generate and store the preconditioning matrix. Moreover there is no need to store the matrices $A^2, A^3, ..., A^m$ as well. The CGM computations were implemented in the following way,

$\mathbf{x}_0$ — initial approximation;

$$\mathbf{r}_0 = C_L(\mathbf{b}_d - A_d\mathbf{x}_0),$$

$$\mathbf{p}_0 = \mathbf{r}_0, \quad \rho_0 = 1,$$

for $k = 1{:}\text{maxit}$

$$\hat{\mathbf{r}}_{k-1} = C_{L_m}\mathbf{r}_{k-1},$$

$$\rho_1 = (\hat{\mathbf{r}}_{k-1}, \hat{\mathbf{r}}_{k-1}),$$

$$b_{k-1} = \frac{\rho_1}{\rho_0},$$

$$\mathbf{p}_k = \hat{\mathbf{r}}_{k-1} + b_{k-1}\mathbf{p}_{k-1},$$

$$\hat{\mathbf{p}}_k = C_{L_m}\mathbf{p}_k,$$

50

$$a_k = \frac{(\hat{\mathbf{r}}_{k-1}, \hat{\mathbf{r}}_{k-1})}{(\mathbf{p}_k, A_d \hat{\mathbf{p}}_k)},$$

$$\mathbf{x}_k = \mathbf{x}_{k-1} + a_k \mathbf{p}_k,$$

$$\mathbf{r}_k = \mathbf{r}_{k-1} - a_k A_d \mathbf{p}_k,$$

$$\rho_0 = \rho_1.$$

end

The products of C_{L_m} times vectors $\mathbf{r}_{k-1}$ and $\mathbf{p}_k$ are computed only once per iteration in the sequential way. For example for $\hat{\mathbf{r}}_{k-1}$ the multiplication procedure is implemented as follows,

$$\mathbf{f} = \mathbf{r}_{k-1},$$

$$\mathbf{q} = \alpha_0 \mathbf{f},$$

for   k = 1:maxit

$$\mathbf{f} = A\mathbf{f},$$

$$\mathbf{q} = \mathbf{q} + \alpha_k \mathbf{f},$$

end

$$\hat{\mathbf{r}}_{k-1} = C_{L_m} \mathbf{r}_{k-1} = \mathbf{q}.$$

The procedure is same for $\mathbf{p}_k$. Such an approach is economical in terms of memory.

3.3.3   Finding the Spectral Bounds.

The approach described in [40] was used for finding the spectral bounds of A_d. The *Orthodir* (A_d, A_d) version of CGM is

$$\mathbf{x}_0 \; - \; \text{initial approximation;}$$

51

$$\mathbf{p}_0 = \mathbf{r}_0, \quad \mathbf{e}_i = \mathbf{x} - \mathbf{x}_i,$$

$$a_i = \frac{(A_d\mathbf{e}_i, \mathbf{p}_i)}{(A_d\mathbf{p}_i, \mathbf{p}_i)} = \frac{(\mathbf{r}_i, \mathbf{p}_i)}{(A_d\mathbf{p}_i, \mathbf{p}_i)}, \tag{3.3.27}$$

$$\mathbf{x}_{i+1} = \mathbf{x}_i + a_i\mathbf{p}_i, \tag{3.3.28}$$

$$\mathbf{r}_{i+1} = \mathbf{r}_i - a_i A_d\mathbf{p}_i, \tag{3.3.29}$$

$$\gamma_i = \frac{(A_d\mathbf{p}_i, A_d\mathbf{p}_i)}{(A_d\mathbf{p}_i, \mathbf{p}_i)}, \tag{3.3.30}$$

$$\sigma_i = \frac{(A_d\mathbf{p}_i, A_d\mathbf{p}_{i-1})}{(A_d\mathbf{p}_{i-1}, \mathbf{p}_{i-1})}, \tag{3.3.31}$$

$$\mathbf{p}_{i+1} = A_d\mathbf{p}_i - \gamma_i\mathbf{p}_i - \sigma_i\mathbf{p}_{i-1}. \tag{3.3.32}$$

The parameters computed by the first k steps of *Orthodir* (A_d, A_d) can give the estimates of c and d. Let P_k be the matrix with columns $\mathbf{p}_0, ..., \mathbf{p}_{k-1}$.

Then

$$P_k^* A_d P_k = D_k = \mathrm{diag}(\delta_{k-1}), \quad \delta_{k-1} = (A_d\mathbf{p}_{k-1}, \mathbf{p}_{k-1}). \tag{3.3.33}$$

The three-term recursion (3.3.32) gives

$$P_k^* A_d A_d P_k = D_k T_k, \tag{3.3.34}$$

where $T_k = \mathrm{tridiag}(1, \gamma_{k-1}, \sigma_k)$ is a tridiagonal matrix.

Define the field of values of symmetric positive definite matrix $\mathcal{G}$ with respect to A inner product as

$$\mathcal{F}_A(\mathcal{G}) = \left\{ \lambda : \lambda = \frac{(A_d\mathcal{G}\mathbf{x}, \mathbf{x})}{(A_d\mathbf{x}, \mathbf{x})} \right\} \tag{3.3.35}$$

for some $\mathbf{x} \in C^n$. If λ is an eigenvalue of T_k with eigenvector $\mathbf{x}$, $T_k\mathbf{x} = \lambda\mathbf{x}$, then

$$\lambda = \frac{(D_k T_k\mathbf{x}, \mathbf{x})}{(D_k\mathbf{x}, \mathbf{x})} = \frac{(A_d\mathcal{G}P_k\mathbf{x}, P_k\mathbf{x})}{(A_d P_k\mathbf{x}, P_k\mathbf{x})} \in \sigma(A_d).$$

Hence if $[\ c_1, \ d_1] = \sigma(T_k)$, then $[\ c_1, \ d_1] \subset [\ c, \ d]$, and c_1 and d_1 can be used as the estimates of c and d.

Consider

$$\tilde{T}_k = D_k^{\frac{1}{2}} T_k D_k^{-\frac{1}{2}} = \text{tridiag}\left(\left(\frac{\delta_{k-1}}{\delta_{k-2}}\right)^{\frac{1}{2}}, \gamma_{k-1}, \sigma_k \left(\frac{\delta_{k-1}}{\delta_k}\right)^{\frac{1}{2}} \right). \qquad (3.3.36)$$

The matrices T_k and $\tilde{T}_k$ are similar, hence they have the same eigenvalues. Since

$$\sigma_k = \frac{(A_d \mathbf{p}_k, A_d \mathbf{p}_{k-1})}{(A_d \mathbf{p}_{k-1}, \mathbf{p}_{k-1})} = \frac{(A_d \mathbf{p}_k, \mathbf{p}_k + \gamma_{k-1} \mathbf{p}_{k-1} + \sigma_{k-1} \mathbf{p}_{k-2})}{(A_d \mathbf{p}_{k-1}, \mathbf{p}_{k-1})} = \frac{(A_d \mathbf{p}_k, \mathbf{p}_k)}{(A_d \mathbf{p}_{k-1}, \mathbf{p}_{k-1})} = \frac{\delta_k}{\delta_{k-1}},$$

$$\sigma_k \left(\frac{\delta_{k-1}}{\delta_k}\right)^{\frac{1}{2}} = \left(\frac{\delta_k}{\delta_{k-1}}\right)^{\frac{1}{2}},$$

then $\tilde{T}_k$ is a symmetric matrix,

$$\tilde{T}_k = \text{tridiag}(\sqrt{\sigma_{k-1}}, \gamma_{k-1}, \sqrt{\sigma_k}). \qquad (3.3.37)$$

A similar procedure can in principle be derived for the classical version of the Conjugate Gradient Method. One just has to rewrite the expressions for $\mathbf{p}_k$ in a similar way.

3.3.4 Jacoby Preconditioning.

The Polynomial Preconditioning is combined with Jacoby Preconditioning for further computational time reduction [39]. This procedure allows one to reduce the difference in the absolute values of the entries from different rows for the symmetric positive definite matrix. For the matrix under consideration there is a difference between the rows which correspond to the inside brain cubes and the ones which represent the cubes from the skull. Instead of the system,

$$A_d \mathbf{u}_d = \mathbf{b}_d,$$

one should consider the system

$$B A_d B \hat{\mathbf{u}}_d = B \mathbf{b}_d, \qquad (3.3.38)$$

53

where $\mathbf{u}_d = B\hat{\mathbf{u}}_d$, B is a diagonal matrix

$$B = \begin{bmatrix} \frac{1}{\sqrt{a_{11}}} & 0 & 0 & 0 & \cdots & 0 \\ 0 & \frac{1}{\sqrt{a_{22}}} & 0 & 0 & \cdots & 0 \\ 0 & 0 & \frac{1}{\sqrt{a_{33}}} & 0 & \cdots & 0 \\ \cdot & \cdot & \cdot & \cdot & \cdots & \cdot \\ 0 & 0 & 0 & 0 & \cdots & \frac{1}{\sqrt{a_{NN}}} \end{bmatrix}, \qquad (3.3.39)$$

where $a_{11}, a_{22}, ..., a_{NN}$ are the diagonal elements of A_d. The matrix BA_dB is symmetric positive definite, its diagonal elements are all equal to 1. The computation of B can be vectorized in practice with the Matlab procedure $diag.m$. This method does not require extra storage or extra CGM operations. It is supposed to improve the conditioning of the matrix A_d. By Gersgorin theorem [18], all the eigenvalues of the symmetric positive definite matrix are located within the union of n intervals,

$$\bigcup_{i=1}^{N} \left\{ |x - a_{ii}| < R_i'(A_d) \right\} \equiv G(A_d),$$

where

$$R_i'(A_d) = \sum_{\substack{j=1 \\ j \neq i}}^{N} |a_{ij}|, \quad 1 \leq i \leq N.$$

The eigenvalues of the matrix BA_dB lie within the interval $(1,2)$. The spectral condition number $\frac{\lambda_{max}(BA_dB)}{\lambda_{min}(BA_dB)}$ is normally less then $\frac{\lambda_{max}(A_d)}{\lambda_{min}(A_d)}$. Usually the Jacoby Preconditioning is combined with other preconditioning strategies.

The realization of the Finite Volume Method is simple enough and can be easily reproduced for an arbitrary grid resolution. The deflated matrix of the forward EEG problem is proved to be positive definite, so the Conjugate Gradient Method can be applied. The computational time can be reduced with the use of preconditioning strategies. The Polynomial Preconditioning is chosen and implemented due to its efficiency. The numerical results are given in Chapter 6. An implementation similar to the one here is given in [42].

54

It is called the finite difference modeling. It leads to a similar matrix but the positive semidefiniteness was not taken into account in [42] and the computational procedures are inferior to the one applied here in terms of speed. The ideas underlying the Finite Volume modeling will allow to extend the implementation in the case of a nonuniform grid. In such a case the deflated matrix will also be positive definite as this property is due to the underlying physics of the problem.

4   Non-iterative Inversion of the System Matrix.

The linear system which corresponds to the forward EEG problem for a single dipole was already described in detail in Chapter 2. The right-hand side of this linear system has only two nonzero entries, corresponding to the positive and negative current sources,

$$
\mathbf{b} = \begin{bmatrix} 0 \\ \cdot \\ b_i \\ 0 \\ \cdot \\ 0 \\ -b_j \\ \cdot \\ 0 \end{bmatrix}.
\tag{4.1}
$$

Here $b_i = b_j = \mathcal{I}$ is the intensity of the source. The indices i and j are defined as follows. Assume that (i_1, j_1, k_1) and (i_2, j_2, k_2) are indices corresponding to positive and negative current sources (see Chapter 3 for details). Then h is a parameter defining grid resolution, f is a function which defines the correspondence between the indexes numbering the system of all the cubes and the system containing only the cubes with nonzero conductivity.

$$
s_1 = \left(i_1 + \left[\frac{1}{h}\right] \right) \left(2\left[\frac{1}{h}\right] + 1 \right)^2 + \left(j_1 + \left[\frac{1}{h}\right] \right) \left(2\left[\frac{1}{h}\right] + 1 \right) + k_1 + \left[\frac{1}{h}\right] + 1,
$$

$$
\tag{4.2}
$$

$$
s_2 = \left(i_2 + \left[\frac{1}{h}\right] \right) \left(2\left[\frac{1}{h}\right] + 1 \right)^2 + \left(j_2 + \left[\frac{1}{h}\right] \right) \left(2\left[\frac{1}{h}\right] + 1 \right) + k_2 + \left[\frac{1}{h}\right] + 1,
$$

$$
i = f(s_1), \quad j = f(s_2.
$$

For the forward problem with a different right-hand side

$$
\mathbf{b}_1 = \begin{bmatrix} 0 \\ \cdot \\ b_{i_1} \\ 0 \\ \cdot \\ 0 \\ -b_{j_1} \\ \cdot \\ 0 \end{bmatrix}.
\tag{4.3}
$$

we can write

$$
\mathbf{b}_1 = \Pi_{ii_1}\Pi_{jj_1}\mathbf{b},
\tag{4.4}
$$

where the matrices Π_{ii_1} and Π_{jj_1} are permutation matrices of the form (4.8) with the properties

$$
\Pi_{ii_1} = \Pi_{i_1 i}, \qquad \Pi_{ii_1}^{-1} = \Pi_{ii_1}.
\tag{4.5}
$$

If $\mathbf{x}$ is the solution of $A\mathbf{x} = \mathbf{b}$, the solution of

$$
A\mathbf{y} = \mathbf{b}_1 = \Pi_{ii_1}\Pi_{jj_1}\mathbf{b}
\tag{4.6}
$$

is related to $\mathbf{x}$ by the formula

$$
\mathbf{y} = A^{-1}P A\mathbf{x}, \quad \text{where} \quad P = \Pi_{ii_1}\Pi_{jj_1}.
\tag{4.7}
$$

57

$$\Pi_{ii_1} = \begin{array}{c} \\ \\ \\ i \\ \\ \\ \\ i_1 \\ \\ \\ \\ \end{array} \begin{bmatrix} 1 & & & & & & \\ & \cdot & & & & & \\ & & 1 & & & & \\ & & & 0 & 0 & \cdot & \cdot & 1 \\ & & & 0 & 1 & & & \cdot \\ & & & & \cdot & \cdot & \cdot & \\ & & & & \cdot & & 1 & 0 \\ & & & 1 & \cdot & \cdot & 0 & 0 \\ & & & & & & & 1 \\ & & & & & & & & \cdot \\ & & & & & & & & & 1 \end{bmatrix},$$

$$\overset{i \qquad\qquad i_1}{}$$

(4.8)

and Π_{jj_1} can be written in the similar way.

Moreover

$$\mathbf{y} = A^{-1}IA\mathbf{x} + A^{-1}(P - I)A\mathbf{x} = \mathbf{x} + A^{-1}(P - I)A\mathbf{x}. \tag{4.9}$$

The matrix $P - I$ has only 4 nonzero elements. As a result the matrix $(P - I)A$ has only four nonzero rows. Therefore a much faster algorithm for the forward problem solution can be developed provided that the structure of the inverse of A is known. In fact for this

58

problem only the columns of A^{-1} with indexes i, i_1, j, j_1 need to be known.

$$
P - I = \begin{bmatrix}
0 & & & & & & & & \\
 & \cdot & & & & & & & \\
 & -1 & \cdot & 1 & & & & & \\
 & & \cdot & \cdot & \cdot & & & & \\
 & 1 & \cdot & -1 & & & & & \\
 & & & & \cdot & & & & \\
 & & & & & -1 & \cdot & 1 & \\
 & & & & & & \cdot & \cdot & \cdot \\
 & & & & & 1 & \cdot & -1 & \\
 & & & & & & & & \cdot \\
 & & & & & & & & 0
\end{bmatrix}
\tag{4.10}
$$

Each row of A has at most 13 nonzero elements and the matrix

$$
(P - I)A = \begin{bmatrix}
0 & 0 & \cdots & 0 \\
a_{i_1 1} - a_{i1} & a_{i_1 2} - a_{i2} & \cdots & a_{i_1 N} - a_{iN} \\
0 & 0 & \cdots & 0 \\
a_{i1} - a_{i_1 1} & a_{i2} - a_{i_1 2} & \cdots & a_{iN} - a_{i_1 N} \\
0 & 0 & \cdots & 0 \\
a_{j_1 1} - a_{j1} & a_{j_1 2} - a_{j2} & \cdots & a_{j_1 N} - a_{jN} \\
0 & 0 & \cdots & 0 \\
a_{j1} - a_{j_1 1} & a_{j2} - a_{j_1 2} & \cdots & a_{jN} - a_{j_1 N} \\
0 & 0 & \cdots & 0
\end{bmatrix}
\tag{4.11}
$$

has only four nonzero rows.

1) *One-dimensional Case.*

Let us first consider the one-dimensional case, i.e. one-dimensional chain of N cubic finite volume elements of unit conductivity connected sequentially.

59

Figure 4: One-dimensional Case.

For such a system the deflated matrix A has the form

$$A = \begin{bmatrix} 2 & -1 & 0 & & \cdots & & & \\ -1 & 2 & -1 & 0 & \cdots & & & \\ 0 & -1 & 2 & -1 & \cdots & & & \\ \cdot & \cdot & \cdot & \cdot & \cdots & \cdot & \cdot & \cdot \\ & & & & \cdots & -1 & 2 & -1 \\ & & & & \cdots & 0 & -1 & 1 \end{bmatrix} . \tag{4.12}$$

Recall that

$$A^{-1} = \frac{1}{\det A}\mathrm{adj}A, \tag{4.13}$$

60

where adj$A$ is the adjoint of A, obtained in the usual way by first taking $A(\{i\}', \{j\}')$ to be the submatrix of A without the i-th row and j-th column, then constructing the matrix of cofactors of A,

$$(-1)^{i+j} \det A(\{i\}', \{j\}'),$$

and finally transposing the latter. For the sake of simplicity we use notations B and b_{ij} to denote $(\text{adj}A)_{ij}$ and its elements

$$b_{ij} = (\text{adj}A)_{ij} = (-1)^{i+j} \det A(\{i\}', \{j\}'). \tag{4.14}$$

Denote by Δ_k the principal minors of A, i.e.

$$\Delta_k = \begin{bmatrix} 2 & -1 & 0 & & \cdots & & & \\ -1 & 2 & -1 & 0 & \cdots & & & \\ 0 & -1 & 2 & -1 & \cdots & & & \\ \cdot & \cdot & \cdot & \cdot & \cdots & \cdot & \cdot & \cdot \\ & & & & \cdots & -1 & 2 & -1 \\ & & & & \cdots & 0 & -1 & 2 \end{bmatrix}, \tag{4.15}$$

$1 \le k \le N = \dim A$.

Define $\Delta_0 = 1$, and $\Delta_1 = \det[2] = 2$. Expansion of $\Delta_k = \|a_{ij}\|_1^k$ with respect to the k-th row yields:

$$\Delta_k = \begin{cases} 2\Delta_{k-1} - \Delta_{k-2} & \text{for } k \ge 2, \\ \Delta_{k-1} - \Delta_{k-2} & \text{for } k = N. \end{cases} \tag{4.16}$$

They can be easily computed:

$$\Delta_2 = 2\Delta_1 - \Delta_0 = 2 \cdot 2 - 1 = 3,$$

$$\Delta_3 = 2\Delta_2 - \Delta_1 = 2 \cdot 3 - 2 = 4,$$

$$\Delta_4 = 2\Delta_3 - \Delta_2 = 2 \cdot 4 - 3 = 5,$$

61

$$\cdots$$

$$\Delta_{N-1} = N,$$

that is,

$$\Delta_k = \begin{cases} k+1, & k = 1, 2, ..., N-1 \\ \det A = \Delta_{N-1} - \Delta_{N-2} = 1, & k = N. \end{cases} \qquad (4.17)$$

A is symmetric, and so is adj A. The cofactors b_{mn} of A, satisfy $b_{mn} = b_{nm}$. If $m = n$, then by (4.14)

$$b_{nn} = (-1)^{2n} \begin{vmatrix} 2 & -1 & 0 & & & | & & & & \\ -1 & 2 & -1 & 0 & & | & & & & \\ 0 & -1 & 2 & -1 & 0 & | & & & & \\ & \cdot & \cdot & \cdot & & | & & & & \\ & & 0 & -1 & 2 & | & & & & \\ - & - & - & - & - & - & - & - & - & - & - \\ & & & & & | & 2 & -1 & 0 & \\ & & & & & | & -1 & 2 & -1 & 0 \\ & & & & & | & & \cdot & \cdot & \cdot \\ & & & & & | & & -1 & 2 & -1 \\ & & & & & | & & & 0 & -1 & 1 \end{vmatrix} = \det \begin{bmatrix} \|a_{ij}\|_1^{n-1} & 0 \\ 0 & F_{N-m} \end{bmatrix},$$

where

$$\|a_{ij}\|_1^{n-1} = \begin{bmatrix} 2 & -1 & 0 & \\ -1 & 2 & -1 & 0 \\ \cdot & \cdot & \cdots & \cdot \\ & & 0 & -1 & 2 \end{bmatrix},$$

62

$$F_{N-m} = \begin{bmatrix} 2 & -1 & 0 & & \cdots & & & \\ -1 & 2 & -1 & 0 & \cdots & & & \\ 0 & -1 & 2 & -1 & \cdots & & & \\ \cdot & \cdot & \cdot & \cdot & \cdots & \cdot & \cdot & \cdot \\ & & & & \cdots & -1 & 2 & -1 \\ & & & & \cdots & 0 & -1 & 1 \end{bmatrix}.$$

F_{N-m} is a matrix of the same structure as A, except that rather than being N by N, it is (N-m) by (N-m). Since $\det F_{N-m} = \det \Delta_N = 1$, we have

$$b_{nn} = \det \|a_{ij}\|_1^{n-1} = \Delta_{n-1} = n. \tag{4.18}$$

Let us now consider nondiagonal elements b_{mn}. More precisely

$$b_{21} = b_{12} = (-1)^{1+2} \det \begin{bmatrix} -1 & 0 & \cdots & 0 \\ -1 & & & \\ 0 & & F_{N-2} & \\ \cdot & & & \\ 0 & & & \end{bmatrix} = (-1)^{1+2} \cdot (-1) \det F_{N-2} = 1,$$

$$b_{31} = b_{13} = (-1)^{1+3} \det \begin{bmatrix} -1 & 0 & \cdot & & \cdot & \cdot \\ 2 & -1 & 0 & & \cdot & \cdot \\ 0 & -1 & \cdot & & \cdot & \cdot \\ 0 & 0 & & & & \\ \cdot & \cdot & & F_{N-3} & & \\ 0 & 0 & & & & \end{bmatrix} = (-1)^{1+3}(-1)^{3-1} \det F_{N-3} = 1,$$

$$\cdots$$

$$b_{n1} = b_{1n} = \det(-1)^{1+k}(-1)^{k-1} \det F_{N-n} = 1, n > 1. \tag{4.19}$$

63

$$b_{23} = b_{32} = (-1)^{2+3} \det \begin{bmatrix} 2 & 0 & \cdot & \cdots & 0 \\ -1 & -1 & 0 & \cdots & 0 \\ 0 & -1 & & & \\ \cdot & 0 & & & \\ \cdot & \cdot & & F_{N-3} & \\ 0 & 0 & & & \end{bmatrix} = 2 \cdot (-1)^{2+3} \cdot (-1) \det F_{N-3} = 2,$$

$$b_{24} = b_{42} = (-1)^{2+4} \det \begin{bmatrix} 2 & 0 & \cdot & \cdot & \cdots & 0 \\ -1 & -1 & 0 & \cdots & & 0 \\ 0 & 2 & -1 & 0 & \cdots & 0 \\ 0 & 0 & -1 & & & \\ \cdot & \cdot & \cdot & & F_{N-4} & \\ \cdot & \cdot & \cdot & & & \end{bmatrix} = 2 \cdot (-1)^{2+4}(-1)^2 \det F_{N-3} = 2.$$

$$\cdots$$

$$b_{n2} = b_{2n} = 2 \cdot (-1)^{2+n}(-1)^{n-2} \det F_{N-n} = 2, \quad n \geq 3. \tag{4.20}$$

$$b_{43} = b_{34} = (-1)^{3+4} \det \begin{bmatrix} 2 & -1 & 0 & \cdot & \cdots & 0 \\ -1 & 2 & 0 & \cdot & \cdots & 0 \\ 0 & -1 & -1 & 0 & \cdots & 0 \\ 0 & 0 & -1 & & & \\ \cdot & \cdot & 0 & & F_{N-4} & \\ \cdot & \cdot & \cdot & & & \end{bmatrix} = (-1)^{3+4} \det \begin{bmatrix} 2 & -1 \\ -1 & 2 \end{bmatrix} \cdot (-1) \det F_{N-4} = 3.$$

64

$$b_{53} = b_{35} = (-1)^{3+5} \det \begin{bmatrix} 2 & -1 & 0 & \cdot & \cdot & \cdots & 0 \\ -1 & 2 & 0 & \cdot & \cdot & \cdots & 0 \\ 0 & -1 & -1 & 0 & \cdot & \cdots & 0 \\ \cdot & 0 & 0 & -1 & & & \\ \cdot & \cdot & \cdot & 0 & & F_{N-5} & \\ \cdot & \cdot & \cdot & \cdot & & & \end{bmatrix} = \det \begin{bmatrix} 2 & -1 \\ -1 & 2 \end{bmatrix} (-1)^2 \det F_{N-5} = 3.$$

$$\cdots$$

$$b_{n3} = b_{3n} = \det \begin{bmatrix} 2 & -1 \\ -1 & 2 \end{bmatrix} \det (-1)^{3+n}(-1)^{n-3} \det F_{N-n} = 3, \quad n \geq 4. \qquad (4.21)$$

There emerges a pattern,

$$b_{nk} = b_{kn} = \det \begin{bmatrix} a_{11} & \cdots & a_{1\ k-1} \\ & \cdot & \\ a_{k-1\ 1} & \cdots & a_{k-1\ k-1} \end{bmatrix} (-1)^{k+n}(-1)^{n-k} \det F_{N-n}$$

$$= \Delta_{k-1} \det F_{N-n} = k. \qquad (4.22)$$

which can be easily proved using mathematical induction. The inverse of A thus has the form:

$$A^{-1} = \begin{bmatrix} 1 & 1 & 1 & 1 & 1 & 1 & 1 & \cdots \\ 1 & 2 & 2 & 2 & 2 & 2 & 2 & \cdots \\ 1 & 2 & 3 & 3 & 3 & 3 & 3 & \cdots \\ 1 & 2 & 3 & \cdots & \cdots & \cdots & \cdots & \cdots \\ 1 & 2 & 3 & \cdots & k-1 & k-1 & k-1 & \cdots \\ 1 & 2 & 3 & \cdots & k-1 & k & k & \cdots \\ 1 & 2 & 3 & \cdots & k-1 & k & k+1 & \cdots \\ \cdots & \cdots & \cdots & \cdots & \cdots & \cdots & \cdots & \cdots \end{bmatrix} \qquad (4.23)$$

In such a case $A^{-1}(P - I)A$ can be trivially computed.

65

2) Two-dimensional Case.

Now consider a less trivial case of the conducting square plate broken up into $N \times N$ cubic finite volume elements of unit conductivity. In this case the matrix A is $N \times N$ and has the following block structure,

$$
A = \begin{bmatrix}
A_1 & -I & & & & \\
-I & A_2 & -I & & & \\
0 & -I & A_2 & -I & & \\
& & \cdot & \cdot & \cdot & \\
& & & -I & A_2 & -I \\
& & & & -I & A_1
\end{bmatrix}, \tag{4.24}
$$

where I is the N by N identity matrix, A_1 and A_2 are tri-diagonal N by N matrices of the form,

$$
A_1 = \begin{bmatrix}
2 & -1 & & & & \\
-1 & 3 & -1 & & & \\
& -1 & 3 & -1 & & \\
& & \cdot & \cdot & \cdot & \\
& & & -1 & 3 & -1 \\
& & & & -1 & 2
\end{bmatrix}, \quad
A_2 = \begin{bmatrix}
3 & -1 & & & & \\
-1 & 4 & -1 & & & \\
& -1 & 4 & -1 & & \\
& & \cdot & \cdot & \cdot & \\
& & & -1 & 4 & -1 \\
& & & & -1 & 3
\end{bmatrix} \tag{4.25}
$$

A can be viewed as an N by N matrix with entries from the $\{A_1, A_1^{-1}\}$-generated ring since $A_2 = A_1 + I$. Thus block entries of A are from the minimal ring generated by A_1.

66

Figure 5: Two-dimensional Case.

Before we compute A^{-1}, let us first invert an $N \times N$ matrix with scalar entries

$$M = \begin{bmatrix} a_1 & -1 & & & & & \\ -1 & a_2 & -1 & & & & \\ & -1 & a_2 & -1 & & & \\ & & & \cdot & & & \\ & & & & \cdot & & \\ & & & & & \cdot & \\ & & & & -1 & a_2 & -1 \\ & & & & & -1 & a_1 \end{bmatrix} , \quad a_2 = a_1 + 1, \qquad (4.26)$$

67

To do this we introduce notations,

$$M_1 = \begin{bmatrix} a_1 \end{bmatrix}, \ M_2 = \begin{bmatrix} a_1 & -1 \\ -1 & a_2 \end{bmatrix}, \ M_3 = \begin{bmatrix} a_1 & -1 & 0 \\ -1 & a_2 & -1 \\ 0 & -1 & a_1 \end{bmatrix}, \ \cdots, \tag{4.27}$$

$$M_k = \begin{bmatrix} a_1 & -1 \\ -1 & a_2 & -1 \\ & -1 & a_2 & -1 \\ & & & . \\ & & & & . \\ & & & & & . \\ & & & & & -1 & a_2 \end{bmatrix}, \ \cdots, M_N = M, \tag{4.28}$$

$$\text{and} \ \ \Delta_k = \begin{cases} 1, & k = 0 \\ \det M_k, & 1 \le k \le N. \end{cases} \tag{4.29}$$

Each three consecutive Δ_k are related by

$$\Delta_k = a_k \Delta_{k-1} - \Delta_{k-2}, \ \text{where} \ a_k = \begin{cases} a_2, & k = 2, ..., N-1, \\ a_1, & k = N. \end{cases} \tag{4.30}$$

Define

$$\xi_k = \begin{bmatrix} \Delta_{k-1} \\ \Delta_k \end{bmatrix}, \ \ 1 \le k \le N. \tag{4.31}$$

Then for $k < N$ (4.30) takes the form:

$$\xi_{k-1} = T\xi_k, \ \ \ T = \begin{bmatrix} 0 & 1 \\ -1 & a_2 \end{bmatrix} = U\mathcal{D}U^{-1},$$

where

$$U = \begin{bmatrix} 1 & 1 \\ \lambda_1 & \lambda_2 \end{bmatrix}, \ \ \mathcal{D} = \begin{bmatrix} \lambda_1 & 0 \\ 0 & \lambda_2 \end{bmatrix}, \ \ U^{-1} = \frac{1}{\lambda_2 - \lambda_1} \begin{bmatrix} \lambda_2 & -1 \\ -\lambda_1 & 1 \end{bmatrix}, \tag{4.32}$$

68

and

$$\lambda_1 = \frac{a_2}{2} + \frac{\sqrt{a_2^2 - 4}}{2}, \quad \lambda_2 = \frac{a_2}{2} - \frac{\sqrt{a_2^2 - 4}}{2}, \quad e_1 = \begin{bmatrix} 1 \\ \lambda_1 \end{bmatrix} \quad \text{and} \quad e_2 = \begin{bmatrix} 1 \\ \lambda_2 \end{bmatrix} \tag{4.33}$$

are the eigenvalues and eigenvectors of T.

(4.30) can be explicitly solved,

$$\xi_{k-1} = T^k \xi_1 = U\mathcal{D}^k U^{-1}\xi_1, \quad k = 1, 2, 3, ..., N - 2 \tag{4.34}$$

and

$$\begin{bmatrix} \Delta_{N-1} \\ \Delta_N \end{bmatrix} = \xi_N = \begin{bmatrix} 0 & 1 \\ -1 & a_1 \end{bmatrix} \xi_{N-1} = \begin{bmatrix} 0 & 1 \\ -1 & a_1 \end{bmatrix} U\mathcal{D}^{N-2}U^{-1}\xi_1. \tag{4.35}$$

The matrix on the right-hand side is

$$F = \begin{bmatrix} 0 & 1 \\ -1 & a_1 \end{bmatrix} U\mathcal{D}^{N-2}U^{-1} = \frac{1}{\lambda_2 - \lambda_1} \begin{bmatrix} f_{11}(\lambda_1, \lambda_2, a_1) & f_{12}(\lambda_1, \lambda_2, a_1) \\ f_{21}(\lambda_1, \lambda_2, a_1) & f_{22}(\lambda_1, \lambda_2, a_1) \end{bmatrix} \tag{4.36}$$

where

$$f_{11} = \lambda_1^{n-1}\lambda_2 - \lambda_2^{n-1}\lambda_1, \quad f_{12} = \lambda_2^{n-1} - \lambda_1^{n-1},$$

$$f_{21} = \lambda_1^{n-2}\lambda_2(a_1\lambda_1 - 1) - \lambda_2^{n-2}\lambda_1(a_1\lambda_2 - 1), \quad f_{22} = \lambda_2^{n-2}(a_1\lambda_2 - 1) - \lambda_1^{n-2}(a_1\lambda_1 - 1).$$

Therefore

$$\Delta_N = \frac{f_{21} + f_{22}a_1}{\lambda_2 - \lambda_1} = \frac{1}{\lambda_2 - \lambda_1}\{\lambda_1^{N-2}\lambda_2(a_1\lambda_1 - 1) - \lambda_2^{N-2}\lambda_1(a_1\lambda_2 - 1)\}$$

$$+ \frac{a_1}{\lambda_2 - \lambda_1}\{\lambda_2^{N-2}(a_1\lambda_2 - 1) - \lambda_1^{N-2}(a_1\lambda_1 - 1)\}$$

$$= \frac{1}{\lambda_2 - \lambda_1}\{\lambda_1^{N-2}(\lambda_2 - a_1)(a_1\lambda_1 - 1) - \lambda_2^{N-2}(\lambda_1 - a_1)(a_1\lambda_2 - 1)\}. \tag{4.37}$$

$$\lambda_1^2 = \frac{a_2^2}{2} + \frac{a_2\sqrt{a_2^2 - 4}}{2} - 1 = a_2(\frac{a_2^2}{2} + \frac{\sqrt{a_2^2 - 4}}{2}) - 1 = a_2\lambda_1 - 1, \tag{4.38}$$

$$\lambda_2^2 = \frac{a_2^2}{2} - \frac{a_2\sqrt{a_2^2 - 4}}{2} - 1 = a_2(\frac{a_2^2}{2} - \frac{\sqrt{a_2^2 - 4}}{2}) - 1 = a_2\lambda_2 - 1. \tag{4.39}$$

69

We can replace the terms $(a_1\lambda_1 - 1)$, $(a_1\lambda_2 - 1)$, $(\lambda_2 - a_1)$ and $(\lambda_1 - a_1)$ in (4.37) with

$$a_1\lambda_1 - 1 = (a_2 - 1)\lambda_1 - 1 = \lambda_1^2 - \lambda_1, \tag{4.40}$$

$$a_1\lambda_2 - 1 = (a_2 - 1)\lambda_2 - 1 = \lambda_2^2 - \lambda_2, \tag{4.41}$$

$$\lambda_2 - a_1 = 1 + \lambda_2 - a_2 = 1 - \frac{a_2}{2} - \frac{\sqrt{a_2^2 - 4}}{2} = 1 - \lambda_1, \tag{4.42}$$

$$\lambda_1 - a_1 = 1 + \lambda_1 - a_2 = 1 - \frac{a_2}{2} + \frac{\sqrt{a_2^2 - 4}}{2} = 1 - \lambda_2. \tag{4.43}$$

This gives us,

$$\Delta_N = \frac{1}{\lambda_2 - \lambda_1}\{\lambda_1^{N-2}(1 - \lambda_1)(\lambda_1^2 - \lambda_1) - \lambda_2^{N-2}(1 - \lambda_2)(\lambda_2^2 - \lambda_2)\}$$

$$= \frac{1}{\lambda_2 - \lambda_1}\{\lambda_1^{N-1}(\lambda_1 - 1)^2 - \lambda_2^{N-1}(\lambda_2 - 1)^2\}. \tag{4.44}$$

Note that $\lambda_1\lambda_2 = 1$.

Δ_N is a polynomial of a_2. To determine its form we take

$$\Delta_N = \frac{1}{\lambda_2 - \lambda_1}\left\{\lambda_1^{N+1} - \lambda_2^{N+1} - 2(\lambda_1^N - \lambda_2^N) + \lambda_1^{N-1} - \lambda_2^{N-1}\right\}. \tag{4.45}$$

and replace λ_1, λ_2 with s and d defined by

$$s = \lambda_1 + \lambda_2 = a_2, \quad d = \lambda_1 - \lambda_2 = \sqrt{a_2^2 - 4}. \tag{4.46}$$

Let

$$q = \max\{m - 1 - k, k\} - \min\{m - 1 - k, k\}, \tag{4.47}$$

$$C_q^t = \frac{q!}{t!(q - t)!}, \tag{4.48}$$

$$\left[\frac{m - 1}{2}\right] = \begin{cases} \frac{m-1}{2}, & \text{if } m \text{ is odd,} \\ \frac{m-2}{2}, & \text{if } m \text{ is even.} \end{cases} \tag{4.49}$$

For arbitrary $m > 1$, the ratio

$$\frac{\lambda_1^m - \lambda_2^m}{\lambda_1 - \lambda_2} = \sum_{k=0}^{m-1} \lambda_1^{m-1-k}\lambda_2^k = \begin{cases} \sum_{k=0}^{[\frac{m-1}{2}]}(\lambda_1^{m-1-k}\lambda_2^k + \lambda_2^{m-1-k}\lambda_1^k), & \text{if } m \text{ is odd,} \\ \sum_{k=0}^{[\frac{m-1}{2}]}(\lambda_1^{m-1-k}\lambda_2^k + 1 + \lambda_2^{m-1-k}\lambda_1^k) & \text{if } m \text{ is even.} \end{cases} \tag{4.50}$$

70

Furthermore using $\lambda_1 \lambda_2 = 1$

$$\sum_{k=0}^{[\frac{m-1}{2}]} (\lambda_1^{m-1-k} \lambda_2^k + \lambda_2^{m-1-k} \lambda_1^k) =$$

$$= \sum_{k=0}^{[\frac{m-1}{2}]} (\lambda_1 \lambda_2)^{\min\{m-1-k,k\}} \left(\lambda_2^{\max\{m-1-k,k\}-\min\{m-1-k,k\}} + \lambda_1^{\max\{m-1-k,k\}-\min\{m-1-k,k\}} \right)$$

$$= \sum_{k=0}^{[\frac{m-1}{2}]} (\lambda_1^q + \lambda_2^q) = \sum_{k=0}^{[\frac{m-1}{2}]} \left\{ \left(\frac{s+d}{2} \right)^q + \left(\frac{s-d}{2} \right)^q \right\}$$

$$= \sum_{k=0}^{[\frac{m-1}{2}]} \frac{1}{2^q} \left(\sum_{t=0}^{q} C_q^t s^{q-t} d^t + \sum_{t=0}^{q} (-1)^t C_q^t s^{q-t} d^t \right),$$

$$= \sum_{k=0}^{[\frac{m-1}{2}]} \frac{1}{2^{q-1}} \sum_{l=0}^{[\frac{q}{2}]} C_q^{2l} a_2^{q-2l} (a_2^2 - 4)^l = P_{[\frac{m-1}{2}]}(a_2). \tag{4.51}$$

Here $P_{[\frac{m-1}{2}]}(a_2)$ is the polynomial of degree $[\frac{m-1}{2}]$ defined by the second last part of the string of identities above. Hence

$$\Delta_N = P_{[\frac{N}{2}]}(a_2) - 2P_{[\frac{N-1}{2}]}(a_2) + P_{[\frac{N-2}{2}]}(a_2). \tag{4.52}$$

For $1 \leq k \leq N - 1$,

$$\begin{bmatrix} \Delta_{k-1} \\ \Delta_k \end{bmatrix} = \xi_k = T^{k-1} \xi_1 = U D^{k-1} U^{-1} \xi_1 = U D^{k-1} U^{-1} \begin{bmatrix} \Delta_0 \\ \Delta_1 \end{bmatrix}$$

$$= \frac{1}{\lambda_2 - \lambda_1} \begin{bmatrix} 1 & 1 \\ \lambda_1 & \lambda_2 \end{bmatrix} \begin{bmatrix} \lambda_1^{k-1} & 0 \\ 0 & \lambda_2^{k-1} \end{bmatrix} \begin{bmatrix} \lambda_2 & -1 \\ -\lambda_1 & 1 \end{bmatrix} \begin{bmatrix} 1 \\ a_1 \end{bmatrix}$$

$$= \frac{1}{\lambda_2 - \lambda_1} \begin{bmatrix} 1 & 1 \\ \lambda_1 & \lambda_2 \end{bmatrix} \begin{bmatrix} \lambda_1^{k-1} & 0 \\ 0 & \lambda_2^{k-1} \end{bmatrix} \begin{bmatrix} \lambda_2 - a_1 \\ a_1 - \lambda_1 \end{bmatrix}$$

$$\frac{1}{\lambda_2 - \lambda_1} \begin{bmatrix} 1 & 1 \\ \lambda_1 & \lambda_2 \end{bmatrix} \begin{bmatrix} \lambda_1^{k-1}(1-\lambda_1) \\ \lambda_2^{k-1}(\lambda_2 - 1) \end{bmatrix}$$

$$= \frac{1}{\lambda_2 - \lambda_1} \begin{bmatrix} \lambda_1^{k-1}(1-\lambda_1) + \lambda_2^{k-1}(\lambda_2 - 1) \\ \lambda_1^k(1-\lambda_1) + \lambda_2^k(\lambda_2 - 1) \end{bmatrix}. \tag{4.53}$$

71

$$\Delta_k = \frac{1}{\lambda_2 - \lambda_1}\left(\lambda_1^k(1 - \lambda_1) + \lambda_2^k(\lambda_2 - 1)\right)$$

$$= \frac{\lambda_1^{k+1} - \lambda_2^{k+1}}{\lambda_1 - \lambda_2} - \frac{\lambda_1^k - \lambda_2^k}{\lambda_1 - \lambda_2} = P_{[\frac{k}{2}]}(a_2) - P_{[\frac{k-1}{2}]}(a_2). \qquad (4.54)$$

Again let b_{ij} denote elements of adj M. For the diagonal elements,

$$b_{11} = \det\begin{bmatrix} a_2 & -1 & & & & \\ -1 & a_2 & -1 & & & \\ & & \cdot & & & \\ & & & -1 & a_2 & -1 \\ & & & & -1 & a_1 \end{bmatrix} = \det\begin{bmatrix} a_1 & -1 & & & & \\ -1 & a_2 & -1 & & & \\ & & \cdot & & & \\ & & & -1 & a_2 & -1 \\ & & & & -1 & a_2 \end{bmatrix} = \Delta_{N-1},$$

$$b_{22} = \det\begin{bmatrix} a_1 & 0 & \cdot & \cdot & \cdot & \cdot & \cdot \\ 0 & a_2 & -1 & & & & \\ \cdot & -1 & a_2 & -1 & & & \\ \cdot & & & \cdot & & & \\ \cdot & & & & -1 & a_2 & -1 \\ \cdot & & & & & -1 & a_1 \end{bmatrix} = a_1 \det\begin{bmatrix} a_2 & -1 & & & \\ -1 & a_2 & -1 & & \\ & & \cdot & & \\ & & -1 & a_2 & -1 \\ & & & -1 & a_1 \end{bmatrix}$$

$$= a_1\Delta_{N-2} = \Delta_1\Delta_{N-2},$$

$$b_{33} = \det\begin{bmatrix} a_1 & -1 & 0 & \cdot & \cdot & \cdot & \cdot \\ -1 & a_2 & 0 & \cdot & \cdot & \cdot & \cdot \\ 0 & 0 & a_2 & -1 & & & \\ 0 & 0 & -1 & a_2 & -1 & & \\ \cdot & \cdot & & & \cdot & & \\ \cdot & \cdot & & & -1 & a_2 & -1 \\ \cdot & \cdot & & & & -1 & a_1 \end{bmatrix} = \det\begin{bmatrix} a_1 & -1 \\ -1 & a_2 \end{bmatrix}\Delta_{n-3} = \Delta_2\Delta_{n-3}.$$

There emerges a pattern

$$b_{ii} = \begin{cases} b_{N+1-i,N+1-i}\Delta_{i-1}\Delta_{N-i}, & 2 \le i \le N-1, \\ \\ \Delta_{N-1}, & i = N. \end{cases} \tag{4.55}$$

As far as the nondiagonal b_{ij}'s are concerned,

$$b_{21} = b_{12} = (-1)^{2+1} \det \begin{bmatrix} -1 & 0 & \cdot & \cdot & \cdot \\ -1 & & & & \\ 0 & & M_{n-2} & & \\ \cdot & & & & \\ \cdot & & & & \end{bmatrix} = \Delta_{N-2},$$

$$b_{31} = b_{13} = (-1)^{3+1} \det \begin{bmatrix} -1 & 0 & \cdot & \cdot & \cdot \\ a_2 & -1 & 0 & \cdot & \cdot \\ 0 & -1 & & & \\ \cdot & 0 & & M_{n-3} & \\ \cdot & \cdot & & & \end{bmatrix} = \det M_{n-3} = \Delta_{n-3}.$$

$$\cdots$$

$$b_{k1} = b_{1k} = (-1)^{k+1}(-1)^{k-1}\Delta_{n-k} = \Delta_{n-k}, \quad 1 \le k \le N. \tag{4.56}$$

$$b_{23} = (-1)^{2+3} \det \begin{bmatrix} a_1 & 0 & \cdot & \cdot & \cdot \\ -1 & -1 & 0 & \cdot & \cdot \\ 0 & -1 & & & \\ \cdot & 0 & & M_{nN-3} & \\ \cdot & \cdot & & & \end{bmatrix} = (-1)^{2+3} \det \begin{bmatrix} a_1 & 0 \\ -1 & -1 \end{bmatrix} \det M_{N-3} = \Delta_1 \Delta_{N-3}.$$

73

$$b_{24} = \det \begin{bmatrix} a_1 & 0 & \cdot & \cdot & & \cdot & \cdot \\ -1 & -1 & 0 & \cdot & & \cdot & \cdot \\ 0 & a_2 & -1 & 0 & & & \cdot & \cdot \\ \cdot & & 0 & -1 & & & \\ \cdot & & \cdot & 0 & & M_{N-4} & \\ \cdot & & \cdot & & \cdot & & \end{bmatrix} = \det \begin{bmatrix} a_1 & 0 \\ -1 & -1 \end{bmatrix} \det M_{N-4} = \Delta_1 \Delta_{N-4}$$

$$b_{2k} = b_{k2} = (-1)^{k+2}(-1)^{k-2} \det \begin{bmatrix} a_1 & 0 \\ -1 & -1 \end{bmatrix} \Delta_{N-k} = \Delta_1 \Delta_{N-k}. \tag{4.57}$$

Again a clear pattern

$$b_{lk} = b_{kl} = (-1)^{l+k}(-1)^{N-l} \Delta_{l-1} \Delta_{N-k} \tag{4.58}$$

emerges and can be proved using mathematical induction.

In summary:

$$\mathrm{adj}M = \begin{bmatrix} \Delta_{N-1} & \Delta_{N-2} & \Delta_{N-3} & \Delta_{N-4} & \cdots & \Delta_1 & \Delta_0 \\ \Delta_{N-2} & \Delta_{N-2}\Delta_1 & \Delta_{N-3}\Delta_1 & \Delta_{N-4}\Delta_1 & \cdots & \Delta_1\Delta_1 & \Delta_1 \\ \Delta_{N-3} & \Delta_{N-3}\Delta_1 & \Delta_{N-3}\Delta_2 & \Delta_{N-4}\Delta_2 & \cdots & \Delta_1\Delta_2 & \Delta_2 \\ \Delta_{N-4} & \Delta_{N-4}\Delta_1 & \Delta_{N-4}\Delta_2 & \Delta_{N-4}\Delta_3 & \cdots & \Delta_1\Delta_3 & \Delta_3 \\ \cdot & \cdot & \cdot & \cdot & \cdots & \cdot & \cdot \\ \cdot & \cdot & \cdot & \cdot & \cdots & \cdot & \cdot \\ \Delta_1 & \Delta_1\Delta_1 & \Delta_1\Delta_2 & \Delta_1\Delta_3 & \cdots & \Delta_1\Delta_{N-2} & \Delta_{N-2} \\ \Delta_0 & \Delta_1 & \Delta_2 & \Delta_3 & \cdots & \Delta_{N-2} & \Delta_{N-1} \end{bmatrix} , \tag{4.59}$$

and

$$M^{-1} = \Delta_N^{-1} \mathrm{adj}M. \tag{4.60}$$

74

Since $A_1 A_2 = A_2 A_1$, A can be thought of as an $N \times N$ matrix with entries from an $\{A_1, A_1^{-1}\}$-generated ring, which we denote by $\mathcal{F}$. We can construct $\mathcal{F}$-valued determinants

$$D_0, D_1, D_2, ..., D_N$$

obtained from

$$\Delta_0, \Delta_1, \Delta_2, ..., \Delta_N,$$

by replacing 1 with I, a_1 with A_1, and a_2 with A_2. Then

$$D_k = \begin{cases} I, & k = 0 \\ A_1, & k = 1 \\ A_2 D_{k-1} - D_{k-2} & 2 \leq k \leq N - 1 \\ A_1 D_{N-1} - D_{N-2} & k = N, \end{cases} \tag{4.61}$$

and

$$A^{-1} = D_N^{-1} \begin{bmatrix} D_{N-1} & D_{N-2} & D_{N-3} & D_{N-4} & \cdots & D_1 & D_0 \\ D_{N-2} & D_{N-2}D_1 & D_{N-3}D_1 & D_{N-4}D_1 & \cdots & D_1 D_1 & D_1 \\ D_{N-3} & D_{N-3}D_1 & D_{N-3}D_2 & D_{N-4}D_2 & \cdots & D_1 D_2 & D_2 \\ D_{N-4} & D_{N-4}D_1 & D_{N-4}D_2 & D_{N-4}D_3 & \cdots & D_1 D_3 & D_3 \\ \cdot & \cdot & \cdot & \cdot & \cdots & \cdot & \cdot \\ \cdot & \cdot & \cdot & \cdot & \cdots & \cdot & \cdot \\ D_1 & D_1 D_1 & D_1 D_2 & D_1 D_3 & \cdots & D_1 D_{N-2} & D_{N-2} \\ D_0 & D_1 & D_2 & D_3 & \cdots & D_{N-2} & D_{N-1} \end{bmatrix} \tag{4.62}$$

Thus the process of inversion of the N^2 by N^2 matrix A can be replaced with the inversion of a much smaller matrix $D_N = P_{\lfloor \frac{m-1}{2} \rfloor}(A_2)$. If f_i are the eigenvalues of A_2 and $\mathcal{U}$ is the matrix whose columns are the eigenvectors of A,

$$D_N^{-1} = \mathcal{U} \cdot \text{diag}\left\{ \frac{1}{P(f_i)} \right\} \cdot \mathcal{U}^{-1}. \tag{4.63}$$

75

For $N = 3$,

$$f_1 = 2, \quad f_2 = 3, \quad f_3 = 5.$$

For $N = 4$,

$$f_1 = 2, \quad f_2 = 4 \quad f_3 = 4 + \sqrt{2}, \quad f_4 = 4 - \sqrt{2}.$$

For $N = 5$,

$$f_{1,2} = \frac{7 \pm \sqrt{5}}{2}, \quad f_3 = 2, \quad f_{4,5} = \frac{9 \pm \sqrt{5}}{2}.$$

For large values of N one needs to compute the eigenvalues of A_2 numerically.

3) *Three-dimensional Case.*

Now consider the three-dimensional case of an $N \times N \times N$ cube of finite volume elements. For such a homogeneous cube the matrix of the forward problem has the form

$$A = \begin{bmatrix} G_1 & -I & & & & & \\ -I & G_2 & -I & & & & \\ & -I & G_2 & -I & & & \\ & & & \cdot & & & \\ & & & & \cdot & & \\ & & & & & \cdot & \\ & & & & -I & G_2 & -I \\ & & & & & -I & G_1 \end{bmatrix}, \tag{4.64}$$

where I is an N^2 by N^2 identity matrix, and the matrices G_1 and G_2 in turn are $N^2 \times N^2$

76

blocks, which have the form

$$
G_1 = \begin{bmatrix}
S_1 & -I & & & & & \\
-I & S_2 & -I & & & & \\
& -I & S_2 & -I & & & \\
& & & \cdot & & & \\
& & & & \cdot & & \\
& & & & & \cdot & \\
& & & & -I & S_2 & -I \\
& & & & & -I & S_1
\end{bmatrix},
\tag{4.65}
$$

$$
G_2 = \begin{bmatrix}
S_2 & -I & & & & & \\
-I & S_3 & -I & & & & \\
& -I & S_3 & -I & & & \\
& & & \cdot & & & \\
& & & & \cdot & & \\
& & & & & \cdot & \\
& & & & -I & S_3 & -I \\
& & & & & -I & S_2
\end{bmatrix},
\tag{4.66}
$$

77

with $N \times N$ blocks S_1, S_2, S_3 of the form

$$S_1 = \begin{bmatrix} 3 & -1 & & & & & \\ -1 & 4 & -1 & & & & \\ & -1 & 4 & -1 & & & \\ & & & \cdot & & & \\ & & & & \cdot & & \\ & & & & & \cdot & \\ & & & & -1 & 4 & -1 \\ & & & & & -1 & 3 \end{bmatrix}, \quad S_2 = \begin{bmatrix} 4 & -1 & & & & & \\ -1 & 5 & -1 & & & & \\ & -1 & 5 & -1 & & & \\ & & & \cdot & & & \\ & & & & \cdot & & \\ & & & & \cdot & & \\ & & & & -1 & 5 & -1 \\ & & & & & -1 & 4 \end{bmatrix},$$

$$S_3 = \begin{bmatrix} 5 & -1 & & & & & \\ -1 & 6 & -1 & & & & \\ & -1 & 6 & -1 & & & \\ & & & \cdot & & & \\ & & & & \cdot & & \\ & & & & \cdot & & \\ & & & & -1 & 6 & -1 \\ & & & & & -1 & 5 \end{bmatrix}$$

78

Figure 6: Three-dimensional Case.
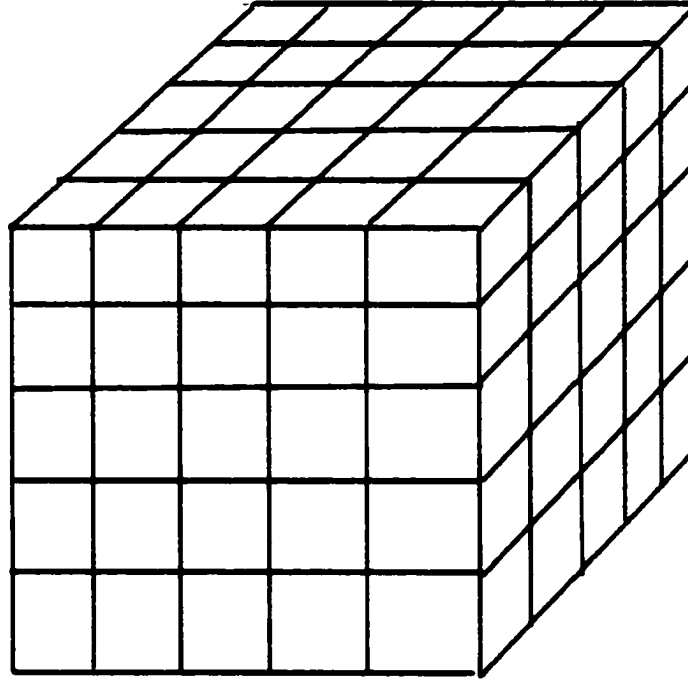
Due to the equalities $S_3 = S_2 + I, S_2 = S_1 + I$ and $G_2 = G_1 + I$, G_1 and G_2 commute, as do S_1, S_2, S_3. We can thus view A as either an $N \times N$ matrix with elements from the $\{G_2, G_2^{-1}\}$-generated ring or an $N^2 \times N^2$ matrix with elements from the $\{S_2, S_2^{-1}\}$-generated ring.

Therefore construction of the inverse of A for the three-dimensional case can be reduced to the construction of the inverse for a much smaller matrix such as for the two-dimensional case.

79

Define

$$
\Gamma_k = \begin{cases}
I, & k = 0; \\
G_1, & k = 1; \\
G_2\Gamma_{k-1} - \Gamma_{k-2}, & \text{for } k = 2, N-1 \\
G_1\Gamma_{N-1} - \Gamma_{N-2}, & k = N.
\end{cases}
\tag{4.67}
$$

As before

$$
A^{-1} = \Gamma_N^{-1}
\begin{bmatrix}
\Gamma_{N-1} & \Gamma_{N-2} & \Gamma_{N-3} & \Gamma_{N-4} & \cdots & \Gamma_1 & \Gamma_0 \\
\Gamma_{N-2} & \Gamma_{N-2}\Gamma_1 & \Gamma_{N-3}\Gamma_1 & \Gamma_{N-4}\Gamma_1 & \cdots & \Gamma_1\Gamma_1 & \Gamma_1 \\
\Gamma_{N-3} & \Gamma_{N-3}\Gamma_1 & \Gamma_{N-3}\Gamma_2 & \Gamma_{N-4}\Gamma_2 & \cdots & \Gamma_1\Gamma_2 & \Gamma_2 \\
\Gamma_{N-4} & \Gamma_{N-4}\Gamma_1 & \Gamma_{N-4}\Gamma_2 & \Gamma_{N-4}\Gamma_3 & \cdots & \Gamma_1\Gamma_3 & \Gamma_3 \\
\cdot & \cdot & \cdot & \cdot & \cdots & \cdot & \cdot \\
\cdot & \cdot & \cdot & \cdot & \cdots & \cdot & \cdot \\
\Gamma_1 & \Gamma_1\Gamma_1 & \Gamma_1\Gamma_2 & \Gamma_1\Gamma_3 & \cdots & \Gamma_1\Gamma_{N-2} & \Gamma_{N-2} \\
\Gamma_0 & \Gamma_1 & \Gamma_2 & \Gamma_3 & \cdots & \Gamma_{N-2} & \Gamma_{N-1}
\end{bmatrix}.
\tag{4.68}
$$

Now the process of the inversion of the N^3 by N^3 matrix A is reduced to the inversion of the N^2 by N^2 matrix Γ_N.

The forward EEG problem can be inverted analytically for the particular case of a chain of finite volume elements. This can be done regardless of the number of cubes in the chain. The basic idea of matrix inversion can be extended to the two-dimensional case of the square plate and the three-dimensional case of the cube assembled from the elementary cubes. Obviously additional research is needed in order to find out whether similar derivations can be carried out for the cube's deformations in fitting it to the realistic head. If so then the forward problem solution can be realized considerably faster than the iterative inversion. The right-hand side of each forward problem has only two nonzero entries, hence only a few rows of the inverse matrix are needed for its solution. This is one more potential opportunity for a reduction of the computational time.

5   The Three-shell Model with a Realistic Source.

So far the three-shell model of the human head was studied under the assumption that the distance between the dipole sources is infinitely small. As we have seen in Chapter 2, this is one of the key assumptions for the derivation of the potential on the surface of the sphere. However anatomy studies show that the distance between the source and sink is finite - of the order of several tenths of a centimeter. Therefore for practical purposes more realistic model is needed which would take this feature into account. In this chapter the expressions for radial and tangential dipole will be derived separately. Then they will be combined into a single expression.

Consider the radial dipole with the finite distance d between the source and sink, each of intensity I, placed inside the homogeneous media of conductivity σ. The potential on the surface of the sphere of radius R will be the difference of the potentials due to the source and the sink, as it was already established in Chapter 2.

$$\Phi = \frac{I}{4\pi\sigma} \sum_{l=0}^{\infty} \left(\frac{\left(b + \frac{d}{2}\right)^l}{R^{l+1}} - \frac{\left(b - \frac{d}{2}\right)^l}{R^{l+1}} \right) P_l(\cos\Theta). \tag{5.1}$$

Using the formula

$$x^l - y^l = (x - y)(x^{l-1} + x^{l-2}y + \dots + xy^{l-2} + y^{l-1}) = (x - y)\sum_{k=0}^{l-1} x^{l-1-k}y^k \tag{5.2}$$

for

$$x = 1 + \frac{d}{2b}, \quad y = 1 - \frac{d}{2b}, \tag{5.3}$$

81

$$\left(b + \frac{d}{2}\right)^l - \left(b - \frac{d}{2}\right)^l = b^l \left\{ \left(1 + \frac{d}{2b}\right)^l - \left(1 - \frac{d}{2b}\right)^l \right\}$$

$$= b^{l-1} d \sum_{k=0}^{l-1} \left(1 + \frac{d}{2b}\right)^{l-1-k} \left(1 - \frac{d}{2b}\right)^k. \tag{5.4}$$

Hence

$$\Phi = \frac{Id}{4\pi\sigma} \sum_{l=0}^{\infty} \frac{f_l(b)}{R^{l+1}} P_l(\cos\Theta) = \frac{m_r}{4\pi\sigma} \sum_{l=0}^{\infty} \frac{f_l(b)}{R^{l+1}} P_l(\cos\Theta), \tag{5.5}$$

where

$$f_l(b) = \sum_{k=0}^{l-1} \left(1 + \frac{d}{2b}\right)^{l-1-k} \left(1 - \frac{d}{2b}\right)^k. \tag{5.6}$$

For $b = 0$,

$$\Phi = \frac{Id}{4\pi\sigma} \sum_{l=1}^{\infty} \frac{h^{l-1}}{R^{l+1}} \frac{P_l(\cos\Theta) - P_l(\cos(\pi - \Theta))}{2}$$

$$= \frac{m_r}{4\pi\sigma h^2} \sum_{l=1}^{\infty} \left(\frac{h}{R}\right)^{l+1} \frac{P_l(\cos\Theta) - P_l(\cos(\pi - \Theta))}{2}. \tag{5.7}$$

Since $P_l(x) = \frac{1}{2^l l!} \frac{d^l}{dx^l} (x^2 - 1)^l$,

$$P_l(-x) = (-1)^l P_l(x), \tag{5.8}$$

hence $\Phi = \frac{m_r}{4\pi\sigma h^2} \sum_{l=1}^{\infty} \frac{h^{l-1}}{R^{l+1}} P_l(\cos\Theta) \frac{(1 - (-1)^l)}{2}. \tag{5.9}$

It is now possible to write the potential on the surface of a three-shell sphere in a way similar to the previous derivations in Chapter 2. The potentials Φ_1, Φ_2, Φ_3 and Φ_4 for the brain, skull, scalp and the surrounding air can be written out as

$$\Psi_1 = \sum_{l=1}^{\infty} \left[A_l r^l + \frac{m_r}{4\pi\sigma b^2} f_l(b) \left(\frac{b}{r}\right)^{l+1} \right] P_l(\cos\Theta),$$

$$\Psi_2 = \sum_{l=1}^{\infty} \left[C_l r^l + D_l r^{-(l+1)} \right] P_l(\cos\Theta), \tag{5.10}$$

$$\Psi_3 = \sum_{l=1}^{\infty} \left[E_l r^l + F_l r^{-(l+1)} \right] P_l(\cos\Theta),$$

$$\Psi_4 = 0.$$

82

The boundary conditions

$$\sigma\frac{\partial\Psi_1}{\partial r}\bigg|_{r=r_1} = \sigma_s\frac{\partial\Psi_2}{\partial r}\bigg|_{r=r_1}, \quad \sigma_S\frac{\partial\Psi_2}{\partial r}\bigg|_{r=r_2} = \sigma\frac{\partial\Psi_3}{\partial r}\bigg|_{r=r_2},$$

(5.11)

$$\frac{\partial\Psi_3}{\partial r}\bigg|_{r=R} = 0,$$

$$\frac{\partial\Psi_1}{\partial\Theta}\bigg|_{r=r_1} = \frac{\partial\Psi_2}{\partial\Theta}\bigg|_{r=r_1}, \frac{\partial\Psi_2}{\partial\Theta}\bigg|_{r=r_2} = \frac{\partial\Psi_3}{\partial\Theta}\bigg|_{r=r_2},$$

(5.12)

result in the following system of equations

$$\sigma\left\{A_l l r_1^{l-1} - \frac{m_r f_l(b)}{4\pi\sigma b^2}b^{l+1}\frac{(l+1)}{r_1^{l+2}}\right\} = \sigma_S\left\{C_l l r_1^{l-1} - D_l\frac{(l+1)}{r_1^{l+2}}\right\}$$

(5.13)

$$\sigma_S\left\{C_l l r_2^{l-1} - D_l\frac{(l+1)}{r_2^{l+2}}\right\} = \sigma\left\{E_l l r_2^{l-1} - F_l\frac{(l+1)}{r_2^{l+2}}\right\}$$

(5.14)

$$E_l l R^{l-1} - F_l\frac{(l+1)}{R^{l+2}} = 0.$$

(5.15)

$$A_l r_1^l + \frac{m_r}{4\pi\sigma b^2}f_l(b)\left(\frac{b}{r_1}\right)^{l+1} = C_l r_1^l + \frac{D_l}{r_1^{l+1}},$$

(5.16)

$$C_l r_2^l + \frac{D_l}{r_2^{l+1}} = E_l r_2^l + \frac{F_l}{r_2^{l+1}}.$$

(5.17)

Again combining equations (5.14) and (5.17)

$$C_l + \frac{D_l}{r_2^{2l+1}} = \frac{K_1 F_l}{r_2^l}$$

(5.18)

$$C_l - \frac{D_l(l+1)}{l r_2^{2l+1}} = \frac{K_1 F_l}{\xi},$$

(5.19)

where

$$K_1 = \frac{(l+1)r_2^l}{l R^{2l+1}} + \frac{1}{r_2^{2l+1}},$$

(5.20)

$$K_2 = \frac{(l+1)}{l}\left(\frac{1}{R^{2l+1}} - \frac{1}{r_2^{2l+1}}\right),$$

(5.21)

83

it is possible to write the following relations between C_l, D_l and F_l,

$$C_l = M_C F_l, \quad \text{where} \quad M_C = \frac{(l+1)}{(2l+1)}\left(\frac{K_1}{r_2^l} - \frac{K_2}{\xi}\right) + \frac{K_2}{\xi}, \tag{5.22}$$

$$D_l = M_D F_l, \quad \text{where} \quad M_D = \frac{lr_2^{2l+1}}{2l+1}\left(\frac{K_1}{r_2^l} - \frac{K_2}{\xi}\right). \tag{5.23}$$

The equations (5.13) and (5.16) can be rewritten as

$$A_l - \frac{m_r}{4\pi\sigma b^2}f_l(b)\frac{l+1}{l}\frac{b^{l+1}}{r_1^{2l+1}} = \xi M_C F_l - \xi M_D F_l \frac{l+1}{l}\frac{1}{r_1^{2l+1}}$$

$$A_l + \frac{m_r}{4\pi\sigma b^2}f_l(b)\frac{b^{l+1}}{r_1^{2l+1}} = M_C F_l + \frac{M_D F_l}{r_1^{2l+1}},$$

in order to get F_l and E_l,

$$F_l = m_r\frac{2l+1}{l}f_l(b)\frac{b^{l-1}}{4\pi\sigma}\frac{1}{M_C r_1^{2l+1}(1-\xi) + M_D\left(1 + \frac{\xi(l+1)}{l}\right)}, \tag{5.24}$$

$$E_l = m_r\frac{(l+1)(2l+1)}{l^2 R^{2l+1}}f_l(b)\frac{b^{l-1}}{4\pi\sigma}\frac{1}{M_C r_1^{2l+1}(1-\xi) + M_D\left(1 + \frac{\xi(l+1)}{l}\right)}. \tag{5.25}$$

Since

$$M_C = \frac{1}{R^{2l+1}}\frac{l+1}{2l+1}\left(\frac{(l+1)}{l} + \frac{1}{\xi}\right) + \frac{l+1}{2l+1}\left(1 - \frac{1}{\xi}\right)\frac{1}{r_2^{2l+1}},$$

$$M_D = \frac{l+1}{2l+1}\left(\frac{r_2}{R}\right)^{2l+1}\left(1 - \frac{1}{\xi}\right) + \frac{\xi l + (l+1)}{\xi(2l+1)},$$

$$\frac{1}{M_C r_1^{2l+1}(1-\xi) + M_D\left(1 + \frac{\xi(l+1)}{l}\right)} =$$

$$\frac{(l+1)}{\xi l(2l+1)l}\left\{ f_1^{2l+1}(1-\xi)\left(\xi(l+1) + l\right) + (\xi-1)\left(\frac{f_1}{f_2}\right)^{2l+1}(1-\xi)l \right.$$

$$\left. + f_2^{2l+1}(\xi-1)(\xi(l+1) + l) + \left(\frac{\xi l}{l+1} + 1\right)(\xi(l+1) + l)\right\},$$

$$f_1 = \frac{r_1}{R}, \quad f_2 = \frac{r_2}{R}.$$

In short

$$\frac{1}{M_C r_1^{2l+1}(1-\xi) + M_D\left(1 + \frac{\xi(l+1)}{l}\right)} = \frac{(l+1)}{\xi l(2l+1)}d_\xi, \tag{5.26}$$

84

where

$$d_\xi = f_1^{2l+1}(1-\xi)\left(\xi(l+1)+l\right) + (\xi-1)\left(\frac{f_1}{f_2}\right)^{2l+1}(1-\xi)l$$

$$+ f_2^{2l+1}(\xi-1)(\xi(l+1)+l) + \left(\frac{\xi l}{l+1}+1\right)(\xi(l+1)+l). \tag{5.27}$$

Hence the potential on the outer surface of the three-shell sphere will be

$$\Psi = \sum_{l=1}^{\infty}\left[E_l R^l + F_l R^{-(l+1)}\right]P_l(\cos\Theta)$$

$$= \sum_{l=1}^{\infty}\left(m_r\frac{b^{l-1}}{R^{l+1}}\frac{f_l(b)}{4\pi\sigma}\frac{2l+1}{l}\left(1+\frac{l+1}{l}\right)\right)\frac{1}{M_C r_1^{2l+1}(1-\xi)+M_D\left(1+\frac{\xi(l+1)}{l}\right)}P_l(\cos\Theta)$$

$$= \sum_{l=1}^{\infty}\frac{m_r}{4\pi\sigma}\frac{b^{l-1}}{R^{l+1}}f_l(b)\frac{(2l+1)^2}{l^2}\frac{1}{M_C r_1^{2l+1}(1-\xi)+M_D\left(1+\frac{\xi(l+1)}{l}\right)}P_l(\cos\Theta)$$

$$= \sum_{l=1}^{\infty}\frac{m_r(2l+1)^2 f_l(b)b^{l-1}}{4\pi\sigma R^{l+1}l^2}\frac{\xi l(2l+1)}{(l+1)d_\xi}P_l(\cos\Theta)$$

$$= \sum_{l=1}^{\infty}\frac{m_r(2l+1)^3\xi f_l(b)b^{l-1}}{4\pi\sigma l(l+1)R^{l+1}d_\xi}P_l(\cos\Theta). \tag{5.28}$$

It is easy to show that for an infinitely small distance d this formula corresponds to the one for the idealistic three-shell model. Since

$$\lim_{d\to 0}f_l(b) = \lim_{d\to 0}\sum_{k=0}^{l-1}\left(1+\frac{d}{2b}\right)^{l-1-k}\left(1-\frac{d}{2b}\right)^k = \sum_{k=0}^{l-1}1 = l,$$

$$\Psi = \lim_{d\to 0}\sum_{l=1}^{\infty}\frac{m_r(2l+1)^3 f_l(b)b^{l-1}}{4\pi\sigma l(l+1)R^{l+1}d_\xi}P_l(\cos\Theta)$$

$$= \sum_{l=1}^{\infty}\frac{m_r(2l+1)^3 b^{l-1}}{4\pi\sigma(l+1)R^{l+1}d_\xi}P_l(\cos\Theta),$$

and this is the formula for the realistic three-shell model.

For $b = 0$, calculations similar to the ones above result in

$$\Psi = \sum_{l=1}^{\infty}\frac{m_r}{4\pi\sigma}\frac{(2l+1)^3\xi}{(l+1)d_\xi}\frac{h^{l-1}}{R^{l+1}}P_l(\cos\Theta)\frac{(1-(-1)^l)}{2}. \tag{5.29}$$

For the tangential dipole the situation is a bit more comlex. The angles Θ_1 and Θ_2 are not necessary close to Θ. First the expressions for $\cos\Theta_1$ and $\cos\Theta_2$ are needed. Consider

85

the tangential dipole in an infinite media of the conductivity σ (Figure 3). The potential on the surface of the sphere of radius R is

$$\Psi = \frac{I}{4\pi\sigma}\left(\frac{1}{r_1} - \frac{1}{r_2}\right) = \frac{1}{4\pi\sigma}\sum_{l=1}^{\infty}\left(b^2 + \left(\frac{d}{2}\right)^2\right)^{\frac{l}{2}}\frac{I}{R^{l+1}}P_l(\cos\Theta_1) - \tag{5.30}$$

$$\frac{1}{4\pi\sigma}\sum_{l=1}^{\infty}\left(b^2 + \left(\frac{d}{2}\right)^2\right)^{\frac{l}{2}}\frac{I}{R^{l+1}}P_l(\cos\Theta_2). \tag{5.31}$$

It is obvious from Figure 7 that

$$r_1^2 = b^2 + \left(\frac{d}{2}\right)^2 + R^2 - 2\sqrt{b^2 + \left(\frac{d}{2}\right)^2}R\cos\Theta_1, \tag{5.32}$$

$$r_2^2 = b^2 + \left(\frac{d}{2}\right)^2 + R^2 - 2\sqrt{b^2 + \left(\frac{d}{2}\right)^2}R\cos\Theta_2. \tag{5.33}$$

On the other hand

$$r_1^2 = d_1^2 + (R\cos\Theta - b)^2, \tag{5.34}$$

$$r_2^2 = d_2^2 + (R\cos\Theta - b)^2, \tag{5.35}$$

where

$$d_1^2 = R\sin^2\Theta + \left(\frac{d}{2}\right)^2 - dR\sin\Theta\cos\beta, \tag{5.36}$$

$$d_2^2 = R\sin^2\Theta + \left(\frac{d}{2}\right)^2 - dR\sin\Theta\cos(\pi - \beta) = R\sin^2\Theta + \left(\frac{d}{2}\right)^2 + dR\sin\Theta\cos\beta. \tag{5.37}$$

Combining these expressions obtain the formulas for $\cos\Theta_1$ and $\cos\Theta_2$,

$$\cos\Theta_1 = \frac{2b\cos\Theta + d\sin\Theta\cos\beta}{2\sqrt{b^2 + \left(\frac{d}{2}\right)^2}}, \tag{5.38}$$

$$\cos\Theta_2 = \frac{2b\cos\Theta - d\sin\Theta\cos\beta}{2\sqrt{b^2 + \left(\frac{d}{2}\right)^2}}. \tag{5.39}$$

86

Figure 7: Tangential Dipole with Finite Distance d Between Source and Sink.
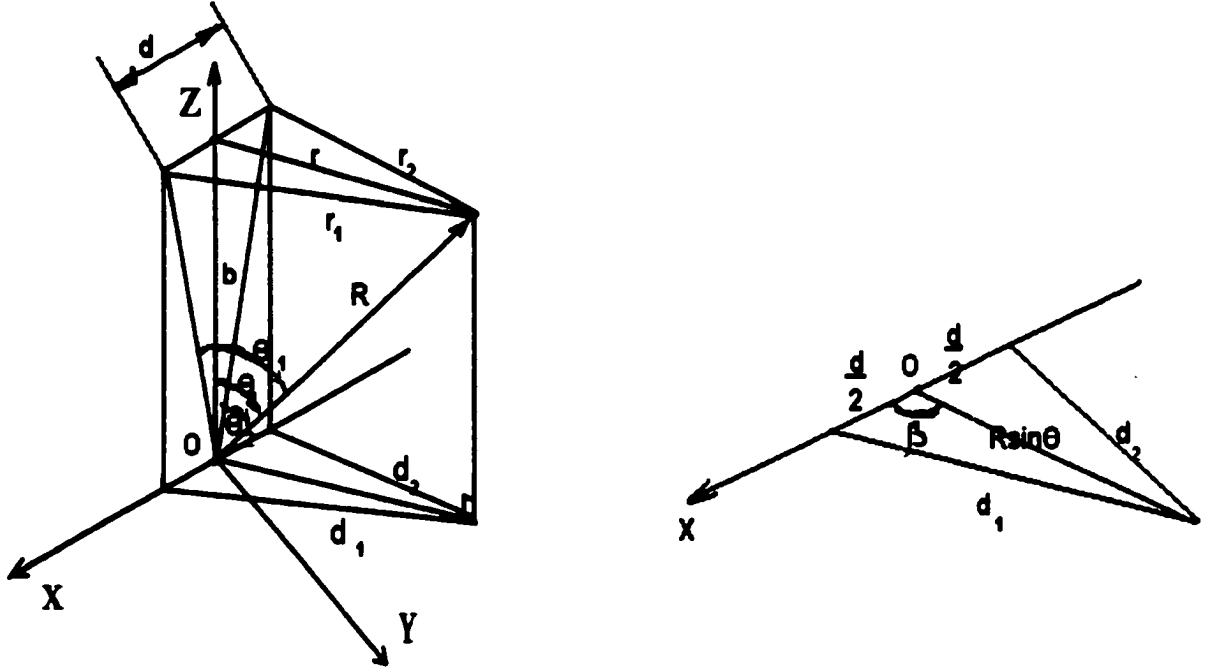
Hence

$$\Psi = \frac{I}{4\pi\sigma} \sum_{l=1}^{\infty} \frac{\left(b^2 + \left(\frac{d}{2}\right)^2\right)^{\frac{l}{2}}}{R^{l+1}} \left\{ P_l\left(k_1 \cos\Theta + k_2 \sin\Theta \cos\beta\right) \right.$$

$$\left. - P_l\left(k_1 \cos\Theta - k_2 \sin\Theta \cos\beta\right) \right\},$$ (5.40)

where

$$k_1 = \frac{1}{\sqrt{1 + \left(\frac{q}{2}\right)^2}}, \quad k_2 = \frac{1}{\sqrt{1 + \left(\frac{2}{q}\right)^2}}, \quad q = \frac{d}{b}.$$ (5.41)

In case $b = 0$,

$$\Psi = \frac{I}{4\pi\sigma} \sum_{l=1}^{\infty} \frac{h^l}{R^{l+1}} \left(P_l(\cos\Theta_1) - P_l(\cos\Theta_2)\right),$$

87

where

$$\cos\Theta_1 = \lim_{b \to 0} \frac{2b\cos\Theta + d\sin\Theta\cos\beta}{2\sqrt{b^2 + \left(\frac{d}{2}\right)^2}} = \sin\Theta\cos\beta, \qquad (5.42)$$

$$\cos\Theta_2 = \lim_{b \to 0} \frac{2b\cos\Theta - d\sin\Theta\cos\beta}{2\sqrt{b^2 + \left(\frac{d}{2}\right)^2}} = -\sin\Theta\cos\beta. \qquad (5.43)$$

Hence

$$\Psi = \frac{I}{4\pi\sigma} \sum_{l=1}^{\infty} \frac{h^l}{R^{l+1}} P_l(\sin\Theta\cos\beta)\frac{(1 - (-1)^l)}{2}. \qquad (5.44)$$

For a homogeneous sphere of radius R and conductivity σ,

$$\Psi = \sum_{l=1}^{\infty} \left(A_l r^l + \frac{I}{4\pi\sigma} \frac{\left(b^2 + \left(\frac{d}{2}\right)^2\right)^{\frac{l}{2}}}{r^{l+1}} \right) \left\{ P_l\left(k_1\cos\Theta + k_2\sin\Theta\cos\beta\right) \right.$$

$$\left. -P_l\left(k_1\cos\Theta - k_2\sin\Theta\cos\beta\right) \right\}.$$

The boundary condition

$$\left. \frac{\partial\Psi}{\partial r} \right|_{r=R} = 0 \qquad (5.45)$$

results in

$$A_l = \frac{(l+1)}{l} \frac{I\left(b^2 + \left(\frac{d}{2}\right)^2\right)^{\frac{l}{2}}}{4\pi\sigma R^{2l+1}}. \qquad (5.46)$$

Therefore the potential for this illustrative case will be

$$\Psi = \frac{(2l+1)}{l} \frac{I\left(b^2 + \left(\frac{d}{2}\right)^2\right)^{\frac{l}{2}}}{4\pi\sigma R^{2l+1}} \left\{ P_l\left(k_1\cos\Theta + k_2\sin\Theta\cos\beta\right) \right.$$

$$\left. -P_l\left(k_1\cos\Theta - k_2\sin\Theta\cos\beta\right) \right\}. \qquad (5.47)$$

For the sake of convenience denote

$$S_l(q,\beta,\Theta) = \left\{ P_l\left(k_1\cos\Theta + k_2\sin\Theta\cos\beta\right) \right.$$

$$\left. - P_l\left(k_1\cos\Theta - k_2\sin\Theta\cos\beta\right) \right\}. \qquad (5.48)$$

88

In a general case of three-shell sphere with conductivities σ and σ_S,

$$\Psi_1 = \sum_{l=1}^{\infty}\left[A_l r^l + \frac{I}{4\pi\sigma}\frac{\left(b^2 + \left(\frac{d}{2}\right)^2\right)^{\frac{l}{2}}}{r^{l+1}}\right]S_l(q,\beta,\Theta),$$

$$\Psi_2 = \sum_{l=1}^{\infty}\left[C_l r^l + D_l r^{-(l+1)}\right]S_l(q,\beta,\Theta),$$

$$\Psi_3 = \sum_{l=1}^{\infty}\left[E_l r^l + F_l r^{-(l+1)}\right]S_l(q,\beta,\Theta),$$

$$\Psi_4 = 0.$$

The boundary conditions (5.11)−(5.12) will result in the system of equations (5.14), (5.15), (5.17) and the following equations

$$\sigma\left\{A_l l r_1^{l-1} - \frac{I}{4\pi\sigma}\left(b^2 + \left(\frac{d}{2}\right)^2\right)^{\frac{l}{2}}\frac{(l+1)}{r_1^{l+2}}\right\} = \sigma_S\left\{C_l l r_1^{l-1} - D_l\frac{(l+1)}{r_1^{l+2}}\right\}, \qquad (5.49)$$

$$A_l r_1^l + \frac{I}{4\pi\sigma}\frac{\left(b^2 + \left(\frac{d}{2}\right)^2\right)^{\frac{l}{2}}}{r_1^{l+1}} = C_l r_1^l + \frac{D_l}{r_1^{l+1}}. \qquad (5.50)$$

Write them as

$$A_l - \frac{I}{4\pi\sigma}\left(b^2 + \left(\frac{d}{2}\right)^2\right)^{\frac{l}{2}}\frac{(l+1)}{l}\frac{1}{r_1^{2l+1}} = \xi C_l - \xi D_l\frac{(l+1)}{l}\frac{1}{r_1^{2l+1}},$$

$$A_l + \frac{I}{4\pi\sigma}\frac{\left(b^2 + \left(\frac{d}{2}\right)^2\right)^{\frac{l}{2}}}{r_1^{2l+1}} = C_l + \frac{D_l}{r_1^{2l+1}}.$$

As before $C_l = M_C F_l$, $D_l = M_D F_l$, where C_l and D_l are given by formulas (5.22) and (5.23), K_1 and K_2 - by (5.20) and (5.21). Hence

$$A_l - \frac{m_t}{4\pi\sigma}\frac{\left(b^2 + \left(\frac{d}{2}\right)^2\right)^{\frac{l}{2}}}{d}\frac{(l+1)}{l}\frac{1}{r_1^{2l+1}} = \xi M_C F_l - \xi M_D F_l\frac{(l+1)}{l}\frac{1}{r_1^{2l+1}}, \qquad (5.51)$$

$$A_l + \frac{m_t}{4\pi\sigma}\frac{\left(b^2 + \left(\frac{d}{2}\right)^2\right)^{\frac{l}{2}}}{dr_1^{2l+1}} = M_C F_l + \frac{M_D F_l}{r_1^{2l+1}}. \qquad (5.52)$$

Therefore

$$F_l = \frac{I}{4\pi\sigma}\frac{2l+1}{l}\left(b^2 + \left(\frac{d}{2}\right)^2\right)^{\frac{l}{2}}\frac{1}{M_C r_1^{2l+1}(1-\xi) + M_D\left(1 + \frac{\xi(l+1)}{l}\right)}, \qquad (5.53)$$

89

$$E_l = \frac{I}{4\pi\sigma} \frac{(2l+1)(l+1)}{l^2 R^{2l+1}} \left(b^2 + \left(\frac{d}{2}\right)^2\right)^{\frac{l}{2}} \frac{1}{M_C r_1^{2l+1}(1-\xi) + M_D\left(1 + \frac{\xi(l+1)}{l}\right)}. \tag{5.54}$$

Eventually the potential on the surface of the sphere is

$$\Psi = \sum_{l=1}^{\infty} \left[E_l R^l + F_l R^{-(l+1)}\right] S_l(q,\beta,\Theta)$$

$$= \sum_{l=1}^{\infty} \frac{I}{4\pi\sigma} \frac{(2l+1)^2}{l^2 R^{l+1}} \left(b^2 + \left(\frac{d}{2}\right)^2\right)^{\frac{l}{2}} \frac{1}{M_C r_1^{2l+1}(1-\xi) + M_D\left(1 + \frac{\xi(l+1)}{l}\right)} S_l(q,\beta,\Theta)$$

$$= \sum_{l=1}^{\infty} \frac{I}{4\pi\sigma} \left(b^2 + \left(\frac{d}{2}\right)^2\right)^{\frac{l}{2}} \frac{(2l+1)^2}{l^2 R^{l+1}} \frac{\xi l(2l+1)}{(l+1)d_\xi} S_l(q,\beta,\Theta),$$

$$= \sum_{l=1}^{\infty} \frac{I}{4\pi\sigma} \frac{\left(b^2 + \left(\frac{d}{2}\right)^2\right)^{\frac{l}{2}}}{R^{l+1}} \frac{(2l+1)^3 \xi}{l(l+1)d_\xi} S_l(q,\beta,\Theta). \tag{5.55}$$

where d_ξ is already defined by (5.27).

For an infinitely small distance between the dipoles, the expression should be identical to the one given in Chapter 2 for the idealistic three-shell model.

Indeed for $d \to 0, b \neq 0, m_t = Id$ fixed,

$$\lim_{d \to 0} \quad I\left(b^2 + \left(\frac{d}{2}\right)^2\right)^{\frac{l}{2}} S_l(q,\beta,\Theta)$$

$$= \lim_{d \to 0} \quad \frac{m_t b}{d} \left\{ P_l\left(\frac{\cos\Theta}{\sqrt{1+\left(\frac{q}{2}\right)^2}} + \frac{\sin\Theta\cos\beta}{\sqrt{1+\left(\frac{2}{q}\right)^2}}\right) \right.$$

$$\left. - P_l\left(\frac{\cos\Theta}{\sqrt{1+\left(\frac{q}{2}\right)^2}} - \frac{\sin\Theta\cos\beta}{\sqrt{1+\left(\frac{2}{q}\right)^2}}\right) \right\}$$

$$= \lim_{d \to 0} \quad \frac{m_t b}{d} \left\{ P_l\left(\cos\Theta + \frac{d}{2b}\sin\Theta\cos\beta\right) \right.$$

$$\left. - P_l\left(\cos\Theta - \frac{d}{2b}\sin\Theta\cos\beta\right) \right\}.$$

Since $\frac{d\cos\beta}{b} \approx d\Theta$,

$$\frac{d}{2b}\sin\Theta\cos\beta = \frac{\sin\Theta d\Theta}{2} = -\frac{1}{2}d(\cos\Theta),$$

90

the above expression can be written as

$$\lim_{d\to 0} \frac{b^{l-1}\cos\beta}{d\Theta}\left\{P_l\left(\cos\Theta - \frac{1}{2}d(\cos\Theta)\right)\right.$$

$$\left. - P_l\left(\cos\Theta + \frac{1}{2}d(\cos\Theta)\right)\right\}$$

$$= - m_t b^{l-1}\cos\beta\frac{dP_l(\cos\Theta)}{d(\cos\Theta)}\frac{d(\cos\Theta)}{d\Theta}$$

$$= - m_t b^{l-1}P_l^1(\cos\Theta)\cos\beta,$$

hence as a whole,

$$\lim_{d\to 0}\sum_{l=1}^{\infty}\frac{I}{4\pi\sigma}\frac{\left(b^2 + \left(\frac{d}{2}\right)^2\right)^{\frac{l}{2}}}{R^{l+1}}\frac{(2l+1)^3\xi}{l(l+1)d_\xi}S_l(q,\beta,\Theta)$$

$$= -\sum_{l=1}^{\infty}\frac{m_t}{4\pi\sigma}\frac{b^{l-1}}{R^{l+1}}\frac{(2l+1)^3\xi}{l(l+1)d_\xi}P_l^1(\cos\Theta)\cos\beta.$$

If $b = 0$,

$$\Psi = \sum_{l=1}^{\infty}\frac{m_t}{4\pi\sigma}\frac{h^{l+1}}{R^{l+1}}\frac{(2l+1)^3\xi}{l(l+1)d_\xi}P_l(\sin\Theta\cos\beta)\frac{(1-(-1)^l)}{2}. \tag{5.56}$$

Finally combining the expressions for the radial and tangential dipole,

$$\Psi = \sum_{l=1}^{\infty}\frac{1}{4\pi\sigma}\frac{(2l+1)^3\xi}{l(l+1)d_\xi}\frac{1}{R^{l+1}}\left\{m_r f_l(b)b^{l-1}P_l(\cos\Theta)\right.$$

$$\left. + I\left(b^2 + \left(\frac{d}{2}\right)^2\right)^{\frac{l}{2}}S_l(q,\beta,\Theta)\right\}. \tag{5.57}$$

The numerical implementation of this solution requires not only the radial m_r and the tangential m_t components to be defined, but also the intensity I and the distance between the sources d to be defined. For the sake of simplicity they are the same for both directions in the preceding formula, as it is not a prime consideration. This implementation of the analytical model can be combined with minimization algorithms in the same way as it was done for the idealistic three-shell model. The new model is more suitable for the tests of the FVM modelling. It corresponds to two distance sources located in the centers of two different finite volume elements.

91

6 Experimental Results.

6.1 Comparison of Numerical and Analytical Models.

For practical source localization it is important to know the accuracy of the computation of the potential by FVM. The accuracy can be estimated by applying the numerical model for the computation of the potential for the biological volume conductor with geometry admitting the known analytical solution. The three-shell spherical models are suitable for this purpose.

The three-shell model with an infinitely small distance between the source and the sink will hereupon be called the *idealistic three-shell model* (I3SM), whereas the one described in Chapter 5 with the finite distance between the source and the sink will be called the *realistic three-shell model* (R3SM).

The standard three-shell setup representing the human head has the following parameters:

$r_1 = 0.87; \quad r_2 = 0.92; \quad R = 1.0;$

$\sigma = 0.0029(\Omega m)^{-1}; \quad \sigma_S = 3.6 \cdot 10^{-5}(\Omega m)^{-1}.$

The system of the finite volume elements with cube size h is defined in the way it was described in Chapter 3. The conductivities for each cube with indexes (i, j, k) are

$x = ih, \quad y = jh, \quad z = kh,$

if $\sqrt{x^2 + y^2 + z^2} \leq r_1$

$\quad\quad \sigma_{ijk} = \sigma;$

else if $\sqrt{x^2 + y^2 + z^2} \leq r_2$

$\quad\quad \sigma_{ijk} = \sigma_S;$

else if $\sqrt{x^2 + y^2 + z^2} \leq R$

$\quad\quad \sigma_{ijk} = \sigma;$

else $\quad \sigma_{ijk} = 0.$

In other words if the center of the cube is within an inside sphere representing the brain or in the outer shell which represents the scalp, the conductivity σ is described for the cube. Otherwise if the center is within an inner layer representing the skull, the conductivity of the cube is σ_S.

The values of the potential on the surface of the sphere will be compared for the points with the following spherical coordinates
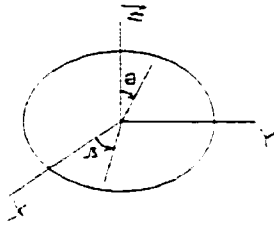
$R = 1;$

for $m = 1{:}90$

$$\Theta = \left(1 + 2 \cdot (m - 1)\right)\frac{\pi}{180};$$

for $n = 1{:}90$

$$\beta = \left(1 + 4 \cdot (m - 1)\right)\frac{\pi}{180};$$

Hence there are 8100 spatial points in total.

93
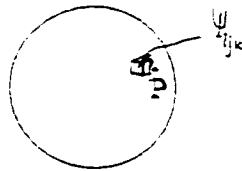
For a given spatial point P on the surface of the sphere, the NM potential computed for the finite volume element with the center closest to P is ascribed, $\Psi_P = \Psi_{ijk}$. The point $X = 1.0, Y = 0.0, Z = 0.0$ is taken to be a reference point, and the finite volume element closest to this point is taken to be a reference finite volume element. The matrix of the linear system is deflated with respect to this element in the way it was described in Chapter 3. Two systems of finite volume elements were generated, first with $N_1 = 267761$ cubes, second with $N_2 = 523305$, they correspond to the cube sizes 0.025 and 0.02. These systems will be denoted as R_1 and R_2.

The potential due to NM was compared to the idealistic three-shell model first for radial and tangential dipoles with centers located at

$$X = 0.0; \quad Y = 0.0;$$

$$Z = 0.0, \ 0.1, \ 0.2, ..., \ 0.7.$$

For the numerical model the source and the sink are assumed to have a unit intensity whereas the distance d between the dipoles is twice the cube's size, i.e. 0.05 for R_1 and 0.04 for R_2. For the I3SM the radial m_r and tangential m_t components are 0.05 for R_1 and 0.04 for R_2. The radial dipole is oriented in the Z-direction, whereas the tangential dipole is oriented in the X-direction.

The scaled difference between the NM and the I3SM for the XZ-plane, $Z = 0.1, 0.4, 0.7$, for the radial dipole is shown on Figure 9. As for the intersection of the surface of the sphere and the XZ-plane, the following expression is mapped:

$$1.0 + s(V_{NM}(\Theta, \beta) - V_{I3SM}(\Theta, \beta)),$$

where s is a scaling factor. Apparently for $Z = 0.7$, i.e. when the dipole is getting closer to the skull, the difference $V_{NM} - V_{I3SM}$ has a positive spike. The value of the potential V_{NM} is higher for the surface area that is immediately above the dipole. The differences

94

1.0 + $s(V_{NM} - V_{I3SM})$ for R_1 and R_2 for are shown in Figure 9. The error norms for the radial dipole are given in Table 1. The same scaled difference for the tangential dipoles is shown in Figure 10. The error growth for the area under the skull is not as large as for the radial dipole. The error norms for the tangential dipole are summarized in Table 2. The higher resolution reduced the error for the radial dipole, except for $Z = 0.7$. The Boundary Element Modeling [35] resulted in 10-20% error for similar multiple-shell models when the dipole was located in areas close to the skull. The finite-difference approach taken in [42] is very similar to the one taken in this work. The resulting matrix is almost the same except the deflation and positive definiteness were not studied. The measure applied in [42] for the error estimates is not a proper measure, since the authors applied *mean relative error*,

$$\Delta_r = \frac{1}{N} \sum_{i=1}^{N} \Delta_{r,i}, \quad \text{where} \quad \Delta_{r,i} = \frac{(V_{NM} - V_{I3SM})_i}{V_{NMi}} \times 100. \tag{6.1}$$

Such a norm implies the summation of the positive and negative values of the error, so for the same actual error such a norm results in lower values.

It is also important to know where and how the realistic three-shell model differs from the idealistic three-shell model. There is the possibility that the increase of the error $V_{NM}(\Theta, \beta) - V_{I3SM}(\Theta, \beta)$ under the skull for the radial dipole can in part be explained by the difference between the model with a finite and infinitely small distance between the source and the sink. Hence the outputs of the two models for the radial dipoles places at the same locations as before were compared.

The scaled difference between R3SM and I3SM for the XZ-plane, $Z = 0.1$, 0.4, 0.7, for the radial and tangential dipoles is shown in Figures 11 and 12, whereas the error norms for the radial and tangential dipoles are given in Tables 3 and 3. Apparently the difference grows while the radial dipole approaches the skull, but for given resolutions this error only is a small percentage of the NM error.

Of course for the radial dipole the error can be further reduced with an increase of

95

the resolution, but the capabilities of the SUN Ultra 30 workstation do not allow further substantial reduction of h. One can use the following simple estimates of the dimension of the arising problem. For the cube which contains the three-shell sphere one needs $\left(2 \cdot \left[\frac{1}{h}\right] + 1\right)^3$ finite volume elements. The ratio of the volume of the sphere of radius h to the volume of the cube with side $2h$ is

$$\frac{\frac{4}{3}\pi h^3}{8h^3} = \frac{\pi}{6} \approx \frac{1}{2}.$$

Hence the dimension of vectors which have to be stored is approximately $\frac{1}{2}\left(2 \cdot \left[\frac{1}{h}\right] + 1\right)^3$. The dimension of matrix A_d is approximately $\frac{7}{2}\left(2 \cdot \left[\frac{1}{h}\right] + 1\right)^3$. If $h = 0.01$, then the dimension of the solution vector should be over 4 million. For $h = 0.005$, the dimension will exceed 30 million.

Nevertheless it is important to know the impact that the error will have on the source localization. In order to find the source in the case of the realistic head [45], a certain number of candidate dipole locations inside the brain is chosen, and the potential corresponding to the dipoles in X, Y and Z directions in those locations is computed. Then the best location and direction (i.e. combination of X, Y and Z components) is chosen [35] in such a way that it is closest to the recorded potential in l_∞ or l_2 norm. It can be seen from the experimental data that there is a growth of the error for the radial dipole as it gets closer to the skull. This means that the potential distribution generated by such a dipole can become closest in l_∞ or l_2 to the recorded potential for the actual dipole which is located even closer to the skull. Nevertheless the effect is significant only for that limited area and the error of source localization will be limited due to geometry - the actual dipole does not have much space to go, it can be located within the brain tissue only.

Figure 8: Error Close to the Skull.

Figure 8: Error Close to the Skull.
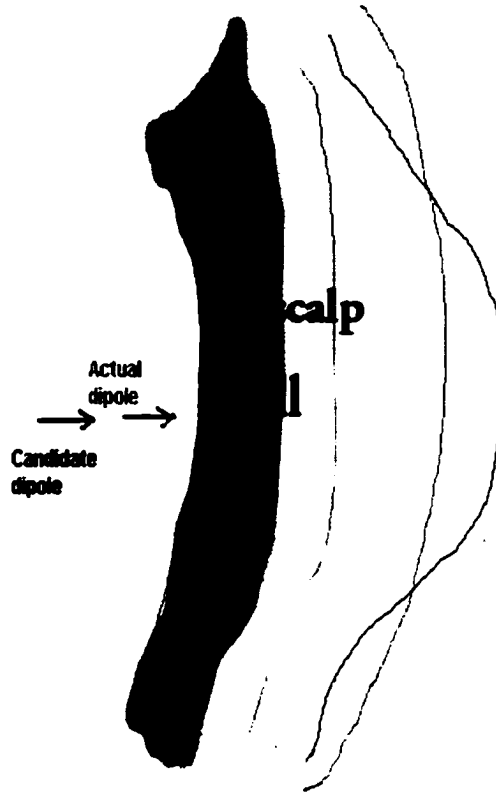
6.2   Polynomial Preconditioning Results.

The Polynomial Preconditioning resulted in a considerable reduction of the number of iterations needed for reaching the absolute error of 10^{-10}. The numerical experiments were made for the matrix corresponding to the $R1$ grid described above. The spectral bounds of the matrix were estimated in the way described in Chapter 3. The number of iterations needed for reaching the absolute error of 10^{-10} as well as the error graphs were obtained for preconditioning polynomials of the order of 1,2,3,5,7,9,....,17,19. The graphs of the absolute error vs. the number of iterations are shown on Figure 13. Apparently even the preconditioning polynomials of the order of 5 or 7 allow the reduction of the number

97

Figure 9: $1.0 + 8.0 \cdot \left(V_{NM} - V_{I3SM} \right)$, Radial Dipole.

Z = 0.1   Z = 0.4   Z = 0.7

R1

R2

98
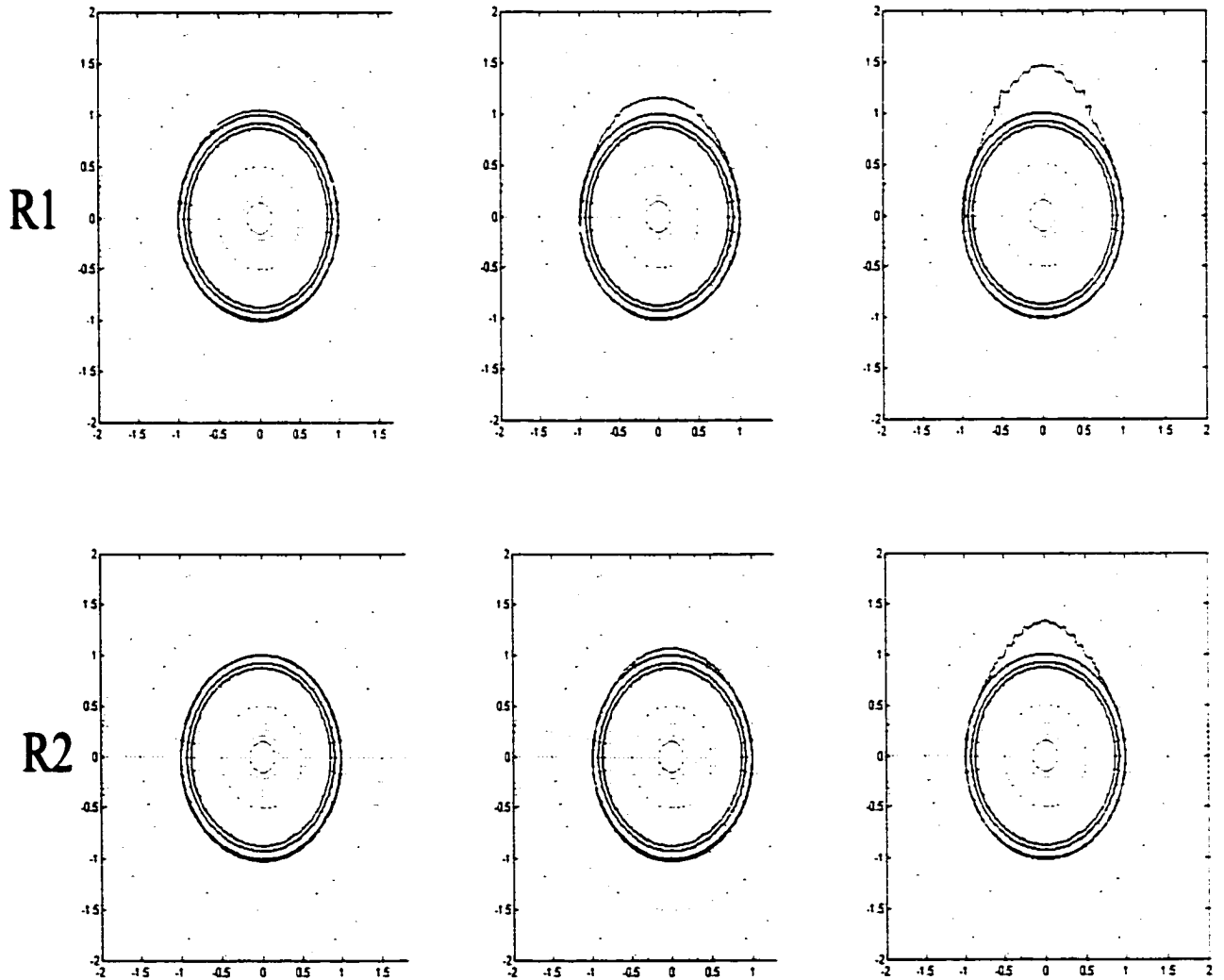
Figure 10: $1.0 + 15.0 \cdot \left(V_{NM} - V_{I3SM} \right)$, Tangential Dipole.
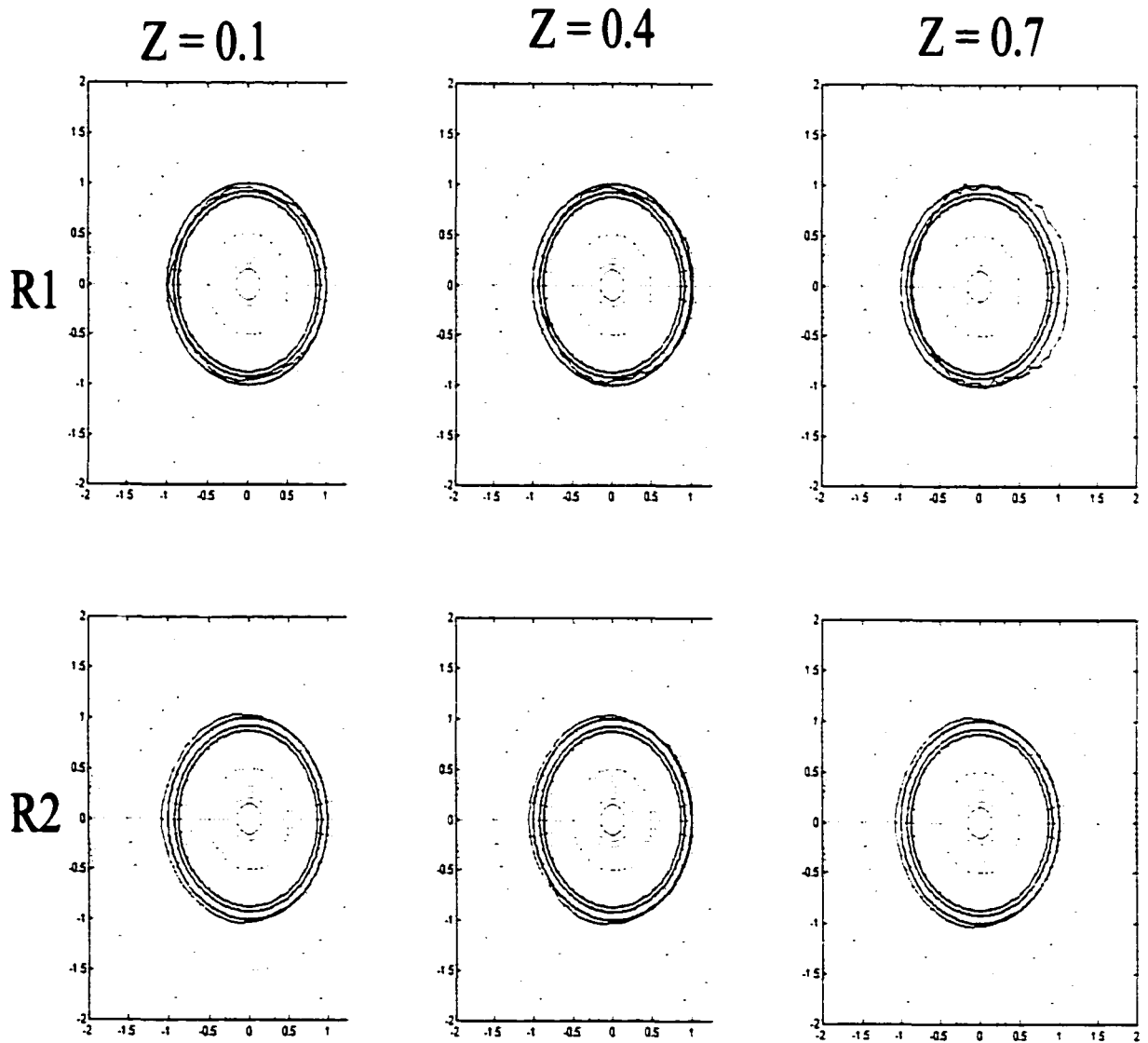
Figure 11: $1.0 + 1000.0 \cdot \left(V_{R3SM} - V_{I3SM} \right)$, Radial Dipole.

Z = 0.1

Z = 0.4

Z = 0.7

100
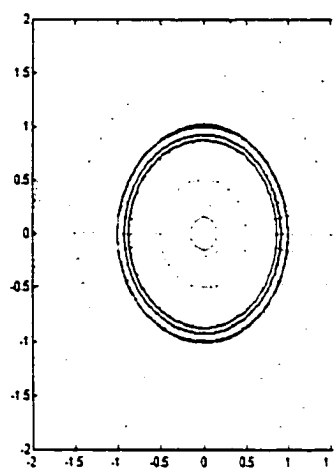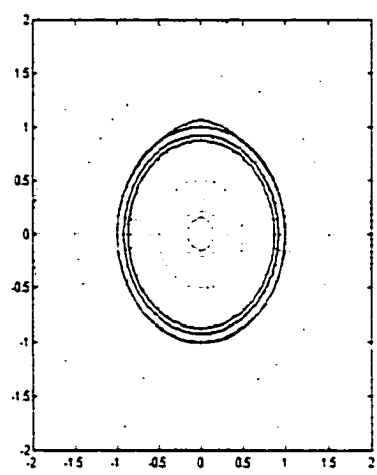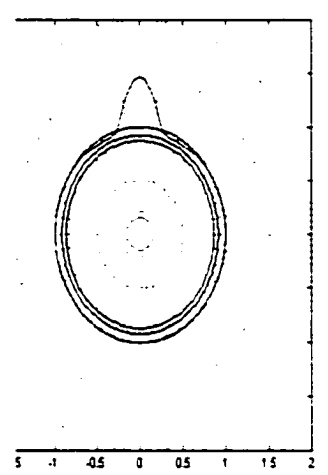
Figure 12: $1.0 + 1000.0 \cdot \left(V_{R3SM} - V_{I3SM} \right)$, Tangential Dipole.

Z = 0.1

Z = 0.4

Z = 0.7

101
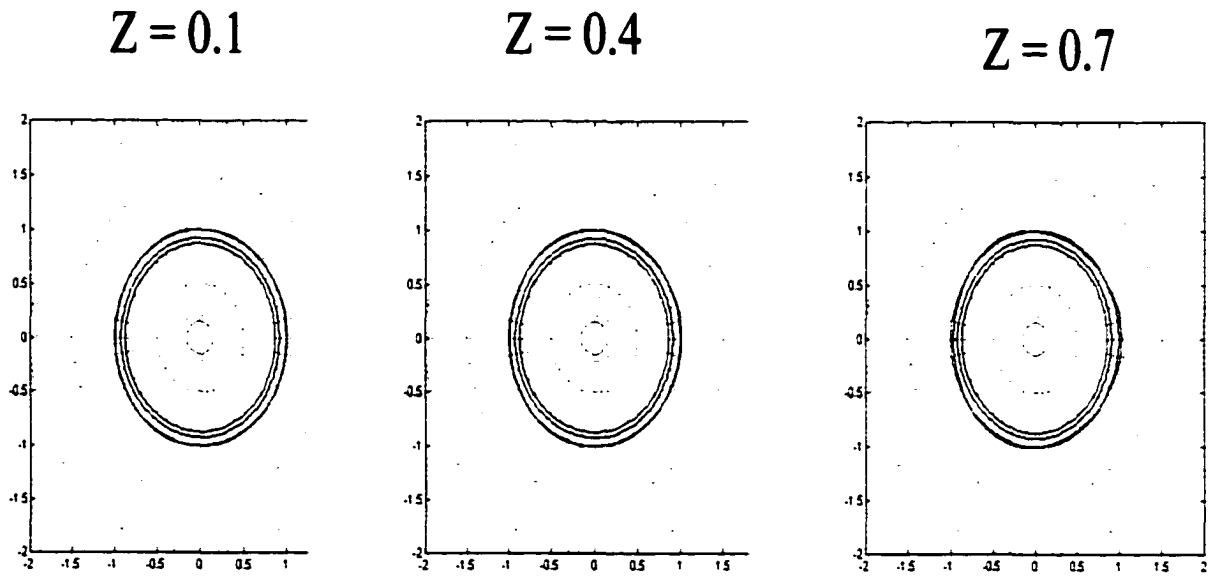
Table 1: Errors of Numerical Model, Radial Dipole.

Z	$\frac{\|V_{NM}-V_{I3SM}\|_\infty}{\|V_{NM}\|_\infty}, \%$		$\frac{\|V_{NM}-V_{I3SM}\|_2}{\|V_{NM}\|_2}, \%$	
	R_1	R_2	R_1	R_2
0.0	5.4	5.2	4.9	4.3
0.1	7.4	4.4	5.5	4.3
0.2	9.4	4.2	7.3	4.8
0.3	11.4	5.9	9.4	6.0
0.4	13.3	8.6	11.5	7.9
0.5	15.3	11.7	13.4	10.3
0.6	17.2	15.2	15.1	13.2
0.7	18.2	18.6	16.4	17.0

102

Table 2: Errors of Numerical model, Tangential Dipole.

Z	$\frac{\|V_{NM}-V_{I3SM}\|_\infty}{\|V_{NM}\|_\infty}$, % R_1
0.0	3.2
0.1	3.2
0.2	3.3
0.3	3.3
0.4	4.4
0.5	5.1
0.6	5.5
0.7	5.2

103

Table 3: Realistic versus Idealistic model, Radial Dipole.

Z	$\dfrac{\|V_{R3SM}-V_{I3SM}\|_\infty}{\|V_{R3SM}\|_\infty}$, %	$\dfrac{\|V_{R3SM}-V_{I3SM}\|_2}{\|V_{R3SM}\|_2}$, %
0.0	0.060	0.044
0.1	0.024	0.016
0.2	0.031	0.018
0.3	0.039	0.022
0.4	0.053	0.030
0.5	0.075	0.042
0.6	0.118	0.065
0.7	0.209	0.117

Table 4: Realistic versus Idealistic model, Tangential Dipole.

Z	$\dfrac{\|V_{R3SM}-V_{I3SM}\|_\infty}{\|V_{R3SM}\|_\infty}$, %	$\dfrac{\|V_{NM}-V_{I3SM}\|_2}{\|V_{NM}\|_2}$, %
0.0	0.061	0.042
0.1	0.020	0.014
0.2	0.021	0.016
0.3	0.022	0.018
0.4	0.030	0.022
0.5	0.046	0.030
0.6	0.078	0.044
0.7	0.154	0.077

of iterations from 210 to 30. The further reduction of the number of iterations gets more time-consuming. In order to reach 10^{-10} in 18 iterations, a preconditioning polynomial of the order of 18-19 is needed. As the order of the preconditioning polynomial increases, the computational time needed for a single iteration increases as well. In order to estimate the increase in computational time, compare the number of operations per one iteration for the CGM with and without preconditioning. The equations needed for only one CGM iteration are shown below, as well as the estimates of the number of operations. It is assumed below that any vector (p.e. $C_L r_{k-1}$) or scalar product needs to be computed only once and can then be stored for further use. For CGM without preconditioning,

$$\rho_1 = (\mathbf{r}_{k-1}, \mathbf{r}_{k-1}) \to 2N,$$

$$b_{k-1} = \frac{\rho_1}{\rho_0} \to 1,$$

$$\mathbf{p}_k = \mathbf{r}_{k-1} + b_{k-1}\mathbf{p}_{k-1} \to 2N,$$

$$a_k = \frac{(\mathbf{r}_{k-1}, \mathbf{r}_{k-1})}{(\mathbf{p}_k, A_d\mathbf{p}_k)} \to 2N + O(N),$$

$$\mathbf{x}_k = \mathbf{x}_{k-1} + a_k\mathbf{p}_k \to 2N,$$

$$\mathbf{r}_k = \mathbf{r}_{k-1} - a_k A_d\mathbf{p}_k \to 2N,$$

$$\rho_0 = \rho_1 \to 1.$$

For CGM with preconditioning,

$$\rho_1 = (C_L\mathbf{r}_{k-1}, C_L\mathbf{r}_{k-1}) \to 2N + mO(N) + 2N,$$

$$b_{k-1} = \frac{\rho_1}{\rho_0} \to 1,$$

$$\mathbf{p}_k = C_L\mathbf{r}_{k-1} + b_{k-1}\mathbf{p}_{k-1} \to 2N,$$

$$a_k = \frac{(C_L\mathbf{r}_{k-1}, C_L\mathbf{r}_{k-1})}{(\mathbf{p}_k, C_L A_d\mathbf{p}_k)} \to 2N + O(N) + mO(N) + 2N,$$

$$\mathbf{x}_k = \mathbf{x}_{k-1} + a_k\mathbf{p}_k \to 2N,$$

$$\mathbf{r}_k = \mathbf{r}_{k-1} - a_k A_d\mathbf{p}_k \to 2N,$$

$$\rho_0 = \rho_1 \to 1.$$

105

Here N is the dimension of the vector and m is an order of the preconditioning polynomial. $O(N)$ is the number of operations, proportional to N, needed for the multiplication of the sparse matrix by an N-dimensional vector. In both cases one also needs $2N$ operations for estimating $\|r_k\|_2$ in order to determine whether this norm satisfies the stopping criterium.

Hence the ratio of the time needed for one iteration of CGM without preconditioning to the one with preconditioning is

$$\frac{t_{npr}}{t_{pr}} = \frac{12N + O(N) + \Delta}{16N + (2m+1)O(N) + \Delta},$$

where Δ is the memory allocation and storage time. The overall gain in time will be achieved if

$$\frac{n_{npr}^{it}}{n_{pr}^{it}} \cdot \frac{t_{npr}}{t_{pr}} > 1,$$

where n_{npr}^{it} and n_{pr}^{it} denote the number of iterations needed for getting the desired accuracy of 10^{-10} for CGM without and with preconditioning. $O(N)$ depends on the sparsity of the matrix. The simple calculations based on the above formula show that up to two times the gain can be achieved, depending on the order m of the preconditioning polynomial. It does not make sense to use the polynomials with m more than 9-10. The experimental values of the ratio of the computational time for preconditioned CGM over the time for CGM without preconditioning are shown on Figure. The condition number for the matrix resulting from $R2$ is not supposed to differ much from $R1$, hence similar results will be obtained for matrix $R2$.

In conclusion the error of the FVM numerical modeling increases for the radial dipole approaching the skull. However as it was shown before, this error will not affect the accuracy of the source localization. The difference between the realistic and idealistic models also grows for the radial dipole approaching the skull, but this difference is not significant in comparison with the difference between the numerical and analytical modeling results.

The number of iterations and computational time can be substantially reduced thanks to the Polynomial Preconditioning. However the computational time here was not reduced that much for the reasons described above.

Figure 13: Relative Error versus the Number of Iterations for Polynomial Preconditioning.
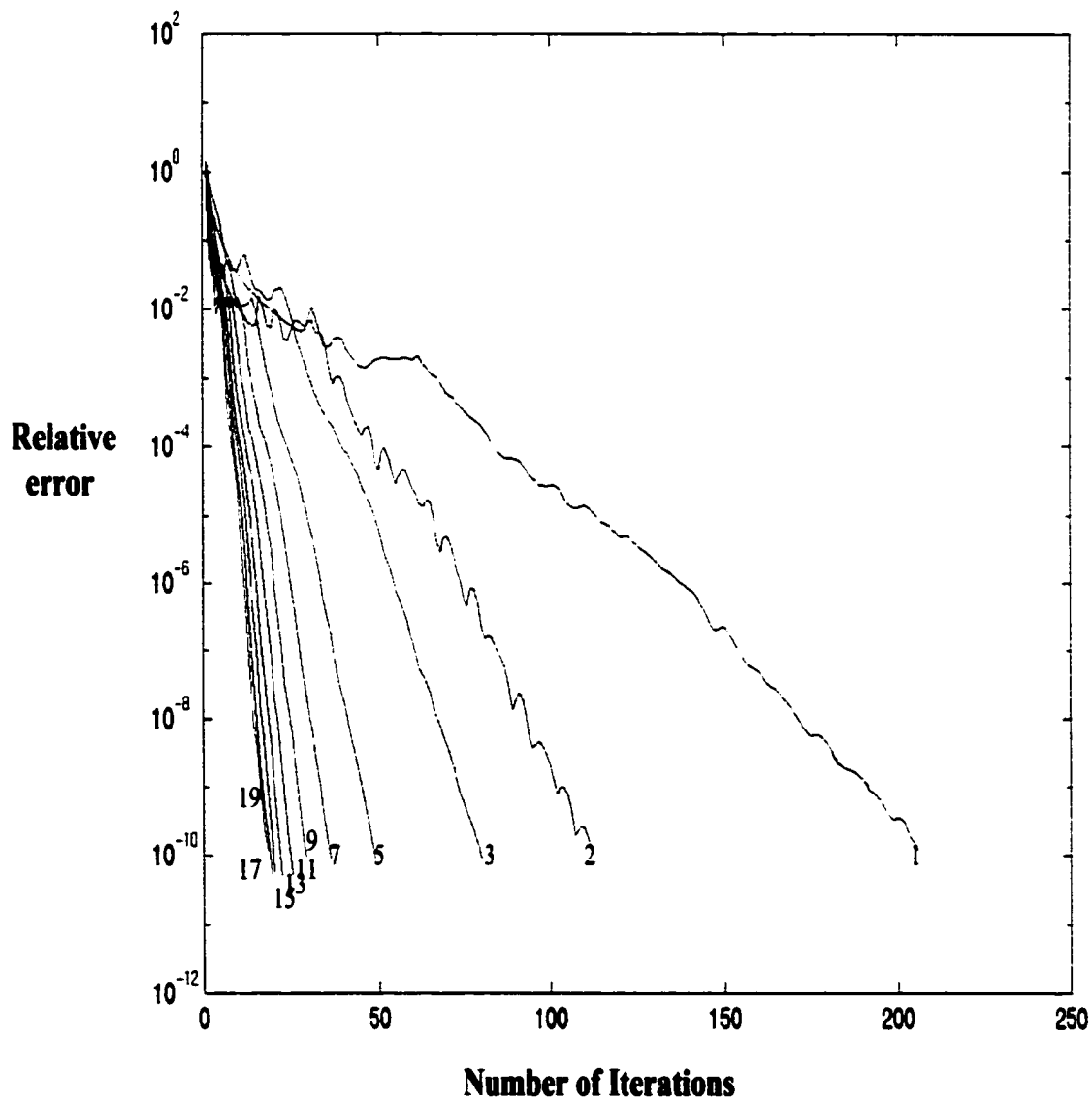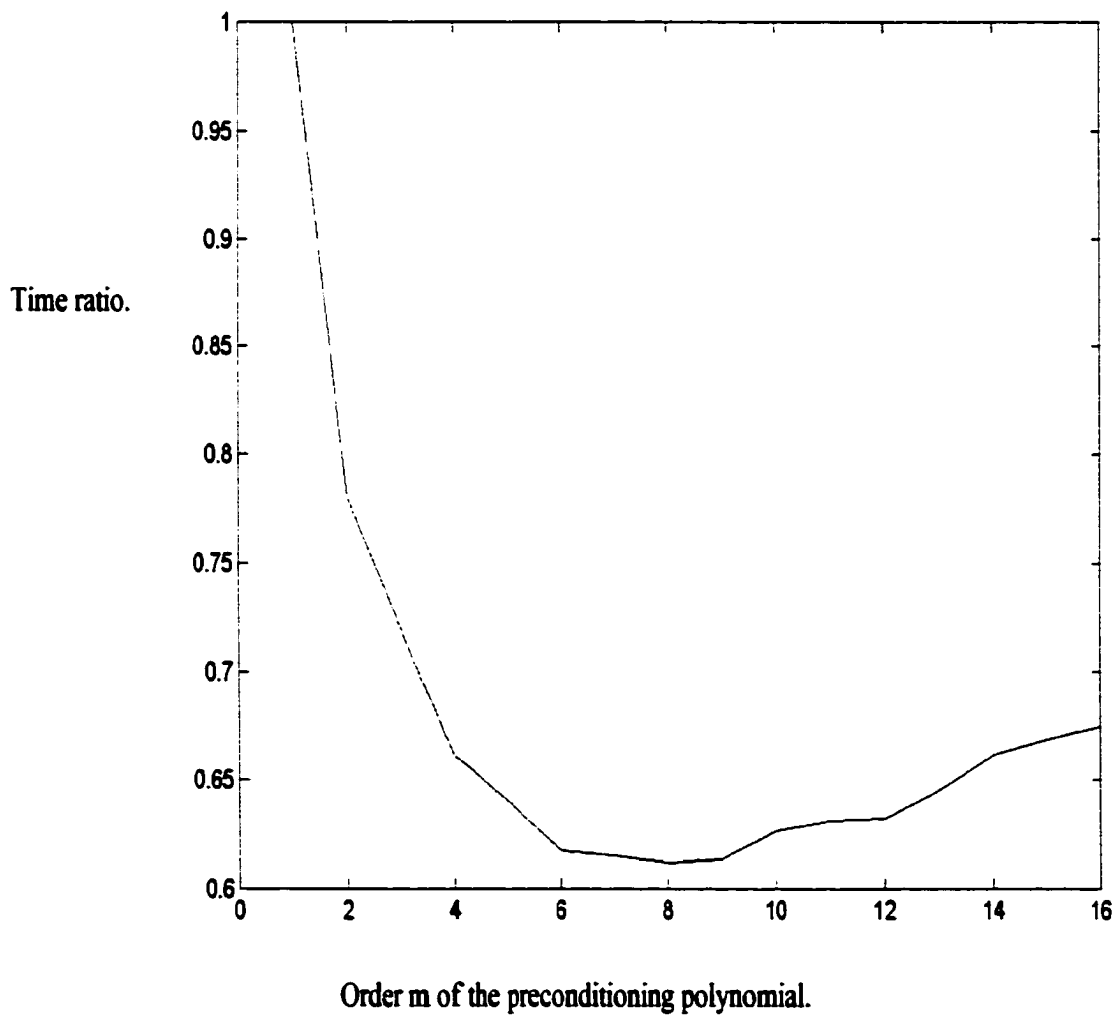

108

Figure 14: Time Ratio for Preconditioned CGM versus the Order of Preconditioning Polynomial.

Time ratio.

Order m of the preconditioning polynomial.

109

7 Summary and Conclusions. Suggestions for future research.

7.1 Summary and Conclusions.

The development of efficient software for high-precision patient-oriented localization of the multiple dipole sources remains one of the major purposes of the EEG research. In Chapter 1 an overview of the basic concepts underlying the Inverse and the Forward EEG problem was given, as well as a very brief overview of the ways of solving it. The objectives of this research are:

1) an acceleration of the numerical solution for the realistic head model;

2) an assessment of the errors involved in the numerical solution of the forward problem by comparison to the analytical solution of the problem in a spherical head model;

3) a search for alternatives to the numerical approach.

In Chapter 2 a review of known methods relevant to the forward problem is given. The three-shell idealistic model allows one to get analytical solutions for a certain geometry. It can also be used for the assessment of errors in numerical modeling. The Boundary and Finite Element Methods have already been used in EEG literature for the numerical solution of the forward problem. In this work the Finite Volume Method for the forward EEG problem was implemented in a way suitable for computing the biopotential for the realistic head model. The Conjugate Gradient Method is described since it provides an efficient way of solving large sparse systems with symmetric and positive definite matrices.

The implementation Finite Volume Method is given in Chapter 3. The approach taken in this work provides a uniform grid which is convenient for source localization. The matrix for the corresponding linear system is symmetric but semidefinite. This is due to the fact that only the potential difference between the given point and a reference point makes physical sense. Therefore the solution is defined up to an arbitrary constant. Hence

the linear system must be deflated. It is proved that the matrix of the deflated system is positive definite. The Polynomial Preconditioning allowes one to accelerate the CGM forward problem computation by about 2 times in comparison with the non-preconditioned CGM. The overall computational procedure becomes much more efficient comparied to the implementations given in [42] and [5].

It is desirable to have an inverse matrix for the Finite Volume Method. This would allow one to avoid numerous repetitions of the forward problem iterative solution for different right-hand sides, needed for the inverse problem of EEG source localization. It is much more desirable to have an analytic expression for the inverse matrix. Thus there would be no need to store it in memory. The very first step in this direction is the idea of the analytic inversion of the forward problem matrix for the uniform cube, given in Chapter 4. First the inverse matrix is found for a one-dimensional chain of cubes. Then the idea is extended for two-dimensional and tri-dimensional cases. In these cases the block matrices are similar to the one-dimensional cases. The analytical expression for the inverse matrix could also be valuable due to the fact that only a limited number of entries of A^{-1} is needed for the particular forward problem solution. Certainly this direction of research has a potential for a given problem, and such an approach may also be extended to a variety of inverse problems of similar nature.

In Chapter 5 a new version of the three-shell analytical model is given. One of the key assumptions of the idealistic three-shell model described in Chapter 2 is that the positive and negative sources are infinitely close to each other. First this assumption is not realistic, as in practice these sources are separated. The distance may vary up to 1 cm. Second the FVM implementation of the forward problem is done in a way that the positive and negative sources cannot be placed into one and the same finite volume element. In such a case the system will have a zero right-hand side. Hence this assumption is removed in a realistic three-shell model. As before the solution is a sum of expressions for the radial

111

and tangential dipoles. It is shown that as the distance between the sources goes to zero, the solution for the realistic three-shell model turns into an expression for the idealistic one.

Chapter 6 contains the description of numerical experiments. First the idealistic and realistic three-shell models are compared. It is quite surprising that the difference does not exceed 1 % in absolute value. The difference is maximal for the radial dipole as it gets closer to the skull. Nevertheless the new model is more convenient for testing the Finite Volume Method. Second the solutions of the forward problem are compared to idealistic and realistic analytical models. The difference between the numerical and analytical solutions can be regarded as an error of the FVM. For the radial dipole, there is an increase in error as it gets closer to the skull. For the tangential dipole, the increase is not very significant. The error of the numerical models cannot be explained by the differences between idealistic and realistic models alone. Similar results are obtained in [35] and [42].

7.2 Suggestions for Future Research

.

For practical diagnostics, it is important to further reduce the computational time, as well as the error of the numerical modeling. Below are the guidelines for an enhancement of the forward, as well as the inverse, problem solution.

1) In order to solve an inverse problem, the forward problem has to be solved thousands of times with different right-hand sides corresponding to the varying dipole locations and orientations. Hence there are parallelization opportunities.

2) A grid with finer resolution is needed for further error reduction. In addition the error can be further reduced by adapting the shapes of the finite volume elements to the edges of the skull and scalp, keeping the grid uniform in the brain area.

3) The system of the finite volume elements should reflect the realistic geometry of the human brain. The conductivity distribution data is obtained through Magnetic Resonance Imaging scans of the realistic head. The proper identification of the edges of the skull and scalp is quite problematic for these scans. There is already a certain progress in the identification of the three-dimensional shapes of the human head [45], however it is important to identify the outer shapes of the skull and scalp and construct an algorithm which will automatically generate the system of finite volume elements with a given resolution for the scans of the human head.

4) In order to make the modeling more realistic the FVM system of equations should be modified in a way that will allow the anisotropy of conductivities. In reality the conductivity of the brain tissue depends on the direction and this fact should be taken into account.

The new model can be combined with the *MUSIC* algorithm for the experimental source localization. One can also use it for the estimation of the FVM error while studying

113

different domain decompositions.

The analytical matrix inversion has a serious potential for an acceleration of the forward problem solution. However in order to put this idea into practice the following should be done:

1) calculations like those in Chapter 4 must be extended for the cube under various deformations;

2) this idea should be extended to a nonuniform conductivity distribution;

3) the problem of matrix deflation has to be studied for two and three-dimensional cases in order to put these solutions into practice.

114

7.3 Acknowledgments

.

I am very grateful to Dr. Koles, Department of Biomedical Engineering, and to Dr. Kovalyov, Department of Mathematics, for their extensive help, numerous discussions and their patience throughout the time this work was under way. The author is also grateful to Dr. Wang, Department of Mathematics, for very valuable remarks on the computational aspects of this thesis. I would like to thank for their kindness and for the practical skills they shared with me Dan Witney, Nora O'Neil and Angela Antoniu, graduate students of Dr. Koles, Department of Biomedical Engineering. I am sure that these talented and hard-working individuals will be able to continue and enhance this direction of research in the future.

115

References

[1] Vinokur M. *An analysis of Finite-Difference and Finite-Volume Formulations of Conservation Laws*. J. of Comput. Phys., 81(1989), pp. 1-52.

[2] Koles Z.J., Lind J.C., Soong A.C.K. *Spatio-temporal Decomposition of the EEG: A General Approach to the Isolation and Localization of Sources*. Electroencephalography & Clinical Neurophysiology, 95 (1995), pp. 219-230.

[3] Abboud S., Rosenfeld M., Luzon J. *Effect of Source Location on the Scalp Potential Assymmetry in a Numerical Model of the Head*. IEEE Transactions on Biomedical Engineering, 43 , N. 7, July 1996, pp. 690-696.

[4] Sydman R.D., Giambalvo V., Allison T., Bergey P. *A Method for Localization of Sources of Human Cerebral Potentials Evoked by Sensory Stimuli*. Sensory Processes, 2. (1978), 116-129.

[5] Rosenfeld M., Abboud S. *Numerical Solution of the Potential Due to Dipole Sources in Volume Conductors With Arbitrary Geometry and Conductivity*. IEEE Transactions on Biomedical Engineering, 43 , N. 7, July 1996, pp. 679-688.

[6] Jackson D. R. et al. *Computational Aspects of Finite Element Modeling in EEG Source Localization*. IEEE Transactions on Biomedical Engineering, 44, N. 8, August 1997.

[7] Raz J., Turetsky B., Fein J. *Frequency Domain Estimation of the Parameters of Human Brain Electrical Dipoles*. Journal of the American Statistical Association. March 1992, Vol. 87, N. 417.

[8] Marchuk G.I. *Methods of Numerical Mathematics*. Springer-Verlag New York Inc., 1982.

[9] Polak E. *Computational Methods in Optimization*. Academic Press, New York and London, 1971.

[10] Mathews J., Walker R.L. *Mathematical Methods of Physics*. W.A.Benjamin, Inc., New York, 1970.

[11] Press W.H., Teukolsky S.A., Vetterling W.T., Flannery B.P. *Numerical Recipes in C. The Art of Scientific Computing*. Cambridge University Press, 1992.

[12] Cuffin B.N. *Effects of Head Shape on EEG's and MEG's*. IEEE Trans. Biomed. Eng., vol. 37, pp. 44-52, 1990.

[13] He B., Musha T., Okamoto Y., Homma S., Nakajima Y., Sato T. *Electric Dipole Tracing in the Brain by means of the boundary element method and its accuracy*. IEEE Trans. Biomed. Eng., vol BME-34, pp. 406-414, 1987.

[14] Yan Y., Nunez P.L., Hart R.T. *Finite-element model of the head: Scalp potentials due to dipole sources*. Med. Biol. Eng. Comp., vol. 29, pp. 475-481, 1991.

[15] Nunez P.L. *Electric fields of the brain*. Oxford University press, 1981.

[16] Brebbia. *Advanced formulations in Boundary Element Method*. Computational Mechanics Publications, London, 1993.

[17] B.M. Horacek, J.C. Klements. *The Inverse Problem of Electrocardiography: A Solution in Terms of Single- and Double-Layer Sources on the Epicardial Surface*. Math. Biosciences, 144 (1997), No. 2, p.p. 83-119.

[18] R. Horn, C. Johnson. *Matrix Analysis*. Cambridge University Press, 1985.

[19] Z.J. Koles, A.C.K. Soong (1998). *EEG source localization: implementing the spatio-temporal decomposition approach*. In press: Electroenceph. clin. Neurophysiol. item

Cuffin B.N. Effects of head shape on EEG's and MEG's. IEEE Trans. Biomed. Eng., vol. 37, pp. 44-52, 1990.

[20] Koles Z.J., Soong A.C.K. *EEG source localization: implementing the spatio-temporal decomposition approach*. Electroencephalography and clinical Neurophysiology, 107: 343-352, 1998.

[21] Jackson D. R. et al. *Computational Aspects of Finite Element Modeling in EEG Source Localization*. IEEE Transactions on Biomedical Engineering, 44, N. 8, August 1997.

[22] Schwarz H.R. *Finite Element Methods*. Academic Press Ltd, San Diego, 1988.

[23] Collatz L. *The Numerical Treatment of Differential Equations*. Springer-Verlag, Berlin, 1966.

[24] Kane J. *Boundary Element Analysis in Engineering Continuum Mechanics*. Prentice-Hall Inc., 1994.

[25] Hubner K.H., Thornton E.A. *The Finite Element Method for Engineers*. John Wiley&Sons, Inc., 1982.

[26] Faber V., Manteuffel T.A. *Orthogonal error methods*. SIAM J. Numer. Anal., 24: 170-187, 1987.

[27] Faber V., Manteuffel T.A. *Necessary and sufficient conditions for the existence of a conjugate gradient method*. SIAM J. Numer. Anal., 21 (1984), p.p. 352-362.

[28] Joubert W.D., Young D.M. *Necessary and sufficient conditions for the simplification of generalized conjugate gradient algorithms*. Linear Algebra Appl., 88/89 (1987), p.p. 449-485.

[29] Magnus W., Oberhettinger F., Soni R.P. *Formulas and theorems for the Special Functions of Mathematical Physics*. Springer-Verlag New York Inc., 1966.

[30] Ashby S.F. *Minimax polynomial preconditioning for Hermitian linear systems*. SIAM J. Matrix Anal., 12:766-789, 1991.

[31] Hageman L.A., Young D.M. *Applied Iterative Methods*. Academic Press, New York, 1981.

[32] Manteuffel T.A. *An Incomplete Factorization Technique for Positive Definite Linear Systems*. Mathematics of Computations, Vol. 34, N. 150, April 1980, p.p. 473-497.

[33] Meijerink J.A., Van der Vorst H.A. *An iterative solution method for linear systems of which the coefficient matrix is a symmetric M-matrix*. Math. Comp., 31:148-162, 1977.

[34] Mosher J.C., Lewis P.S., Leathy R.M. *Multiple dipole modelling and Localization from Spatio-Temporal MEG Data*. IEEE Transactions on Biomedical Engineering, Vol. 39, No. 6, June 1992.

[35] Mosher J.C., Lewis P.S., Leathy R.M. *EEG and MEG: Forward Solutions for Inverse Methods*. IEEE Transactions on Biomedical Engineering, Vol. 46, No. 3, March 1999.

[36] Korn G.A., Korn T.M. *Mathematical handbook for scientists and engineers*. Mc. Graw-Hill, Inc., 1968.

[37] Faddeev D.K., Faddeeva V.N. *Computational Methods of Linear Algebra*. San Francisco: H.W. Freeman, 1963.

[38] John, F. *Partial differential equations*. New York, Springer-Verlag, 1982.

[39] Bruaset A.M. *A survey of preconditioned iterative methods*. Longman Scientific &Technical, 1995.

[40] Ashby S.F., Manteuffel T.A., Saylor P.E. *A taxonomy for conjugate gradient methods.* SIAM J. Numer. Anal., Vol. 27, No. 6, pp. 1542-1568, December 1990.

[41] Prasolov V.V. *Problems and Theorems in Linear Algebra.* American Math. Society, 1994.

[42] Lemieux L., McBride A., Hand J. *Calculation of electrical potentials on the surface of a realistic head model by finite differences.* Phys. Med. Biol., Vol. 41, pp. 1079-1091, 1996.

[43] Hestenes, Steiffel. *Methods of conjugate gradients for solving linear systems.* J. Res. Nat. Bur. Stand., Vol 49, 1952, 409-436.

[44] Agapov V., Kovalyov M., Koles Z.J. *The error in EEG Source Localization due to a homogeneous head model.* In: Proceedings of the 24th Conference of the Canadian Medical and Biological Engineering Society, 16-17, Edmonton, AB, 1998.

[45] Agapov V.E., Koles Z.J., Javidan M., O'Neill N.S. *Estimation of the Locations of Seizure Onset in the Scalp EEG.* In: Proceedings of the 9th World Congress of the International Society for Brain Electromagnetic Topography (ISBET), New Orleans, LA, 1988.

[46] Rush S., Driscoll D.A. *EEG electrode sensitivity - an application of reciprocity.* IEEE Trans. Bio-Med. Eng. 16, 15-22 (1969).

[47] Blum E.K. *Numerical Analysis. Theory and Practice.* Addison-Wesley, 1972.

[48] Chebyshev P.L. *Collected works.* Moscow-Leningrad, 1947, p.p. 23-51.

[49] de Munck J.C. *The potential distribution in a layered anisotropic spheroidal volume conductor.* J. Appl. Phys., Vol. 64(2), 15 July 1988.